

Universitätsbibliothek Kiel
850 00 159 711 6



**TK
5804**

**Quantification of methane fluxes and authigenic
carbonate formation at cold seeps along the
continental margin offshore Costa Rica:
A numerical modeling approach**

**DISSERTATION
zur Erlangung des Doktorgrades
an der Mathematisch-Naturwissenschaftlichen Fakultät
der Christian-Albrechts-Universität zu Kiel**

vorgelegt von

Deniz Karaca

Kiel 2011

**Bitte streichen Sie
in unseren Büchern
nichts an.
Es stört spätere Benutzer
Ihre Universitätsbibliothek**

TK 5804

Quantification of methane fluxes and authigenic
carbonate formation at cold seeps along the
continental margin offshore Costa Rica:
A numerical modelling approach

DISSERTATION
zur Erlangung des Doktorgrades
an der Mathematisch-Naturwissenschaftlichen Fakultät
der Christian-Albrechts-Universität zu Kiel

vorgelegt von

Deniz Karaca

Kiel 2011

**Quantification of methane fluxes and authigenic
carbonate formation at cold seeps along the
continental margin offshore Costa Rica:
A numerical modeling approach**

DISSERTATION
zur Erlangung des Doktorgrades
an der Mathematisch-Naturwissenschaftlichen Fakultät
der Christian-Albrechts-Universität zu Kiel

Reisepass: Prof. Dr. Klaus Weilmann
Korridor: Dr. PD Dr. Mark Schmidt
Tag der mündlichen Prüfung: 28.01.2011
Zum Druck genehmigt: 11.02.2011

vorgelegt von

Deniz Karaca

Kiel 2011

Der Dekan

A numerical modeling approach
continental margin offshore Costa Rica
carbonate formation at cold seeps along the
Quantification of methane fluxes and autigenic

MTK 5804

UNIVERSITÄTSBIBLIOTHEK KIEL
- ZENTRALBIBLIOTHEK -

Hiermit erkläre ich, dass ich die vorliegende Doktorarbeit selbständig und ohne
Zuhilfenahme unerlaubter Hilfsmittel erstellt habe. Weiterhin wurde diese noch eine inhaltliche Arbeit
wurde an einer anderen Universität oder Hochschule im Rahmen eines

Referent:Prof. Dr. Klaus Wallmann
Koreferent:.....PD. Dr. Mark Schmidt
Tag der mündlichen Prüfung:28.01.2011
Zum Druck genehmigt:..... 11.02.2011

Demit Kurca

Der Dekan

11.02.2011

11.02.2011

Zum Druck genehmigt:
Tag der mündlichen Prüfung:
Korridor:
Rechner:
Prof. Dr. Klaus Wallmann
PD. Dr. Marc Schmidt
28.01.2011
11.02.2011

Dr. Doka

Hiermit erkläre ich, dass ich die vorliegende Doktorarbeit selbständig und ohne Zuhilfenahme unerlaubter Hilfsmittel erstellt habe. Weder diese noch eine ähnliche Arbeit wurde an einer anderen Abteilung oder Hochschule im Rahmen eines Prüfungsverfahrens vorgelegt, veröffentlicht oder zur Veröffentlichung vorgelegt. Ferner versichere ich, dass die Arbeit unter Einhaltung der Regeln guter wissenschaftlicher Praxis der Deutschen Forschungsgemeinschaft entstanden ist.

Deniz Karaca

Hiermit bestätige ich, dass ich die vorliegende Doktorarbeit selbstständig und ohne
Zuflüsse anderer Hilfen verfasst habe. Weiterhin bestätige ich, dass die Arbeit
nicht an einer anderen Stelle veröffentlicht oder in irgendeiner Weise
öffentlich zugänglich gemacht wurde. Ich bestätige auch die Richtigkeit der
Angaben in der Zusammenfassung und der Bibliographie. Ich bestätige
des Weiteren die Richtigkeit der Angaben in der Zusammenfassung und der
Bibliographie.

Dennis Kasper

Acknowledgements

First of all I would like to express my gratitude to Dr. Christian Hühner for valuable discussions and recommendations as well as his encouraging and patient guidance which have provided a good basis for the present thesis.

I am very thankful to my supervisor Prof. Dr. Wolfgang Wagner for his detailed and constructive criticism which has helped me to improve my work. His wide knowledge and biological way of thinking have been very helpful for me. I also would like to thank PD Dr. Mark Sørensen for acting as a co-referee for this dissertation.

Lower my most sincere gratitude to Dr. Ingo Klauke and Tina Seifrieder for providing me very useful data and for their constant help and extensive discussions.

I wish to extend my thanks for all those who gave me technical help and support during my work, especially my sincere thanks are due to Dr. Başak Kaşıkçı and Nur Demir as well as to my colleagues and friends in IEM-GEOMAR and SFB-574.

I also appreciate the indispensable support by Roger Lutz and Matthias Häckel concerning the handling of C-CANTH during my stay here in transport reaction modeling.

Finally, my deep and sincere gratitude are due to my parents for their love, support and encouragement.

THE UNIVERSITY OF CHICAGO
LIBRARY

Table of contents

Abstract

Acknowledgements

First of all I would like to express my gratitude to Dr. Christian Hensen for valuable discussions and recommendations as well as his encouraging and personal guidance, which have provided a good basis for the present thesis.

I am very thankful to my supervisor Prof. Dr. Klaus Wallmann for his detailed and constructive comments which greatly improved this thesis. His wide knowledge and his logical way of thinking have been of great value for me. I also would like to thank PD Dr. Mark Schmidt for acting as a co-referee for this dissertation.

I owe my most sincere gratitude to Dr. Ingo Klaucke and Tina Schleicher for providing me very useful data and for their constant help and extensive discussions.

I wish to extend my thanks for all those who gave me untiring help and support during my work, especially my sincere thanks are due to Dr. Başak Kısakürek and Nur Demir as well as to my colleagues and friends in IFM-GEOMAR and SFB-574.

I also appreciate the indispensable support by Roger Luff and Matthias Haeckel concerning the handling of C.CANDI during my first steps in transport reaction modeling.

Finally, my deep and sincere gratitude are due to my parents for their love, support and encouragement.

Deniz Karaca
December, 2010

Acknowledgements

References

Acknowledgements

First of all I would like to express my gratitude to Dr. Christian Hees for valuable discussions and recommendations as well as his encouraging and personal feedback, which have provided a great basis for the present thesis.

I am very thankful to my supervisor Prof. Dr. Klaus Welton for his detailed and constructive comments which greatly improved this thesis. His wide knowledge and his logical way of thinking have been of great value for me. I also would like to thank PD Dr. Frank Schmitt for acting as a reviewer for this dissertation.

I owe my most sincere gratitude to Dr. Inga Klauke and Tan Schreiber for providing me very useful data and for their constant help and extensive discussions.

I wish to extend my thanks for all those who gave me lasting help and support during my work, especially my sincere thanks are due to Dr. Heiko Kraschick and Norbert as well as to my colleagues and friends in IEM-GEOMAR and 57B-57a.

I also appreciate the indispensable support by Roger Jull and Matthias Heesckel concerning the handling of CANDI during my first steps in transport reaction modeling.

Finally, my deep and sincere gratitude are due to my parents for their love, support and encouragement.

Denis Kraschick
December 2010

Table of contents

Abstract	iii
Kurzfassung	v

Chapter I.

General Introduction

I.1. Diagenetic processes in marine sediments	2
I.1.1. Methanogenesis	3
I.1.2. Sulfate reduction and anaerobic oxidation of methane	4
I.1.3. Authigenic carbonate precipitation	6
I.2. Transport processes of methane	7
I.3. Cold seep areas along the Costa Rica fore arc	8
I.4. Thesis outline	10
References	11

Chapter II.

Controls on authigenic carbonate precipitation at cold seeps along the convergent margin off Costa Rica

Abstract	19
II.1. Introduction	21
II.2. Study Area	22
II.3. Sampling Techniques and Chemical Analysis	24
II.4. Model Description and Methodology	25
II.5. Results and Discussion	30
II.5.1. Numerical modeling of measured data	30
II.5.1.1. Advection rates, methane turnover and AOM	35
II.5.1.2. Precipitation of authigenic carbonates	36
II.5.2. Systematics of calcium carbonate precipitation	40
II.5.3. Quantification of CaCO ₃ accumulation at cold seeps	43
II.5.4. Fluxes of TCO ₂ and TA across the sediment-water interface	45
II.6. Conclusions	48
Acknowledgements	49
References	50

Chapter III.**Quantification of dissolved methane discharge at mud mounds offshore Costa Rica**

Abstract	57
III.1. Introduction	59
III.2. Study Area	60
III.3. Material and Methods	62
III.4. Model set-up	65
III.5. Results	68
III.5.1. Seafloor observations	68
III.5.2. Modeling of advection rates and methane turnover	70
III.5.2.1. Mound 11	71
III.5.2.2. Mound 12	71
III.5.3. Estimation of regional methane release	76
III.6. Discussion	80
III.6.1. Upward advection and AOM	80
III.6.2. Estimation of methane emission at Mound 11 and Mound 12	81
III.6.3. Methane emission compared to other mud volcanoes	83
III.7. Conclusions	86
References	87

Chapter IV.**Quantification of methane emission at bacterial mats offshore Costa Rica**

Abstract	91
IV.1. Introduction	93
IV.2. Study Area	94
IV.3. Material and Methods	96
IV.4. Reaction-transport model	97
IV.5. Results and discussion	100
IV.5.1. Seafloor observations	100
IV.5.2. Porewater geochemistry	102
IV.5.2.1. Transport of dissolved species	103
IV.5.2.2. Upward fluid flow velocities	107
IV.5.3.3. AOM efficiency and methane turnover	108
IV.5.3. Methane release at bacterial mats	109
IV.6. Conclusions	112
References	113

Abstract

The expulsion of liquids, gases and fluids at continental margins covers a wide range of processes including not only mud volcanism, mud diapirism and gas flares, but also continuously seeping methane-rich fluids leading to cold vent sites and even outbursts of over-pressured gases. Seepage of fluids frequently leads to precipitation of authigenic carbonates that modify sedimentary processes along the margin, and finally, the fluids constitute the energy source for a number of diverse and complex ecosystems. During the last two decades, researchers gained significant knowledge about the impact of fluid seepage on local ecosystems and the biogeochemical processes that result in carbonate formation via the anaerobic oxidation of methane (AOM). However, all the knowledge was gained in different areas and geological settings of the world ocean but left a regional gap in our knowledge about seeps at the continental margin offshore Costa Rica. Those processes including authigenic carbonate precipitation, quantification of the impact of fluid seepage and methane budgets are documented in the present thesis.

Chapter II presents comprehensive results from five cold seep structures at the Costa Rican continental margin addressing the relationship between fluid advection, dissolved calcium concentrations in upward migrating fluids, and authigenic calcium carbonate precipitation. A numerical transport-reaction model was used to determine rates of AOM, CaCO_3 precipitation, and benthic fluxes of solutes. Production of carbonate alkalinity and formation of authigenic carbonates is most intense at intermediate flow rates ($3\text{-}40\text{ cm a}^{-1}$) and reduced under low and high flux conditions (0.1 and 200 cm a^{-1}). Systematic model runs showed that high Ca concentrations in ascending fluids enhance the rate of authigenic carbonate production at moderate flow rates leading to an almost quantitative fixation of deeply derived Ca in authigenic carbonates. Hence, CaCO_3 precipitation is not only controlled by Ca diffusing into the sediment from bottom water, but also by the Ca concentration in ascending fluids. Based on average precipitation rates deduced from the systematic model runs the global Ca-fixation at cold seeps ($\sim 2 \cdot 10^{10}\text{ mol Ca a}^{-1}$) suggesting that cold seeps are most likely not of key importance with respect to Ca cycling in the ocean.

Chapter 3 comprises the quantitative estimates of dissolved methane discharge from well-studied mud mounds (Mound 11 and Mound 12) at the submarine section of the Costa Rica fore-arc combining geochemical and geoacoustic data. The study is supported by 75 kHz sidescan sonar data, pore-water analysis and visual sea-floor observations by remotely operated vehicle (ROV). A numerical transport reaction model was applied to determine dissolved methane fluxes considering AOM and upward fluid flow. Model results reveal that a significant portion of methane from greater depth is discharged into the bottom water only at high fluid flow velocities that are not sufficiently moderate to allow for AOM. The overall amount of dissolved methane released from the entire mud mounds into the water column was moderate with a discharge of $0.36 \cdot 10^6 \text{ mol a}^{-1}$ at Mound 11 whereas it was calculated as $0.58 \cdot 10^6 \text{ mol a}^{-1}$ at Mound 12. Compared to other active cold seeps (mainly mud volcanoes), mud mounds at the submarine section of the Costa Rica fore arc do not represent a pathway for significant methane discharge from the seafloor.

Sea floor methane emissions from bacterial mat sites of a submarine slide at the Costa Rica continental margin are presented in Chapter IV. The estimates of methane fluxes into the water column are based on (i) detailed mapping in order to determine the abundance of seeps, and thus the spatial validity of the flux measurements; and (ii) application of numerical model to estimate the amount of methane that is transported into the bottom water. Model results illustrate that the majority of the studied seeps transport rather limited amount of methane into the water column due to medium to low advection rates (average 10 cm a^{-1}) allowing high methane consumption by AOM (average 45%) and limiting the methane discharge into the water column. Depth-integrated AOM rates ($56\text{-}1538 \text{ } \mu\text{mol CH}_4 \text{ cm}^{-2} \text{ a}^{-1}$) are comparable with the values reported at other very active vents sites, suggesting that the Quepos Slide should be regarded as one of the most active sites at the seafloor. The overall amount of dissolved methane released from the entire bacterial mat sites into the water column is determined as $0.56 \cdot 10^6 \text{ mol a}^{-1}$. This conservative estimate, relying on rather accurate determinations of sea floor methane fluxes out of bacterial mats emphasizes the importance of submarine slides as sites of natural methane seepage.

Kurzfassung

Die Freisetzung von Fluiden an Kontinentalrändern resultiert in Phänomenen wie Schlammvulkanismus, aufsteigenden Gasblasen in der Wassersäule, dem Auftreten von kalten Quellen sowie der spontanen Freisetzung großer Gasmengen durch im Untergrund erzeugten Überdruck. Der Aufstieg von Fluiden führt häufig zur Bildung authigener Karbonate, welche sedimentäre Prozesse an Kontinentalrändern entscheidend beeinflussen können. Ferner fungieren die Fluide als Energiequelle für diverse und komplexe Ökosysteme. In den vergangenen zwei Jahrzehnten haben Wissenschaftler wichtige Erkenntnisse darüber gewonnen, wie die Freisetzung von Fluiden am Meeresboden und die durch anaerobe Methanoxidation (AMO) induzierte authigene Karbonatbildung, submarine Ökosysteme beeinflussen können. Diese Erkenntnisse wurden in unterschiedlichen Gebieten mit unterschiedlichen geologischen Rahmenbedingungen erzielt. Der Kontinentalrand von Costa Rica fand dabei keine Berücksichtigung. Folglich beschäftigt sich die vorliegende Arbeit mit unterschiedlichen Aspekten der authigenen Karbonatbildung vor Costa Rica, der anaeroben Methanoxidation und der Methanfreisetzung an den kalten Quellen vor Costa Rica.

Kapitel 2 behandelt auf Grundlage eines umfassenden Datensatzes den Zusammenhang zwischen Fluidaufstiegsgeschwindigkeit, der Kalziumkonzentration im Porenwasser und der Fällung authigener Karbonate an kalten Quellen am Kontinentalrand von Costa Rica. Ein numerisches Transport-Reaktions-Modell wurde angewendet, um AMO-Raten, Fällungsraten für Kalziumkarbonat sowie benthische Stoffflüsse zu bestimmen. Die Produktion von Karbonatalkalinität und die Fällung authigener Karbonate sind bei mittleren Aufstiegsgeschwindigkeiten ($3-40 \text{ cm a}^{-1}$) am intensivsten, bei niedrigen und hohen Aufstiegsgeschwindigkeiten (0.1 und 200 cm a^{-1}) jedoch reduziert. Systematische Modellläufe haben gezeigt, dass hohe Kalziumkonzentrationen in den aufsteigenden Fluiden bei mittleren Aufstiegsgeschwindigkeiten die Karbonatfällungsrate erhöhen, so dass das aus der Tiefe aufsteigende Kalzium fast vollständig in authigene Karbonate eingebaut wird. Die CaCO_3 -Fällung wird damit nicht nur von dem aus dem Bodenwasser ins Sediment diffundierenden Kalzium, sondern auch von der Kalziumkonzentration im aufsteigenden Fluid bestimmt. Durchschnittliche Fällungsraten, die aus systematischen Modellläufen abgeleitet wurden, zeigen, dass die Kalziumfixierung an kalten Quellen scheinbar nicht von großer Bedeutung für den ozeanischen Kalziumkreislauf ist.

Kapitel 3 beschäftigt sich mit der auf geochemischen und geoakustischen Methoden gestützten, quantitativen Abschätzung der Methanfreisetzung an zwei kalten Quellen (Mound 11 und Mound 12) am Kontinentalrand von Costa Rica. Die Studie basiert auf 75 kHz Seitenansichtsonar- und Porenwasseranalysen sowie auf visuellen Meeresbodenbeobachtungen, welche mit Hilfe eines ferngesteuerten Unterwasserfahrzeugs durchgeführt wurden. Ein numerisches Transport-Reaktions-Modell, welches AMO und aufwärtsgerichteten Fluidtransport berücksichtigt, wurde angewandt, um Methanflüsse zu bestimmen. Die Modellergebnisse zeigen, dass nur bei hohen Fluidaufstiegsgeschwindigkeiten die AMO-Aktivität unterbunden wird und signifikante Methanmengen ins Bodenwasser entweichen können. Die Gesamtmengen des an in die Wassersäule abgegebenen Methans war moderat und betrug $0.36 \times 10^6 \text{ mol a}^{-1}$ an Mound 11 und $0.58 \times 10^6 \text{ mol a}^{-1}$ an Mound 12. Verglichen mit anderen aktiven kalten Quellen (v.a. Schlammvulkane), stellen jene am Kontinentalrand von Costa Rica keine signifikante Methanquelle in der Wassersäule dar.

In Kapitel 4 wird die Freisetzung von Methan aus Bakterienmatten an submarinen Rutschungen vor Costa Rica untersucht. Dies basiert auf (i) detaillierten Kartierungen welche die Verteilung kalter Quellen und damit die räumliche Anwendbarkeit der Flussmessungen dokumentieren; und (ii) der Anwendung eines numerischen Modells, um die Menge des ins Bodenwasser transportierten Methans zu bestimmen. Die Modellergebnisse zeigen, dass die meisten kalten Quellen nur geringe Mengen Methan in die Wassersäule transportieren, was mit den mittleren bis geringen Fluidaufstiegsgeschwindigkeiten (durchschnittlich 10 cm a^{-1}) und dem daraus resultierenden intensiven Methanverbrauch durch AMO (durchschnittlich 45 %) zusammen hängt. Tiefenintegrierte AMO-Raten ($56\text{-}1538 \text{ } \mu\text{mol CH}_4 \text{ cm}^{-2} \text{ a}^{-1}$) am Quepos-Slide sind vergleichbar mit Werten anderer sehr aktiver kalter Quellen, weswegen diese Rutschung als besonders aktiv anzusehen ist. Die Gesamtmenge des an Bakterienmatten abgegebenen gelösten Methans beträgt $0.56 \times 10^6 \text{ mol a}^{-1}$. Diese konservative Abschätzung, welche auf relativ exakten Methanflussbestimmungen an Bakterienmatten basiert, unterstreicht die Bedeutung von submarinen Rutschungen als natürliche Gasquellen am Meeresboden.

Chapter I

General Introduction

Atmospheric time series observations over the past two decades have documented an increase in the atmospheric mixing ratio of methane, and a great deal of activity has focused on the cause and climate consequences of this increase. The primary sources of atmospheric methane are: (i) human modifications to the landscape via cultivation; (ii) natural emissions from swamps, peats, termite activities; and (iii) thawing permafrost environments, which came into focus more recently (Prather et al., 1995; Walter et al., 2006). However, it is only relatively recently that gas seeps have been recognized as a potential source of atmospheric methane, and therefore a contributor to the "Greenhouse Effect".

The ocean contributes a relatively small amount of methane to the global net atmospheric methane budget and thought to account for just 2-4 % of the total methane released to the atmosphere (Cicerone and Oremland, 1988; Bates et al., 1996). Since the discovery of new seeps, vents and mud volcanoes related to the sedimentary gas hydrates, estimates of the methane emission rate to the atmosphere from the sea floor have been revised and range from 4-9 % (Hornafius et al., 1999; Judd et al., 2002; Kvenvolden and Rogers, 2005). The estimates of the amount of methane stored in gas hydrates, mostly common in productive continental margins range between 1 to $5 \cdot 10^{15}$ m³ (Kvenvolden, 1988; 1993; Milkov, 2004). These ice-like compounds, which are stable at water depths below 300-500 m depending on conditions of pressure and temperature (Kvenvolden, 1993) represent a significant reservoir and a potential source for methane carbon to the ocean (Kvenvolden, 2002; Dickens, 2003).

Seeps and mud volcanoes, which are common at many active and passive continental margins were specifically identified as sources of methane to the water column (e.g. Hovland et al., 1993; Heeschen et al., 2003; Sauter et al., 2006; Wallmann et al., 2006; de

Beer et al., 2006). However, the global contribution of submarine mud volcanoes remains very uncertain because the number of mud volcanoes as well as their gas release is unknown. Despite these additions to the ocean water column, microbially-mediated aerobic and anaerobic oxidation reactions effectively consume the added methane to low nanomolar levels, so that most of the ocean volume is undersaturated with respect to the atmosphere (Reeburgh, 2007 and references therein). Although cold seeps at continental margins are not expected to play a role in the contemporary atmospheric methane increase (Judd et al., 2002; Milkov et al, 2003), they are a window into the deeper geosphere and may provide crucial information about petroleum and gas systems. During the last two decades, researchers gained significant knowledge about the biogeochemical processes that result in carbonate formation via the anaerobic oxidation of methane (AOM), the formation and dissociation processes of hydrates and their role as temporal storage reservoir for methane.

1.1. Diagenetic processes in marine sediments

Sediments deposited at active continental margins experience a number of diagenetic processes which may include organic matter degradation, formation of biogenic and thermogenic methane and gas hydrate, sulfate reduction coupled to AOM and precipitation of authigenic minerals.

The content of organic carbon in marine surface sediments from different environments of the present-day oceans varies over several orders of magnitude depending on the extent of supply of organic matter. A statistical evaluation of data from the early phase deep-sea drilling (Deep Sea Drilling Project Legs 1-31) showed deep-sea sediments to have mean organic carbon contents of 0.1 - 0.3% (McIver, 1975). Fine grained near-shore sediments on continental shelves and slopes usually have considerably higher organic carbon contents. Typical hemipelagic sediments on outer shelves and continental slopes range between 0.3-1 % C_{org} (Rullkötter, 2006).

Within the sediment, the organic carbon content decreases with increasing depth due to microbiological degradation processes. The microbial decomposition takes place in a complex redox system where organic matter is the electron donor and a variety of substrates are electron acceptors. The major electron acceptors are dissolved oxygen,

nitrate (NO_3^-), sulfate (SO_4^{2-}) and carbon dioxide (CO_2) as well as solid manganese (Mn(IV)) and iron (Fe(III)) in the form of oxyhydroxides. The redox zone in the example given in Figure 1 is restricted to a depositional environment with anoxic surface sediment and comprises only sulfate reduction and methanogenesis.

1.1.1. Methanogenesis

Methane is generally considered to originate from one of two sources: the microbial degradation of organic matter in shallow sediments, or the thermocatalytic breakdown of complex organic molecules as part of the petroleum-generating processes occurring deep within sedimentary basins (Whiticar, 1986, 1999). Methane of these two origins, microbial (biogenic) and thermogenic can be distinguished by their carbon and hydrogen isotope signatures (Whiticar, 1999).

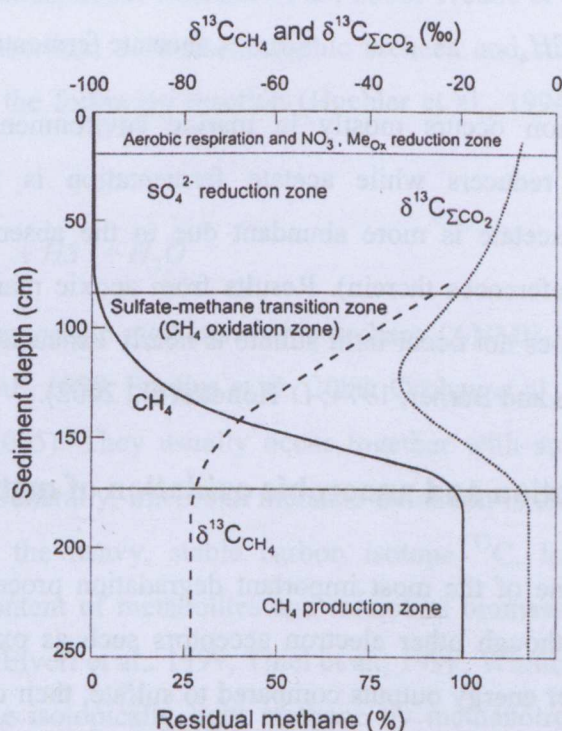
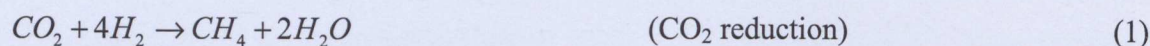


Figure 1. Organic carbon remineralization, sediment depth profile of methane concentration and carbon isotopic composition of dissolved inorganic carbon and methane in marine sediments (Whiticar, 1996).

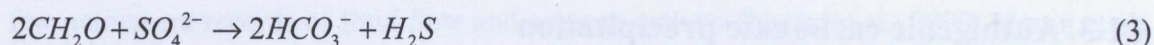
Biogenic or microbial methane is generally considered to have a $\delta^{13}\text{C}$ -value (wherein the delta notation denotes the isotopic ratios of ^{13}C to ^{12}C in the sample relative to a known standard, namely PeeDee belemnite, in permil unit) of less than -55 ‰ (Claypool, et al., 1974) while thermogenic methane is isotopically heavier, with $\delta^{13}\text{C}$ -value of greater than -55 ‰. Biological methane production or methanogenesis is the last step in the remineralization of complex organic matter in anaerobic systems (Kiene, 1991). The formation of methane at a depth level, where all sulfate has been consumed, involves a group of strictly anaerobic archaea, collectively methanogens. They use a small number of substances together with elemental hydrogen (Rudd and Taylor, 1980), which are in turn formed by bacterial fermentation from more complex organic substrates during early diagenesis. The most prominent pathways are the reduction of carbon dioxide with molecular hydrogen and the transformation of acetic acid into methane and carbon dioxide:



Bacterial CO_2 reduction occurs mostly in marine environments because of acetate depletion by sulfate reducers while acetate fermentation is favored in freshwater environments, where acetate is more abundant due to the absence of sulfate reducers (Whiticar, 1999 and references therein). Results from anoxic marine sediments indicate that methanogenesis does not occur until sulfate is nearly exhausted and sulfate reduction rates decrease (Martens and Berner, 1974; D'Hondt et al., 2002).

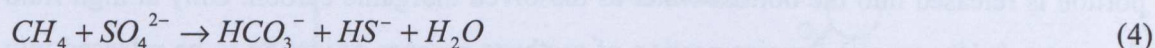
1.1.2. Sulfate reduction and anaerobic oxidation of methane

Sulfate reduction is one of the most important degradation processes of organic matter (Jørgensen, 1982). Although other electron acceptors such as oxygen, nitrate, iron and manganese yield higher energy outputs compared to sulfate, their combined concentration at the sediment water interface are more than 50 times lower compared to the total sulfate concentration (D'Hondt et al., 2002). Most of the known sulfate reducers are bacteria, but also some thermophilic archaea belong to this group (Rabus et al., 2004; Stetter et al., 1993). The sulfate reducing bacteria use sulfate as the terminal electron acceptor for their anaerobic respiration, where sulfate is consumed and dissolved inorganic carbon (DIC) is produced (Claypool and Kaplan, 1974):



Sulfate reduction occurs in anoxic and even in suboxic to oxic sediments where the produced sulfide is rapidly reoxidized (Jørgensen and Bak, 1991). In the deep sea, the metal oxides may be exhausted only several meters below the surface and little organic material is available once it becomes buried down into the sulfate reduction zone. The sulfate reduction in sediments is therefore very sensitive to the organic deposition rate (Jørgensen and Kasten, 2006).

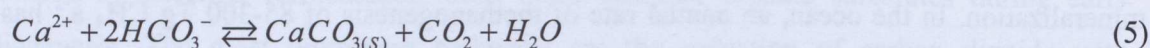
Below the sulfate zone, methanogenesis is the main terminal pathway of organic carbon mineralization. In the ocean, an annual rate of methanogenesis of 85-300 Tg $\text{CH}_4 \text{ a}^{-1}$ has been estimated, of which > 90% is consumed by anaerobic oxidation of methane (AOM) (Hinrichs and Boetius, 2002; Reeburgh, 2007). AOM is a major geochemical process that functions as an important sink in oceanic methane geochemistry (Iversen and Jørgensen, 1985; Hinrichs and Boetius, 2002; Nauhaus et al., 2002; Treude et al., 2003). This process is performed by a consortium of methanotrophic archaea and sulfate-reducing bacteria, which gain energy by the following reaction (Hoehler et al., 1994; Hinrichs et al., 1999; Boetius et al., 2000):



So far two groups of anaerobic methanotrophic archaea (ANME-1, ANME-2) have been identified (Hinrichs et al., 1999; Boetius et al., 2000; Orphan et al., 2001; Michaelis et al., 2002; Knittel et al., 2005). They usually occur together with sulfate reducing bacteria (Knittel et al., 2003). Generally, microbial methane oxidation is characterized by a strong discrimination against the heavy, stable carbon isotope ^{13}C , leading to a significant depletion in the ^{13}C -content of metabolites and microbial biomass (Whiticar et al., 1986; Summons et al., 1994; Elvert et al., 1999; Thiel et al., 1999; Whiticar et al., 1999). During the consumption of the isotopically light methane by methanotrophs, a second step of carbon fractionation is involved. Thus, the methane-derived carbon that is incorporated into methanotrophic biomass reveals a very light signal. In the search for the organisms involved in AOM, scientist found methanogen-specific lipids, named crocetane, archeol and hydroxyarchaeol, in active methane seeps (Elvert et al., 1999; Hinrichs et al., 1999; Pancost et al., 2000; Thiel et al., 2001).

I.1.3. Authigenic carbonate precipitation

During AOM, upward migrating methane and downward diffusing sulfate are consumed at the sulfate-methane interface and DIC, predominantly bicarbonate (HCO_3^-), and bisulfide (HS^-) are produced (Reeburgh, 1976, Berner, 1980). This reaction converts methane carbon into HCO_3^- , enriching the pore water DIC pool with ^{13}C depleted carbon and increasing the carbonate alkalinity of the water at the sulfate-methane interface. This alkalinity increase will stimulate the formation of authigenic carbonates at the sulfate-methane interface (e.g. Greinert et al., 2001; Aloisi et al., 2002):



Carbonate chimneys, crusts and concretions commonly form at or near the sea floor in areas of methane seepage (Greinert et al., 2001; Aloisi et al., 2004; Takeuchi et al., 2007). Carbonate horizons in sediment also mark sulfate-methane interfaces in areas of moderate upward methane flux (Aloisi et al., 2004; Berelson et al., 2005). Studies from the well-studied cold vent sites on Hydrate Ridge (Luff and Wallmann, 2003) show that about 10 – 20 % of methane carbon is precipitated in authigenic carbonates while the remaining portion is released into the bottom water as dissolved inorganic carbon. Only at high fluid flow rates ($>10 \text{ cm yr}^{-1}$) a major portion of methane escapes oxidation to be released into the overlying water column. The modeling further revealed that authigenic carbonate crusts form only over a rather narrow range of fluid flow rates (20 – 90 cm yr^{-1}); (Luff et al., 2005; Luff et al., 2004). Lower rates induce the formation of carbonate cements while higher rates lead to the growth of carbonate chimneys in the water column.

The occurrence of high-Mg calcite and low-Mg calcite, aragonite, dolomite and other less common carbonate minerals has been documented by various studies (e.g. Claypool and Kaplan, 1974; Greinert et al., 2001; Greinert and Derkachev, 2004; Orphan et al., 2004). The carbon isotopic composition of these carbonates can vary by as much as 85 ‰, indicating an almost equally wide range of geochemical processes involved in carbonate precipitation. Oxygen isotopes of authigenic carbonates also show considerable variations, documenting the effects of temperature and/or fluid composition on carbonate formation. Regardless of their mineralogical and isotopic composition, however, seep-related authigenic minerals provide an important geological archive, as they represent one of the

few permanent records of fluid flow and seepage activity (Naehr et al., 2000; Martin et al., 2004; Hein et al., 2006).

I.2. Transport processes of methane

Figure 2 is a schematic diagram showing the range of methane fluxes to the ocean water column from a variety of sources, the lateral size-scale of the sources, and an indication of the depth of origin of the methane. The left-hand side of the diagram illustrates diffusion controlled coastal sediments, where methane formed below the sulfate-methane interface is subjected to anaerobic methane oxidation, so that only a small amount escapes to the water column. The middle of the diagram illustrates seeps, where methane from scarps, fractures, and decomposing hydrates is introduced in fluids and as gas streams. This methane has a deeper origin, and fluxes are high enough to overwhelm sediment oxidation processes.

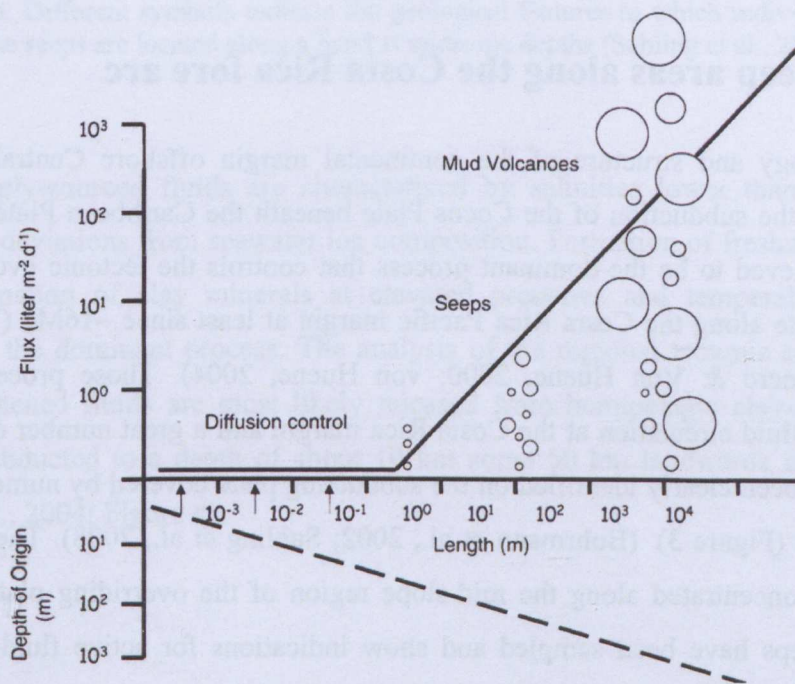


Figure 2. Schematic diagram showing the length, and flux scales of methane additions from a range of sources to the ocean water column (Reeburgh, 2007).

Methane reaches the ocean surface in only a few examples. The right-hand side of the diagram illustrates methane contributions by large seeps and mud volcanoes. Most of the methane emitted from submarine mud volcanoes deeper than 75 m, particularly during quiescent periods, dissolves before it reaches the atmosphere (Dimitrov, 2002). Milkov et al. (2003) estimate that 5000 submarine mud volcanoes release 13 Tg a^{-1} during quiescent periods and 14 Tg a^{-1} during eruptions, and most of this remains in the ocean. The atmospheric flux from mud volcanoes was estimated to be $6\text{--}9 \text{ Tg CH}_4 \text{ a}^{-1}$ (Etiope and Milkov, 2004; Milkov and Etiope, 2005). Eruptive activity is infrequent, but spectacular.

The most recent summary of methane released from geological sources is presented by Kvenvolden and Rogers (2005), who estimate the atmospheric contribution of seeps, mud volcanoes, and miscellaneous sources at $45 \text{ Tg of CH}_4 \text{ a}^{-1}$. However, all the knowledge was gained in different areas and geological settings of the world ocean but left a regional gap in our knowledge about seeps in the W Pacific at the continental margin offshore Costa Rica.

I.3. Cold seep areas along the Costa Rica fore arc

The morphology and structure of the continental margin offshore Central America is controlled by the subduction of the Cocos Plate beneath the Caribbean Plate. Subduction erosion is believed to be the dominant process that controls the tectonic evolution of the overriding plate along the Costa Rica Pacific margin at least since $\sim 16\text{Ma}$ (Vannucchi et al., 2003; Ranero & Von Huene, 2000; von Huene, 2004). Those processes provide pathways for fluid circulation at the Costa Rica margin and a great number of dewatering features have been clearly identified on the subducting plate covered by numerous mound-like structures (Figure 3) (Bohrmann et al., 2002; Sahling et al., 2008). The fluid-escape features are concentrated along the mid-slope region of the overriding plate. Several of these cold seeps have been sampled and show indications for active fluid seepage and emission of methane-rich fluids (Hensen et al., 2004; Linke et al., 2005; Mau et al., 2006) and the occurrence of authigenic carbonates and chemosynthetic communities (Sahling et al., 2008).

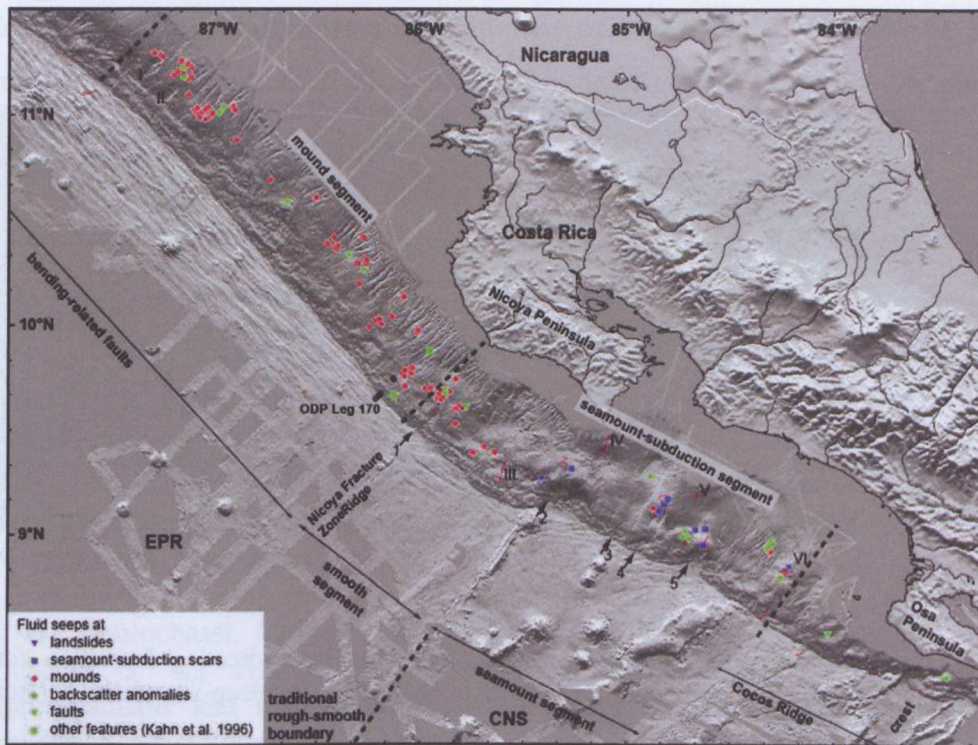


Figure 3. Overview map of locations of 112 methane seeps at the continental margin of Costa Rica and Nicaragua. Different symbols indicate the geological features to which individual fluid seeps are related. The seeps are located along a band at midslope depths (Sahling et al., 2008).

Overall, deeply-sourced fluids are characterized by salinities lower than seawater and conspicuous deviations from seawater ion composition. Formation of freshwater driven by the transformation of clay minerals at elevated pressures and temperatures has been identified as the dominant process. The analysis of the regional tectonic setting revealed that the freshened fluids are most likely released from hemipelagic clay-rich sediments which are subducted to a depth of about 10 km some 50 km landwards from the trench (Hensen et al., 2004; Figure 4).

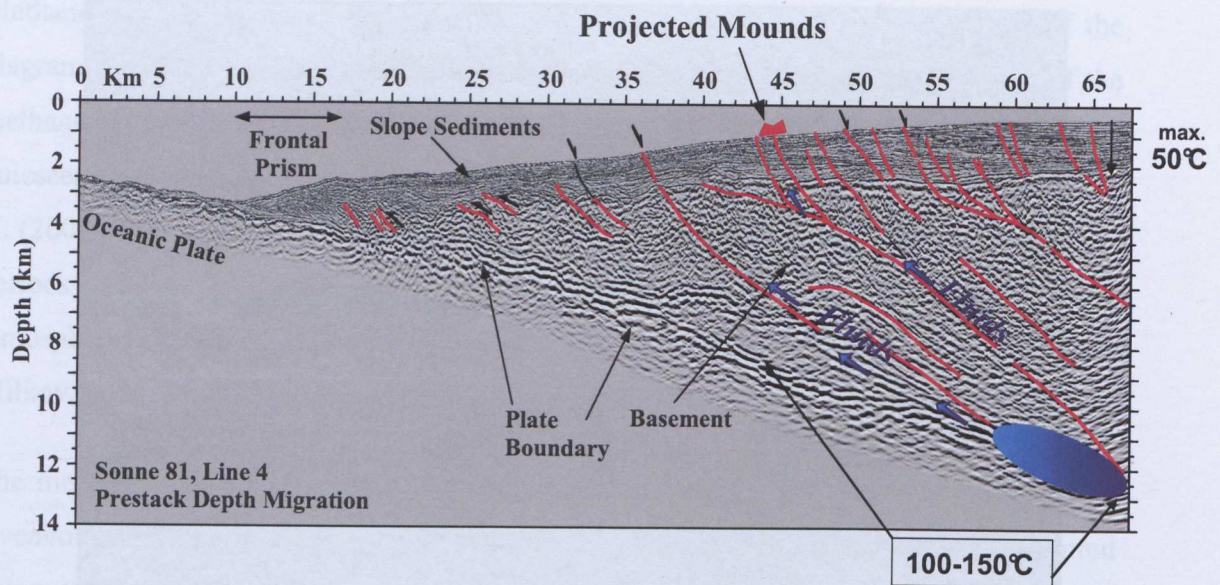


Figure 4. Geological structure along the seismic line SO 81-4 indicating formation zone and pathways (cutting through basement and upper-plate sediments) for deep-seated fluids (Hensen et al., 2004).

I.4. Thesis outline

The following three chapters represent stand-alone articles which have been published or will be submitted for publication in peer-reviewed scientific journals. Each of the Chapters II, III and IV contains a separate introduction, description of methods, presentation of data, results and discussion as well as a separate reference list. Chapter II has already been published in *Geochemistry, Geophysics, Geosystems*; Chapters III and IV will be submitted to peer-reviewed journals and might be subject to revisions.

Chapter II presents comprehensive results from five cold seep structures at the Costa Rican continental margin addressing the relationship between fluid advection, dissolved calcium concentrations in upward migrating fluids, and authigenic calcium carbonate precipitation. A numerical transport-reaction model was used to determine rates of anaerobic oxidation of methane (AOM), CaCO_3 precipitation, and benthic fluxes of solutes. Results reveal the importance of Ca-enriched fluids that potentially offers a reason for enhanced subsurface calcium carbonate precipitation and the occurrence of widespread carbonate caps on top of dewatering structures in the Central American Fore arc.

Chapter III and Chapter IV comprise the quantitative estimates of dissolved methane discharge from well-studied mud mounds and a submarine landslide at the submarine segment of the Costa Rica fore-arc margin. Studies are based on fauna distribution mapping related to methane emission by remotely operated vehicle (ROV) Quest and application of numerical model to estimate the amount of methane that is transported into the bottom water considering AOM, molecular diffusion and upward advection. This approach provides a realistic flux estimate compared to other geochemically and hydroacoustically determined fluxes.

References

- Aloisi, G., Bouloubassi, I., Heijs, S. K., Pancost, R. D., Pierre, C., Damste, J. S. S., Gottschal, J. C., Forney, L. J., and Rouchy, J. M., 2002. CH₄-consuming microorganisms and the formation of carbonate crusts at cold seeps. *Earth and Planetary Science Letters* 203, 195-203.
- Aloisi, G., Wallmann, K., Haese, R., and Saliège, J.-F., 2004. Chemical, biological and hydrological controls on the ¹⁴C content of cold seep carbonate crusts: numerical modeling and implications for convection at cold seeps. *Chemical Geology* 213, 359-383.
- Bates, T. S., Kelly, K. C., Johnson, J. E., and Gammon, R. H., 1996. A reevaluation of the open ocean source of methane to the atmosphere. *Journal of Geophysical Research-Atmospheres* 101, 6953-6961.
- Berelson, W. M., Prokopenko, M., Sansone, F. J., Graham, A. W., McManus, J., and Bernhard, J. M., 2005. Anaerobic diagenesis of silica and carbon in continental margin sediments: Discrete zones of TCO₂ production. *Geochimica et Cosmochimica Acta* 69, 4611-4629.
- Berner, R. A., 1980. *Early diagenesis: A theoretical approach*, Princeton University Press, 241pp., New York.
- Boetius, A., Ravensschlag, K., Schubert, C. J., Rickert, D., Widdel, F., Giesecke, A., Amann, R., Jørgensen, B. B., Witte, U., and Pfannkuche, O., 2000. A marine microbial consortium apparently mediating anaerobic oxidation of methane. *Nature* 407, 623-626.
- Bohrmann, G., Heeschen, K., Jung, C., Weinrebe, W., Baranov, B., Cailleau, B., Heath, R., Hühnerbach, V., Hort, M., Masson, D., and Trummer, I., 2002. Widespread fluid expulsion along the seafloor of the Costa Rica convergent margin. *Terra Nova* 14, 69-79.

- Cicerone, R. J., and Oremland, R.S., 1988. Biogeochemical aspects of atmospheric methane. *Global Biogeochemical Cycles*, 2(4), 299-327.
- Claypool, G. E. and Kaplan, I. R., 1974. The origin and distribution of methane in marine sediments, In: *Natural gases in marine sediments*, 99-139.
- de Beer, D., Sauter, E., Niemann, H., Kaul, N., Foucher, J. P., Witte, U., Schluter, M., and Boetius, A., 2006. In situ fluxes and zonation of microbial activity in surface sediments of the Hakon Mosby Mud Volcano. *Limnology and Oceanography* 51, 1315-1331.
- D'Hondt, S., Rutherford, S., and Spivack, A. J., 2002. Metabolic activity or subsurface life in deep-sea sediments. *Science*, 295, 2067-2070.
- Dickens, G. R., 2003. Rethinking the global carbon cycle with a large, dynamic and microbially mediated gas hydrate capacitor. *Earth Planet. Sci. Lett.* 213, 169-183.
- Dimitrov, L. I., 2002. Mud volcanoes - the most important pathway for degassing deeply buried sediments. *Earth-Sci. Rev.* 59, 49-76.
- Elvert, M., Suess, E., and Whiticar, M. J., 1999. Anaerobic methane oxidation associated with marine gas hydrates: superlight C-isotopes from saturated and unsaturated C-20 and C-25 irregular isoprenoids. *Naturwissenschaften* 86, 295-300.
- Etioppe, G. and Milkov, A. V., 2004. A new estimate of global methane flux from onshore and shallow submarine mud volcanoes to the atmosphere. *Environmental Geology* 46, 997-1002.
- Greinert, J., Bohrmann, G., and Suess, E., 2001. Gas hydrate-associated carbonates and methane-venting at Hydrate Ridge: classification, distribution, and origin of authigenic lithologies. *Geophy. Monograph* 124, 99-113.
- Greinert, J. and Derkachev, A., 2004. Glendonites and methane-derived Mg-calcites in the Sea of Okhotsk, Eastern Siberia: implications of a venting-related ikaite/glendonite formation. *Mar. Geol.* 204, 129-144.
- Heeschen, K. U., Trehu, A. M., Collier, R. W., Suess, E., and Rehder, G., 2003. Distribution and height of methane bubble plumes on the Cascadia Margin characterized by acoustic imaging. *Geophysical Research Letters* 30.
- Hein, J. R., Normark, W. R., McIntyre, B. R., Lorenson, T. D., and Powell, C. L., 2006. Methanogenic calcite, C-13-depleted bivalve shells, and gas hydrate from a mud volcano offshore southern California. *Geology* 34, 109-112.
- Hensen, C. and Wallmann, K., 2004. Methane fluxes and gas hydrate reservoirs in slope sediments along Costa Rica continental margin EGU, Nice, France.
- Hinrichs, K. U. and Boetius, A., 2002. The anaerobic oxidation of methane: new insights in microbial ecology and biogeochemistry. In: G. Wefer, D. Billett, D. Hebbeln et al (Eds), *Ocean Margin Systems*. Springer-Verlag, Berlin, pp 457-477.

- Hinrichs, K. U., Hayes, J. M., Sylva, S. P., Brewer, P. G., and DeLong, E. F., 1999. Methane-consuming archaeobacteria in marine sediments. *Nature* 398, 802-805.
- Hoehler, T. M., Alperin, M. J., Albert, D. B., and Martens, C. S., 1994. Field and laboratory studies of methane oxidation in an anoxic marine sediment: Evidence for a methanogen-sulfate reducer consortium. *Global Biogeochem. Cycles* 8, 451-463.
- Hornafius, J. S., Quigley, D., and Luyendyk, B. P., 1999. The world's most spectacular marine hydrocarbon seeps (Coal Oil Point, Santa Barbara Channel, California): Quantification of emissions. *Journal of Geophysical Research-Oceans* 104, 20703-20711.
- Hovland, M., Judd, A. G., and Burke, J. R. A., 1993. The global flux of methane from shallow submarine sediments. *Chemosphere* 26, 559-578.
- Iversen, N. and Jørgensen, B. B., 1985. Anaerobic methane oxidation rates at the sulfate-methane transition in marine sediments from Kattegat and Skagerrak (Denmark). *Limnol. Oceanogr.* 30, 944-955.
- Jørgensen, B. B., 1982. Mineralization of organic matter in the sea bed - the role of sulphate reduction. *Nature* 296, 643-645.
- Jørgensen, B. B. and Bak, F., 1991. Pathways and microbiology of thiosulfate transformation and sulfate reduction in a marine sediment (Kattegat, Denmark). *Applied and Environmental Microbiology* 57, 847-856.
- Jørgensen, B. B. and Kasten, S., 2006. Sulfur Cycling and Methane Oxidation. In: *Marine Geochemistry*; (Eds) Shulz, H.D. and Zabel, M., Springer Verlag, Berlin, pp. 271-309.
- Judd, A. G., Hovland, M., Dimitrov, L. I., Gil, S. G., and Jukes, V., 2002. The geological methane budget at continental margins and its influence on climate change. *Geofluids* 2, 109-126.
- Kiene, R. P., 1991. In: *Microbial Production and Consumption of Greenhouse Gases: Methane, Nitrogen Oxides, Halomethanes*; (Eds) Rogers, J.E., Whitman, W.B., American Society for Microbiology; Washington Dc, pp 111-146.
- Knittel, K., Boetius, A., Lemke, A., Eilers, H., Lochte, K., Pfannkuche, O., Linke, P., and Amann, R., 2003. Activity, distribution, and diversity of sulfate reducers and other bacteria in sediments above gas hydrate (Cascadia margin, Oregon). *Geomicrobiology Journal* 20, 269-294.
- Knittel, K., Losekann, T., Boetius, A., Kort, R., and Amann, R., 2005. Diversity and distribution of methanotrophic archaea at cold seeps. *Applied and Environmental Microbiology* 71, 467-479.
- Kvenvolden, K. A., 1988. Methane hydrates-a major reservoir of carbon in the shallow geosphere? *Chemical Geology* 71, 41-51.

- Kvenvolden, K. A., 1993. Gas hydrates-geological perspective and global change. *Rev. Geophys.* 31, 173-188.
- Kvenvolden, K. A., 2002. Methane hydrate in the global organic carbon cycle. *Terra Nova* 14, 302-306.
- Kvenvolden, K. A. and Rogers, B. W., 2005. Gaia's breath--global methane exhalations. *Marine and Petroleum Geology* 22, 579-590.
- Linke, P., Wallmann, K., Suess, E., Hensen, C., and Rehder, G., 2005. In-situ benthic fluxes from an intermittently active mud volcano at the Costa Rica convergent margin. *Earth and Planetary Science Letters* 235, 79-95.
- Luff, R., Greinert, J., Wallmann, K., Klauke, I., and Suess, E., 2005. Simulation of long-term feedbacks from authigenic carbonate crust formation at cold vent sites. *Chemical Geology* 216, 157-174.
- Luff, R. and Moll, A., 2004. Seasonal dynamics of the North Sea sediments using a three-dimensional coupled sediment-water model system. *Cont. Shelf Res.* 24, 1099-1127.
- Luff, R. and Wallmann, K., 2003. Fluid flow, methane fluxes, carbonate precipitation and biogeochemical turnover in gas hydrate-bearing sediments at Hydrate Ridge, Cascadia Margin: Numerical modeling and mass balances. *Geochim. Cosmochim. Acta* 67, 3403-3421.
- Martens, C. S. and Berner, R. A., 1974. Methane Production in the Interstitial Waters of Sulfate-Depleted Marine Sediments. *Science* 185, 1167 - 1169.
- Martin, J. B., Day, S. A., Rathburn, A. E., Perez, M. E., Mahn, C., and Gieskes, J., 2004. Relationships between the stable isotopic signatures of living and fossil foraminifera in Monterey Bay, California. *Geochemistry Geophysics Geosystems* 5.
- Mau, S., Sahling, H., Rehder, G., Suess, E., Linke, P., and Soeding, E., 2006. Estimates of methane output from mud extrusions at the erosive convergent margin off Costa Rica. *Mar. Geol.* 225, 129-144.
- McIver, R. (1975). Hydrocarbon occurrences from JODIES Deep Sea Drilling Project, Proceedings of the 9th World Petroleum Congress (Tokyo), 2, Applied Science Publishers, Barking, pp. 269-280
- Michaelis, W., Seifert, R., Nauhaus, K., Treude, T., Thiel, V., Blumenberg, M., Knittel, K., Gieseke, A., Peterknecht, K., Pape, T., Boetius, A., Amann, R., Jørgensen, B. B., Widdel, F., Peckmann, J., Pimenov, N. V., and Gulin, M. B., 2002. Microbial reefs in the Black Sea fueled by anaerobic oxidation of methane. *Science* 297, 1013-1015.
- Milkov, A. V. (2004), Global estimates of hydrate-bound gas in marine sediments: How much is really out there?, *Earth Sci. Rev.*, 66, 183-197.

- Milkov, A. V. and Etiope, G., 2005. Global methane emission through mud volcanoes and its past and present impact on the Earth's climate—a comment. *International Journal of Earth Sciences* 94, 490-492.
- Milkov, A. V., Sassen, R., Apanasovich, T. V., and Dadashev, F. G., 2003. Global gas flux from mud volcanoes: A significant source of fossil methane in the atmosphere and the ocean. *Geophysical Research Letters* 30.
- Naehr, T. H., Stakes, D. S., and Moore, W. S., 2000. Mass wasting, ephemeral fluid flow, and barite deposition on the California continental margin. *Geology* 28, 315-318.
- Nauhaus, K., Boetius, A., Kruger, M., and Widdel, F., 2002. In vitro demonstration of anaerobic oxidation of methane coupled to sulphate reduction in sediment from a marine gas hydrate area. *Environmental Microbiology* 4, 296-305.
- Orphan, V. J., House, C. H., Hinrichs, K. U., McKeegan, K. D., and DeLong, E. F., 2001. Methane-consuming archaea revealed by directly coupled isotopic and phylogenetic analysis. *Science* 293, 484-487.
- Orphan, V. J., Ussler, W., Naehr, T. H., House, C. H., Hinrichs, K. U., and Paull, C. K., 2004. Geological, geochemical, and microbiological heterogeneity of the seafloor around methane vents in the Eel River Basin, offshore California. *Chemical Geology* 205, 265-289.
- Pancost, R. D., Damste, J. S. S., de Lint, S., van der Maarel, M., and Gottschal, J. C., 2000. Biomarker evidence for widespread anaerobic methane oxidation in Mediterranean sediments by a consortium of methanogenic archaea and bacteria. *Applied and Environmental Microbiology* 66, 1126-1132.
- Prather, M. J., Derwent, R., Ehhalt, D., Fraser, P., Sanhueza, E., and Zhou, X., 1995. Other trace gases and atmospheric chemistry. In: Houghton, J.T., Meira-Filho, L.G., Bruce, J.P., Lee, H., Callander, B.A., Haites, E.F., Harris, N., Mashell, K. (Eds.), *Climate Change* (1994). Cambridge University Press, UK, pp. 73–126.
- Rabus, R., Hansen, T., and Widdel, F., 2004. Dissiliatory Sulfate-and Sulfur Reducing Prokaryotes. In: Dworkin, M. et al. (Eds), *The Prokaryotes: An Evolving Electric Resource for the Microbiology Community*, 3rd edition, Springer-Verlag, New York, (<http://springer-ny.com/link/service/books/10125/>).
- Ranero, C. R. and Von Huene, R., 2000. Subduction erosion along the Middle America convergent margin. *Nature* 404, 748-752.
- Reeburgh, W. S., 1976. Methane consumption in Cariaco Trench waters and sediments. *Earth and Planetary Science Letters* 28, 337 - 344.
- Reeburgh, W. S., 2007. Oceanic methane biogeochemistry. *Chemical Reviews* 107, 486-513.
- Rudd, J. W. M. and Taylor, C. D., 1980. *Advance Aquatic Microbiology*, 2, 77.

- Rullkötter, J. (2006). Organic Matter: The Driving Force for Early Diagenesis. In: *Marine Geochemistry*; (Eds) Shulz, H.D. and Zabel, M. 125-168, Springer Verlag, Berlin.
- Sahling, H., Masson, D. G., Ranero, C. R., Hühnerbach, V., Weinrebe, W., Klauke, I., Bürk, D., Brückmann, W., and Suess, E., 2008. Fluid seepage at the continental margin offshore Costa Rica and southern Nicaragua. *G-cubed* 9.
- Sauter, E. J., Muyakshin, S. I., Charlou, J.-L., Schlüter, M., Boetius, A., Jerosch, K., Damm, E., Foucher, J.-P., and Klages, M., 2006. Methane discharge from a deep-sea submarine mud volcano into the upper water column by gas hydrate-coated methane bubbles. *Earth and Planetary Science Letters* 243, 354-365.
- Stetter, K. O., Huber, R., Blochl, E., Kurr, M., Eden, R. D., Fielder, M., Cash, H., and Vance, I., 1993. Hyperthermophilic Archaea Are Thriving in Deep North-Sea and Alaskan Oil-Reservoirs. *Nature* 365, 743-745.
- Summons, R. E., Jahnke, L. L., and Roksandic, Z., 1994. Carbon Isotopic Fractionation in Lipids from Methanotrophic Bacteria - Relevance for Interpretation of the Geochemical Record of Biomarkers. *Geochimica Et Cosmochimica Acta* 58, 2853-2863.
- Takeuchi, R., Matsumoto, R., Ogihara, S., and Machiyama, H., 2007. Methane-induced dolomite "chimneys" on the Kuroshima Knoll, Ryukyu Islands, Japan. *Journal of Geochemical Exploration* 95, 16-28.
- Thiel, V., Peckmann, J., Richnow, H. H., Luth, U., Reitner, J., and Michaelis, W., 2001. Molecular signals for anaerobic methane oxidation in Black Sea seep carbonates and a microbial mat. *Marine Chemistry* 73, 97-112.
- Thiel, V., Peckmann, J., Seifert, R., Wehrung, P., Reitner, J., and Michaelis, W., 1999. Highly isotopically depleted isoprenoids: Molecular markers for ancient methane venting. *Geochim. Cosmochim. Acta* 63, 3959-3966.
- Treude, T., Boetius, A., Knittel, K., Wallmann, K., and Jørgensen, B. B., 2003. Anaerobic oxidation of methane above gas hydrates. *Mar. Ecol. Prog. Ser.* 264, 1-14.
- Vannucchi, P., Ranero, C. R., Galeotti, S., Straub, S. M., Scholl, D. W., and McDougall-Ried, K., 2003. Fast rates of subducting erosion along the Costa Rica Pacific margin: Implications for nonsteady rates of crustal recycling at subduction zones. *Journal of Geophysical Research* 108, doi:10.1029/2002JB002207.
- von Huene, R., Ranero, C. R., and Watts, P., 2004. Tsunamigenic slope failure along the Middle America Trench in two tectonic settings. *Mar. Geol.* 203, 303-317.
- Wallmann, K., Drews, M., Aloisi, G., and Bohrmann, G., 2006. Fluid expulsion from the Dvurechenskii mud volcano (Black Sea): Part II. Methane fluxes and new estimates of global methane discharge into the ocean via submarine mud volcanism. *Earth and Planetary Science Letters* 248, 544-559.

- Walter, K. M., Zimov, S. A., Chanton, J. P., Verbyla, D., and Chapin, F. S., 2006. Methane bubbling from Siberian thaw lakes as a positive feedback to climate warming. *Nature* 443, 71-75.
- Whiticar, M. J., 1999. Carbon and hydrogen isotope systematics of bacterial formation and oxidation of methane. *Chemical Geology* 161, 291-314.
- Whiticar, M. J., 1996. Isotope tracking of microbial methane formation and oxidation. *Mitt.Internat. Verein.Limnol.*, 25, 39-54.
- Whiticar, M. J., Faber, E., and Schoell, M., 1986. Biogenic methane formation in marine and freshwater environments: CO₂ reduction vs. acetate fermentation-Isotope evidence. *Geochimica et Cosmochimica Acta* 50, 693-709

Abstract

Five sediment cores from cold seeps at the margin off Costa Rica were used to explore the relationship between fluid advection, dissolved Ca concentrations in upward migrating fluids, and authigenic CaCO₃ precipitation. A numerical reactive-transport model was used to determine rates of anaerobic oxidation of methane (AOM), CaCO₃ precipitation, and benthic fluxes of solutes. Production of carbonate authigenicity and formation of authigenic carbonates is most intense at intermediate flow rates (1–10 cm a⁻¹) and reduced under low and high flow conditions (0.1 and 200 cm a⁻¹). Dissolved Ca concentrations observed in the vent fluids off Costa Rica cover a wide range (0.05–4.31 mM), clearly exceeding seawater concentrations at two locations. Systematic model runs showed that high Ca concentrations in ascending fluids enhance the rate of authigenic carbonate production at moderate flow rates leading to an upward migration of deeply derived Ca in

Chapter II

Controls on authigenic carbonate precipitation at cold seeps along the convergent margin off Costa Rica

Deniz Karaca^{1*}, Christian Hensen^{1,2}, Klaus Wallmann^{1,2}

¹Sonderforschungsbereich 574, IFM-GEOMAR, Wischhofstraße 1-3, D-24148 Kiel, Germany

²Leibniz-Institute of Marine Sciences, IFM-GEOMAR, Wischhofstraße 1-3, D-24148 Kiel, Germany

Published in 2010, *Geochemistry, Geophysics, Geosystems*, 11, Q08S27,

doi:10.1029/2010GC003062

Abstract

Five sediment cores from cold seeps at the forearc off Costa Rica were used to explore the relationship between fluid advection, dissolved Ca concentrations in upward migrating fluids, and authigenic CaCO₃ precipitation. A numerical transport-reaction model was used to determine rates of anaerobic oxidation of methane (AOM), CaCO₃ precipitation, and benthic fluxes of solutes. Production of carbonate alkalinity and formation of authigenic carbonates is most intense at intermediate flow rates (3–40 cm a⁻¹) and reduced under low and high flux conditions (0.1 and 200 cm a⁻¹). Dissolved Ca concentrations observed in the vent fluids off Costa Rica cover a wide range between 4–31 mM, clearly exceeding seawater concentrations at two locations. Systematic model runs showed that high Ca concentrations in ascending fluids enhance the rate of authigenic carbonate production at moderate flow rates leading to an almost quantitative fixation of deeply derived Ca in

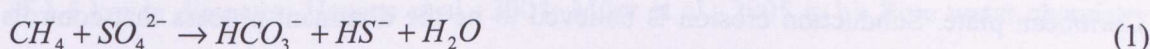
authigenic carbonates. Hence, CaCO_3 precipitation is not only controlled by Ca diffusing into the sediment from bottom water, but also by the Ca concentration in ascending fluids. Thus, Ca enriched fluids offer a reason for enhanced subsurface CaCO_3 precipitation and the occurrence of carbonate caps on dewatering structures in the Central American fore-arc. Based on average precipitation rates deduced from the systematic model runs it is possible to give a rough estimate of the global Ca-fixation at cold seeps ($\sim 2 \cdot 10^{10} \text{ mol Ca a}^{-1}$), which suggests that cold seeps are most likely not of key importance with respect to Ca cycling in the ocean.

* Corresponding author (D. Karaca). Fax: +49 431 6002928. E-mail address: dkaraca@ifm-geomar.de

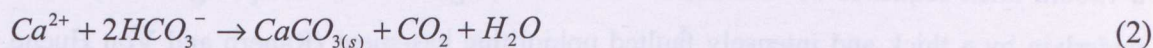
II.1. Introduction

Cold seeps are ubiquitous features along active convergent margins and are direct links between deeply buried sediments and the global ocean reservoir. Hence, they provide insight into deep geochemical and structural processes (e.g. Martin et al., 1996; Aloisi et al., 2004; Hensen et al., 2004). Usually, emanating fluids are highly enriched in methane from deeper horizons that fuels microbial oxidation processes and abundant growth of chemosynthetic communities in near-surface sediments (e.g. Boetius and Suess, 2004; Boetius et al., 2000; Wallmann et al., 1997). Since methane is a potent greenhouse gas, it is important to know how much of this gas reaches the bottom water.

Much of the dissolved methane that ascends to the sediment surface is consumed by a consortium of bacteria and archaea performing the anaerobic oxidation of methane (AOM). Methane is oxidized by pore water sulfate releasing hydrogen sulfide and bicarbonate into the pore water:



Authigenic carbonates may precipitate due to production of inorganic carbon and alkalinity during AOM.



TA increase related to AOM favors the accumulation of authigenic carbonates in pore space and fluid channels if sedimentation and bioturbation rates are low (Luff et al., 2004). Cold-vent carbonates may occur as centimeter-to-decimeter thick crusts or void-filling chimneys formed at shallow depth in the sediment, where intense AOM and, hence, carbonate super saturation prevail (Han et al., 2004).

Numerical experiments by Luff and Wallmann (2003) have shown that the flux of methane, and hence the location of the AOM zone are largely controlled by upward fluid flow velocities. At higher methane fluxes, the depth of the AOM zone is shifted upward (Borowski et al., 1996) and thereby reducing the effectiveness of alkalinity removal by calcium carbonate precipitation.

For the present study, we used the numerical model C.CANDI (Luff et al., 2000) to investigate the main biogeochemical processes at cold vents off Costa Rica. The purpose of our study was to quantify AOM-rates and benthic fluxes as well as to constrain key parameters, which determine vent-driven CaCO_3 precipitation under these specific environmental conditions. Since calcium concentrations in the upward migrating fluids are well above seawater levels at some of the investigated dewatering sites, Ca-enriched fluids potentially offer a reason for enhanced subsurface calcium carbonate precipitation and the occurrence of widespread carbonate caps on top of dewatering structures in the Central American Fore arc. We present comprehensive results from five cold seep locations at the Costa Rican continental margin in order to address the relationship between fluid advection, calcium concentrations, and authigenic calcium carbonate precipitation.

II.2. Study Area

At the Pacific continental margin off Costa Rica, the Cocos Plate subducts beneath the Caribbean plate. Subduction erosion is believed to be the dominant process that controls the tectonic evolution along the Costa Rica Pacific margin since at least ~16Ma (Vannucchi et al., 2003). The overriding plate is covered by numerous mound-like structures at water depths between 500 and 2500m. These structures are situated on top of a 1500m thick sequence of siliciclastic sediments (organic-rich, hemipelagic mud) that is underlain by a thick and intensely faulted ophiolitic basement (Ranero and Von Huene, 2000). Overpressuring of subducted sediments due to clay mineral dehydration and subsequent upward migration of released fluids is thought to significantly affect fluid flow in upper plate sediments, and hence the formation of cold seeps (Hensen et al., 2004; Ranero et al. 2008). More than 100 of these typical dewatering features have been clearly identified up to date (Ranero et al., 2008; Sahling et al., 2008; Fig. 1). Commonly they are referred to as mounds since no clear categorization into structural types such as mud volcanoes or mud diapirs has been accomplished. In many cases the surface of the mounds is covered by crusts, boulders or pavements of authigenic carbonates.

Our study is based on five sediment cores taken from four locations, Mound 11, Quepos Slide, Pockmark and Culebra Fault, which were surveyed on R/V Meteor and Sonne expeditions between 2002 and 2005 (M54; M66; SO173) (Tab 1; Fig. 1). Below, we give a

brief summary of the sampling sites: (1) Mound 11, where station M54-138 is located on, is a fluid escape structure situated 30 km arcward from the trench on the mid slope off Costa Rica at around 1000 m water depth. It is characterized by strong venting activity of methane-rich fluids and by the occurrence of gas hydrate deposits in surface sediments (Hensen et al., 2004; Schmidt et al., 2005; Linke et al., 2005) and is partly covered by carbonate crusts and bacterial mats (Bohrmann et al., 2002). (2) Stations SO173-63 and SO173-73 are from Quepos Slide, which is located close to Mound 11 at shallower water depth (400 m). Quepos Slide is a submarine slide, which is possibly related to intense fluid emanation. Much of the area below the head wall is densely covered by bacterial mats. (3) Station M66-PC30 is situated on Pockmark which describes a flat structure with a total diameter of about 400m and a slightly elevated rim (a few meters in height) on the lower slope at about 1900m water depth. A well developed crater wall is covered by bacterial mats indicating the release of methane-rich fluids (Brückmann et al, 2009). (4) Station SO173-49 (Culebra Fault) is situated on a normal fault at 1500 m water depth. The fault crops out at the seafloor close to Mound Culebra (a large-scale, carbonate-capped Mound of 1.5 km in diameter; Hensen et al., 2004; Mörz et al., 2005 a, b). Pore water chemistry from all five dewatering sites shows that fluids are significantly depleted with respect to seawater chloride and other major elements, suggesting that fresh water addition by clay mineral dewatering (Hensen et al., 2004) is a driving force of overpressuring and fluid advection.

Table 1. Details of sampling sites included in this study and list of selected reference cores within the working area.^a

Station	Core	Gear	Region	Latitude (°N)	Longitude (°W)	Water depth (m)	Research Vessel	CaCO ₃ (wt.%)
1	M54-138	TV-MUC	Mound 11	8°55.35'	84°18.23'	1024	R/V Meteor	22.64
2	SO173-63	TV-MUC	Quepos Slide	8°51.11'	84°13.08'	406	R/V Sonne	15.71
3	SO173-73	TV-MUC	Quepos Slide	8°51.06'	84°13.12'	404	R/V Sonne	21.23
4	M66/D78-PC30	PC	Pockmark	8°55.37'	84°18.23'	1917	R/V Meteor	17.78
5	SO173-49	GC	Culebra Fault	10°15.94'	86°16.60'	1530	R/V Sonne	11.54
Reference cores								
	M54-9	TV-MUC	-	11°20.11'	87°18.26'	1184	R/V Meteor	7.56
	M54-41/2	TV-MUC	-	9°49.00'	86°02.67'	2422	R/V Meteor	1.36
	M54-81/2	TV-MUC	-	9°09.19'	84°41.99'	932	R/V Meteor	3.80

^a CaCO₃ concentrations at the sediment surface are higher at the seep sites compared to the reference cores, and indicate authigenic carbonate precipitation. Reference cores represent the pelagic CaCO₃ input, which is used as the upper boundary condition for all subsequent model runs.

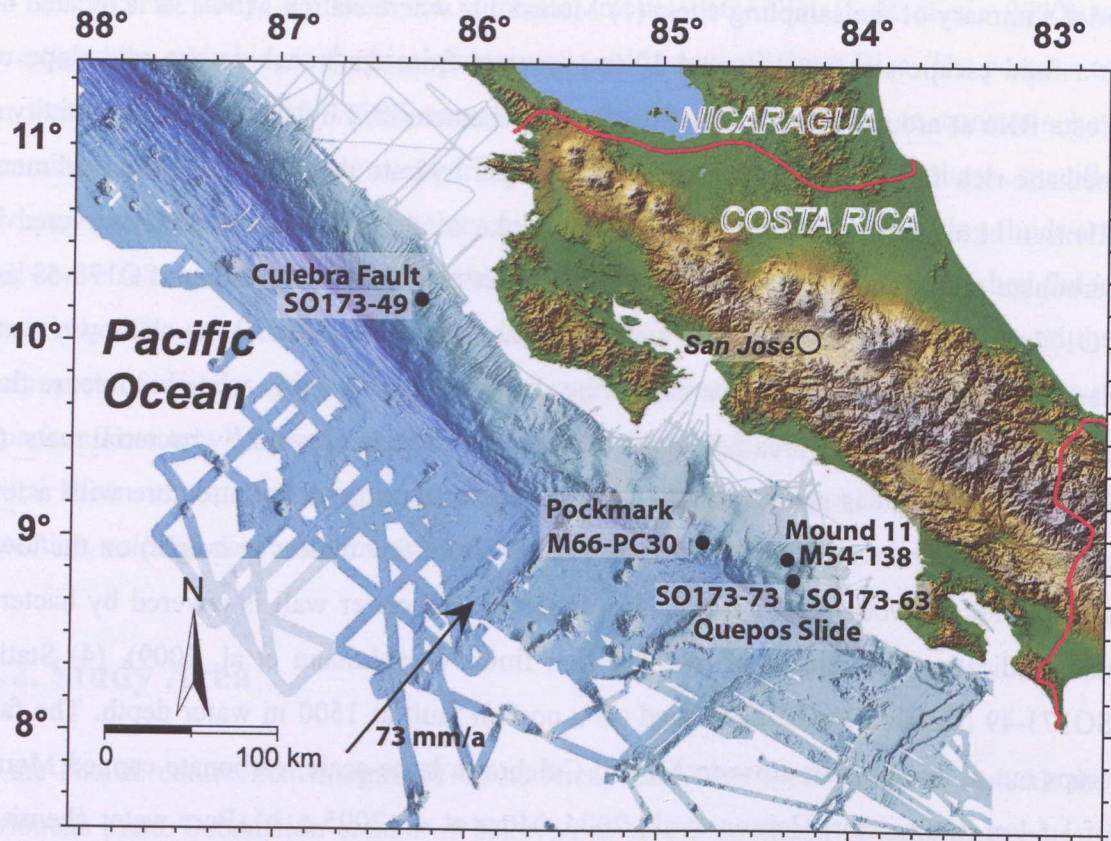


Figure 1. Location map of coring stations offshore Costa Rica.

II.3. Sampling Techniques and Chemical Analysis

Pore water and sediment samples for this study were obtained on cruises M54, SO173, and M66 in 2002, 2003 and 2005, respectively, using TV-guided multi-corers (TV-MUC), ROV-directed push coring (ROV) and a gravity corer (GC) onboard RVs Meteor and Sonne (Tab 1). TV-MUC and ROV were deployed at bacterial mat sites. All cores were transferred in a cooling room in order to maintain in situ temperatures of about 4° C and cut into slices of up to 1 cm resolution. Pore water recovery was done by pressure filtration (argon gas, 2-5 bar). Pore waters were filtered through 0.2 μm cellulose-acetate membrane filters and then divided into aliquots for shipboard and shore-based analyses. Sub-samples for dissolved cation analysis were acidified (HCl or HNO₃, suprapur) to prevent any mineral precipitation or adsorption. The pore waters were analyzed onboard for dissolved ammonia, hydrogen sulfide, chloride, sulfate, methane, and total alkalinity (TA) within a few hours after recovery. Total dissolved sulfide (TH₂S) was measured using a standard

photometric procedure (Grasshoff et al., 1997). TA measurements were done by titration (Ivanenkov and Lyakhin, 1978) immediately after pore water separation. Chlorinity was determined by ion chromatography (761 IC-Compact, Metrohm) or titration with 0.01 N AgNO_3 (Grasshoff et al., 1997). Sulfate analyses were carried out by ion chromatography. Ammonium was analyzed photometrically applying the indophenol-blue method (Grasshoff et al., 1997). Ca analyses were carried out in the shore-based laboratory by inductively coupled plasma optical emission spectrometry (ICP-OES, JY 170 Ultrace, Jobin Yvon). The analytical precision with respect to IAPSO seawater standard is generally <5 % for all methods. For headspace analyses of methane 3 ml of sediment were immediately taken in syringes with the needle-ends cut off, extruded into 20 ml vials and suspended in 5 ml 1 M NaOH to avoid biological degradation. The vials were immediately sealed and shaken for 24 h to establish headspace equilibrium. 100 μl sub-samples of the gas phase were taken by gas-tight syringes and detected with a gas chromatograph (Shimadzu), equipped with a Haysep D column and a flame ionization detector. A 1% CH_4 standard was used. Precision of gas chromatography was $\pm 5\%$.

Total organic carbon was determined by flash combustion of freeze-dried and ground sediment using a Carlo Erba element analyzer (NA1500) with a relative standard deviation of about 1% for replicate measurements. Porosity was calculated from the water content, which was determined by freeze-drying of wet samples assuming a dry solid density of 2.5 g cm^{-3} . More detailed information on sampling techniques and analysis are given in Wallmann et al. (2006a) and are available at <http://www.ifm-geomar.de/index.php?id=1858&L=1>.

II.4. Model Description and Methodology

The reactive-transport model C.CANDI (Luff et al., 2000) was applied to quantitatively study biogeochemical processes at the sample locations. The model was used to simulate the turnover of 10 dissolved and 2 solid species in the sediment and the pore water (SO_4 , TNH_4 , CH_4 , HS, H_2S , HCO_3 , CO_3 , CO_2 , Cl, Ca, CaCO_3 (aragonite), CaCO_3 (calcite)) considering pore water advection, molecular diffusion, bioturbation and biogeochemical reactions. Primary and secondary redox reactions, precipitation and dissolution reactions, as well as thermodynamically controlled acid/base reactions were taken into account while pH calculations were performed using the advancement approach (see Luff et al., 2000 and

Luff and Wallmann, 2003 for a more detailed model description). In general, the model solves the following two equations after Berner (1980) for dissolved (3) and solid (4) species:

$$\phi \frac{\partial C_w}{\partial t} = \frac{\partial}{\partial x} \left(\phi(x) D(x) \frac{\partial C_w}{\partial x} \right) - \frac{\partial}{\partial x} (v(x) \phi(x) C_w) + \phi(x) \sum R_w \quad (3)$$

$$(1 - \phi) \frac{\partial C_s}{\partial t} = \frac{\partial}{\partial x} \left((1 - \phi(x)) D_B(x) \frac{\partial C_s}{\partial x} \right) - \frac{\partial}{\partial x} \left(\omega(x) (1 - \phi(x)) \frac{\partial C_s}{\partial x} \right) + (1 - \phi(x)) \sum R_s \quad (4)$$

where C_w is the concentration of dissolved species (mmol cm^{-3}), C_s is the concentration of solids in dry sediment (wt.%), $D(x)$ is the molecular diffusion coefficient corrected for tortuosity ($\text{cm}^2 \text{a}^{-1}$), $D_B(x)$ is the bioturbation coefficient ($\text{cm}^2 \text{a}^{-1}$), $v(x)$ is the pore water velocity (cm a^{-1}), $\omega(x)$ is burial velocity (cm a^{-1}), Φ is the porosity, and $\sum R_w$ ($\mu\text{mol cm}^{-3} \text{a}^{-1}$) and $\sum R_s$ (in wt %) are the rates of all diagenetic reactions affecting dissolved and solid species, respectively. Sediment compaction and the down-core decrease in porosity were considered applying an exponential function fitted to the porosity data:

$$\phi = (\phi_0 - \phi_\infty) * \text{Exp}(-\text{const} \cdot x) + \phi_\infty \quad (5)$$

where ϕ_∞ and ϕ_0 are the porosity at infinite depth and at sediment surface, and const is the attenuation coefficient for the exponential decrease of porosity with depth. The upward flow velocity v_0 was determined by fitting the model (fit by eye) to the dissolved chloride profiles. The upward directed pore water flux is composed of the downward burial component modified by compaction and the upward fluid advection:

$$v(x) = \frac{\omega_\infty \cdot \phi_\infty - v_0 \cdot \phi_0}{\phi(x)} \quad (6)$$

where $v(x)$ represents the depth-dependent fluid flow velocity (in cm a^{-1}) and v_0 is the surface value of the fluid flow velocity (in cm a^{-1}). Burial of solids is expressed as steady-state compaction with:

$$\omega(x) = \frac{(1 - \phi_\infty) \cdot \omega_\infty}{(1 - \phi(x))} \quad (7)$$

where $\omega(x)$ represents the depth-dependent burial velocity (in cm a^{-1}) and ω_∞ is the sedimentation rate at the lower boundary in cm a^{-1} . The average sedimentation rate for the studied section of the Costa Rica continental margin was previously determined as $\omega_\infty = 0.03 \text{ cm a}^{-1}$ (Kutterolf et al., 2008). Temperature-dependent molecular diffusion coefficients of dissolved species were calculated after Boudreau (1997) and corrected for porosity decrease:

$$D_s(x) = \frac{D_0(x)}{1 - \ln(\phi(x))^2} \quad (8)$$

where D_0 is the molecular diffusion coefficient in seawater in $\text{cm}^2 \text{ a}^{-1}$. Since bioturbation coefficients were not determined at the studied sites, the $D_B(x)$ values given in Luff and Wallmann (2003) were applied for the modeling.

The precipitation rates (R_{PPT}) of calcite and aragonite depend on saturation state and the kinetic constant (k_{PPT}) either for aragonite or calcite:

$$R_{PPT} = k_{PPT} \left(\frac{[Ca^{2+}][CO_3^{2-}]}{K_{SP}} - 1 \right) \quad (9)$$

Values for k_{PPT} were taken from Luff and Wallmann (2003) and are listed in Table 3. In the model, the degree of saturation (Ω) at the lower boundary is a sensitive parameter controlled by the ion concentration product $[Ca^{2+}][CO_3^{2-}]$ and the stoichiometric equilibrium constant (K_{SP}) defining aragonite or calcite solubility:

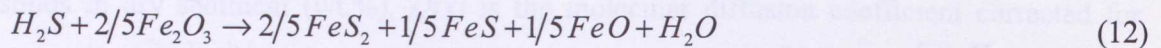
$$\Omega = \frac{[Ca^{2+}][CO_3^{2-}]}{K_{SP}} \quad (10)$$

For all standard runs it was assumed that upward migrating fluids are saturated with respect to calcite at the lower boundary of the model column. The rate of anaerobic methane oxidation was calculated using second order kinetics:

$$R_{AOM} = k_{AOM} [CH_4] [SO_4^{2-}] \quad (11)$$

The kinetic constant of AOM (k_{AOM}) was determined by fitting the model to the pore water profiles of sulfate, TA, and hydrogen sulfide.

Dissolved sulfide may be removed from pore waters by the precipitation of iron sulfide minerals. The following stoichiometry was assumed for sulfide precipitation processes where sulfide is fixed in pyrite (FeS_2) and iron mono sulfides (FeS) (Wallmann et al., 2008):



This equation also considers the reduction of ferric iron in clay minerals, i.e. the conversion of Fe_2O_3 into FeO . This formulation implies that dissolved sulfide removal has no effect on the TA. Precipitation kinetics of sulfidic minerals were simulated applying the following equation assuming that the availability of reactive ferric iron is decreasing exponentially with sediment depth (Wallmann et al., 2008):

$$R_{SP} = k_{SP} \frac{[HS]}{[HS] + K_{SP}} \cdot e^{-r_{SP} \cdot x} \quad (13)$$

where k_{SP} is the kinetic constant, K_{SP} is the Monod constant and r_{SP} is the attenuation constant for sulfide removal.

Constant concentrations were prescribed at the upper and lower boundary of the model column (Dirichlet boundary conditions). In general, upper boundary conditions were chosen to represent regional seawater composition (for pore water constituents) and uppermost surface sediment concentrations (for solids), respectively, while lower boundary values reflect the composition of the deep fluid (for pore water constituents). The upper boundary value of 4.24 wt-% of total calcium carbonate ($CaCO_3$), which was applied for all stations, represents the mean value of three reference cores within the study area and

hence, was chosen to be representative for the pelagic CaCO_3 input (Tab. 1). All simulations were performed assuming steady state conditions ($dc/dt \approx 0$). The vertical resolution of the model grid was set to 1000 layers in order to resolve the steep pore water gradients for the overall simulation time of 100,000 years. Parameter values chosen for each model run are listed in Table 2.

Table 2. Summary of parameter values used for the steady state simulations at all seep locations. ^a

Parameter	Mound 11	Quepos Slide	Quepos Slide	Pockmark	Culebra Fault	Unit
	M54-138	SO173-63	SO173-73	M66-PC30	SO173-49	
Model parameter values						
Length of simulated core	27.5	41.50	32.50	15	810	cm
Number of model layers	1000	1000	1000	1000	3000	-
Temperature	4.43	9.59	9.59	2.66	3.18	°C
Salinity	34.58	34.59	34.59	34.61	34.61	PSU
Pressure	100.40	39.54	39.54	200.41	152.41	Atm
Sedimentation rate	0.03	0.03	0.03	0.03	0.03	cm a^{-1}
Porosity at sediment surface	0.872	0.911	0.910	0.668	0.744	
Porosity at large sediment depth	0.726	0.73	0.725	0.607	0.708	
Bioturbation coefficient at the sediment surface	0.01	0.01	0.01	0.01	0.01	$\text{cm}^2 \text{a}^{-1}$
Depth where bioturbation coefficient is zero	3	3	3	3	3	cm
Kinetic constant for sulfide removal	-	-	300*	-	0.24*	wt-S a^{-1}
Monod constant for sulfide removal	-	-	1*	-	1*	mmol dm^{-3}
Attenuation constant for sulfide removal	-	-	0.5*	-	0.001*	a^{-1}
Pore water concentration upper / lower boundary						
BW Cl / BS Cl	551/210	522/321	555/324	551/381	550/291	mM
BW SO_4 / BS SO_4	28.19/0	28.19/0.1	28.32/0	26.93/0.37	28.77/0	mM
BW Ca / BS Ca	10/9.16	10/4.11	10/6.55	10/31.10	10/22.43	mM
BW CH_4 / BS CH_4	0/68	0/92	0/92	0/61	0/63	mM
BW THN4 / BS THN4	0/1.74	0/2.56	0/2.90	0/3.58	0/6.56	mM
BW TH_2S / BS TH_2S	0/0	0/0.085	0/0	0/0.2	0/0.0025	mM
Solid phase concentrations upper boundary						
CaCO_3	4.24	4.24	4.24	4.24	4.24	% wt

^a The average sedimentation rate of 0.03 cm a^{-1} represents a mean value for this section of the Costa Rica continental margin (Kutterolf et al., 2008). BW indicates concentrations of dissolved species at the upper boundary of the model column; whereas BS indicates concentrations of dissolved species at the bottom of the sediment column.

* modified after Wallmann et al. (2008).

II.5. Results and Discussion

II.5.1. Numerical modeling of measured data

Measured concentration profiles of chloride, sulfate, total hydrogen sulfide (TH₂S), methane, ammonia, dissolved calcium, and total alkalinity (TA) of all cores are presented in Figures 2-6. Overall, there is a general decrease in chlorinity, which is accompanied by a significant increase in ammonium. Profiles of these constituents are indicative for the advection of deeply rooted fluids which are affected by mineral dehydration (freshening) and intense organic matter degradation (Hensen et al., 2004; Hensen and Wallmann, 2005; Lu et al., 2007). The depletion of sulfate within the uppermost cm to dm coincides with peak concentrations of TA and TH₂S and the simultaneous occurrence of high methane levels indicating the zone of AOM. Calcium concentrations in migrating fluids are different at all sites. Specifically, fluids at Pockmark and Culebra Fault are enriched in calcium relative to seawater. In contrast, fluids of Mound 11 and Quepos Slide remain at low levels below the AOM-zone.

Model runs with combinations of parameter values and boundary conditions listed in Table 2 and Table 3 produced good fits to the measured pore water profiles. All simulations were run into steady-state, which was achieved after a maximum time of ~80,000 years (Culebra Fault). Considerable deviations exist only for methane profiles where measured concentrations are considerably lower than simulated values. This discrepancy has been reported elsewhere and is due to the loss of methane from the sediment that degasses during sample retrieval (e.g. Hensen et al., 2007). Methane profiles were simulated assuming methane saturation of the upward migrating fluid with respect to methane hydrate (Tishchenko et al., 2005) at the lower boundary.

The rates for upward fluid flow, AOM, and calcium carbonate precipitation were determined by fitting the model to the data. Because there are very high concentrations of products from organic matter decomposition (e.g. NH₄) in the upward migrating fluids, it is very difficult to constrain *in situ* POC degradation rates. Since POC-profiles (not shown) do not display a systematic decrease over depth, it is assumed that POC-degradation is generally low at these sites and does not significantly affect the processes discussed in the following sections. Previous studies showed that the overall biogeochemical turnover at

seep sites is dominated by AOM and associated processes (Luff and Wallmann 2003; Wallmann et al. 2006b).

Table 3. Summary of parameter values determined by fitting the steady state simulations to measured data.

	Mound 11	Quepos Slide	Quepos Slide	Pockmark	Culebra Fault		
	M54-138	SO173-63	SO173-73	M66-PC30	SO173-49		
Parameter	Value					Unit	Reference
Upward fluid velocity	200	40	4	3	0.1	cm a ⁻¹	This study
Kinetic constant of aragonite dissolution	0.01	0.01	0.01	0.01	0.01	a ⁻¹	Modified after Luff&Wallmann (2003)
Kinetic constant of aragonite precipitation	100	100	100	10	100	mmol cm ⁻³ a ⁻¹	Luff&Wallmann (2003)
Kinetic constant of calcite dissolution	0.01	0.01	0.01	0.01	0.01	a ⁻¹	Modified after Luff&Wallmann (2003)
Kinetic constant of calcite precipitation	10	10	10	1	10	mmol cm ⁻³ a ⁻¹	Luff&Wallmann (2003)
Kinetic constant for anaerobic methane oxidation	1	12	5	1.20	0.5	cm ³ mmol ⁻¹ a ⁻¹	Modified after Luff&Wallmann (2003)

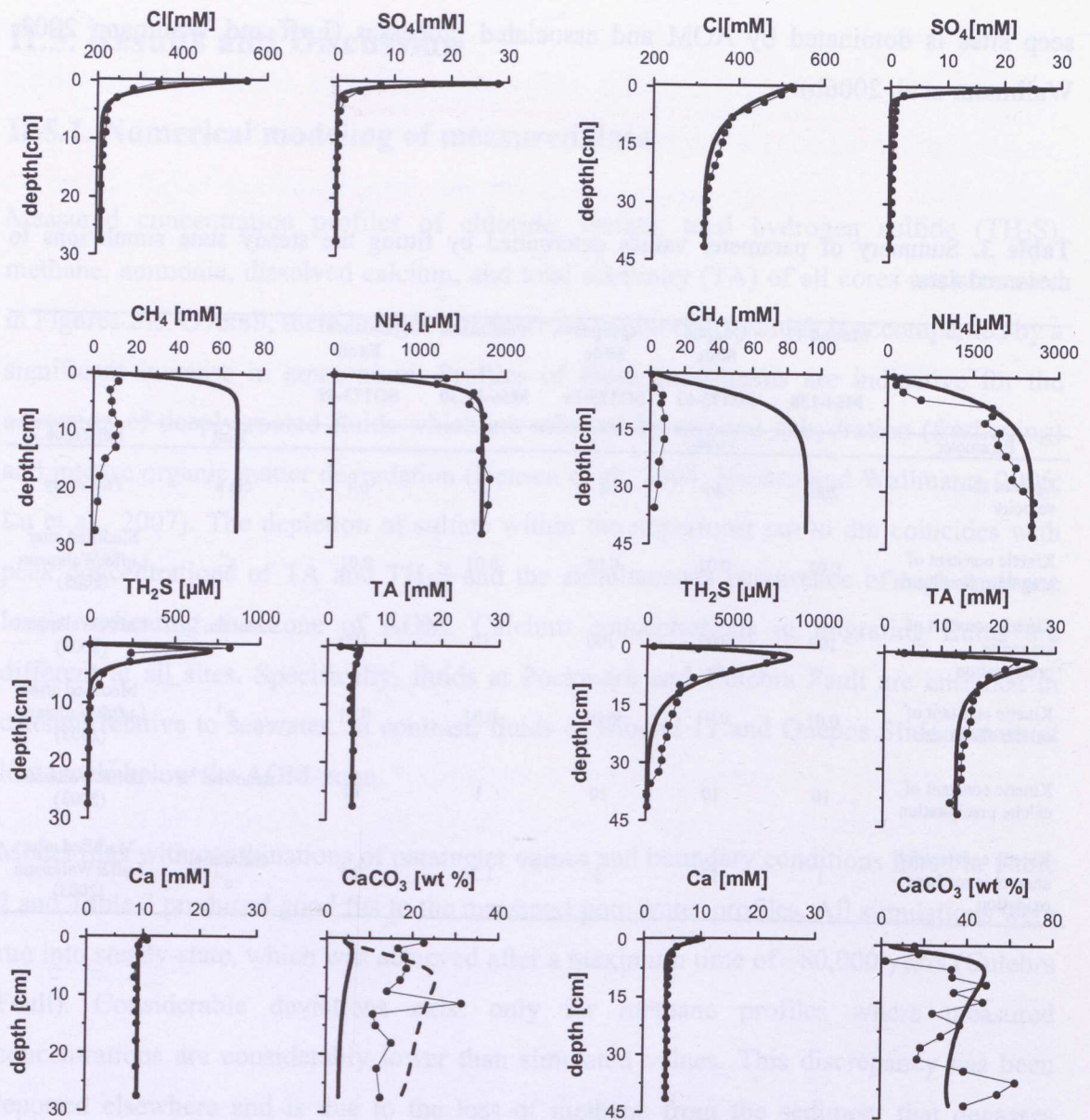


Figure 2. Measured (dots) and simulated (solid lines) concentration profiles at M54-138 (Mound 11). The broken line indicates carbonate concentrations calculated in an additional model run with reduced fluid flow velocity (see text for further explanations).

Figure 3. Measured (dots) and simulated (solid lines) concentration profiles at SO173-63 (Quepos Slide).

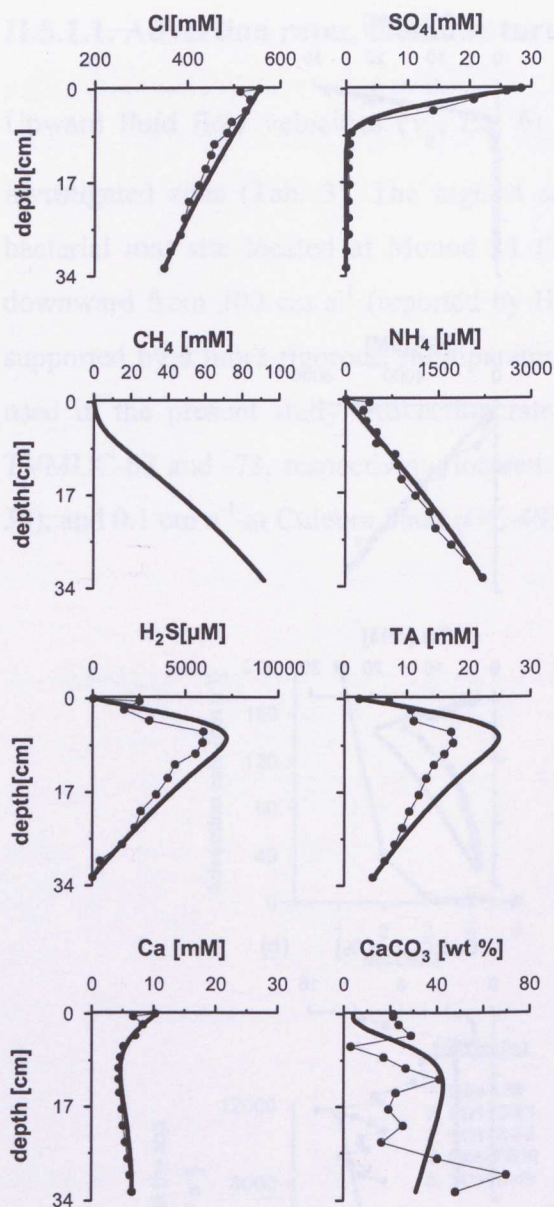


Figure 4. Measured (dots) and simulated (solid lines) concentration profiles at SO173-73 (Quepos Slide). No CH_4 concentrations available for this core.

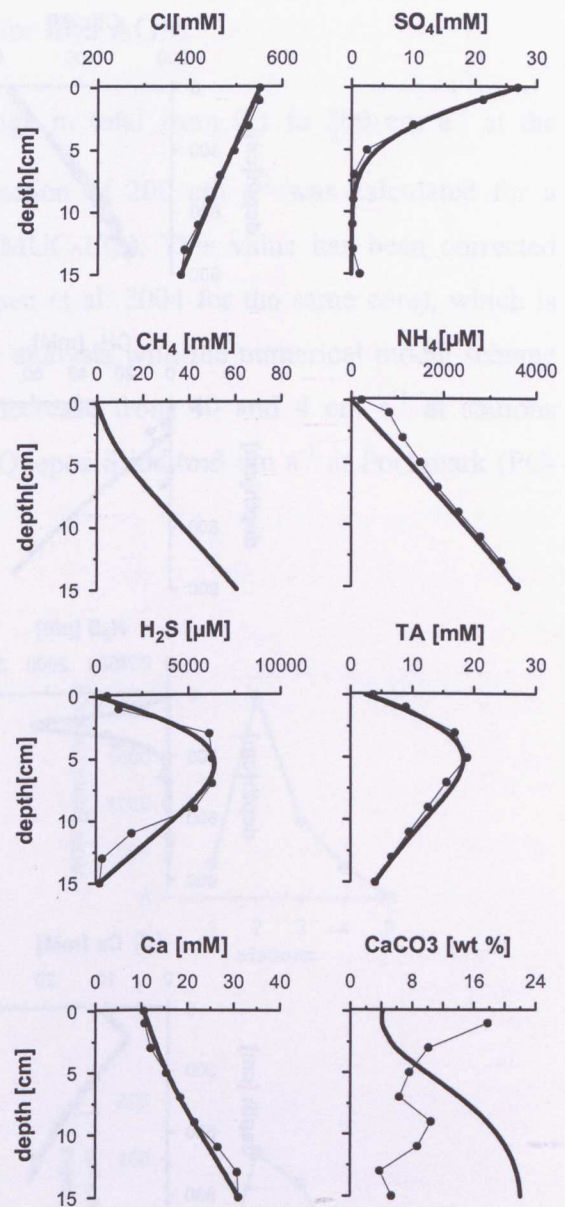


Figure 5. Measured (dots) and simulated (solid lines) concentration profiles at M66-PC30 (Pockmark). No CH_4 concentrations available for this core.

Figure 7. Advective flow (1000 $\mu\text{m s}^{-1}$) through a 10 μm pore of a 10 μm thick layer of CaCO_3 (a) and CaCO_3 (b) below the sediment-water interface and 10 μm deep-integrated pore profiles of CaCO_3 at all depths (c) and (d) calculated from (a) & (b) according to using in Table 1.

High flow rates (>40 $\mu\text{m s}^{-1}$) reduce the efficiency of CH_4 oxidizing microbes (Fig. 7b) and cause an increased efflux of dissolved methane and the water column (Fig. 7c, Tab. 4). AQM is most efficient at intermediate rates (1-40 $\mu\text{m s}^{-1}$) where methane supply is sufficiently high to enhance microbial activity, but still low enough to prevent significant

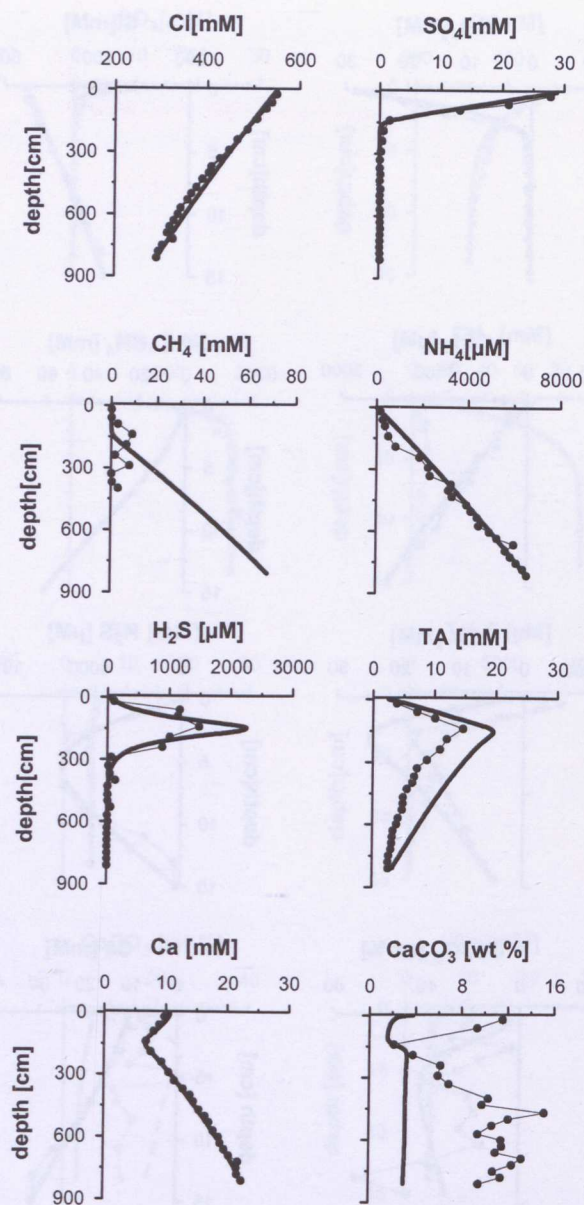


Figure 6. Measured (dots) and simulated (solid lines) concentration profiles at SO173-49 (Culebra Fault).

II.5.1.1. Advection rates, methane turnover and AOM

Upward fluid flow velocities (v_0 , Eq. 6) range in total from 0.1 to 200 cm a^{-1} at the investigated sites (Tab. 3). The highest advection of 200 cm a^{-1} was calculated for a bacterial mat site located at Mound 11 (TVMUC-138). This value has been corrected downward from 300 cm a^{-1} (reported by Hensen et al. 2004 for the same core), which is supported by a more rigorous, multiparameter analysis with the numerical model scheme used in the present study. Advection rates decrease from 40 and 4 cm a^{-1} at stations TVMUC-63 and -73, respectively, located at Quepos Slide to 3 cm a^{-1} at Pockmark (PC-30), and 0.1 cm a^{-1} at Culebra Fault (GC-49).

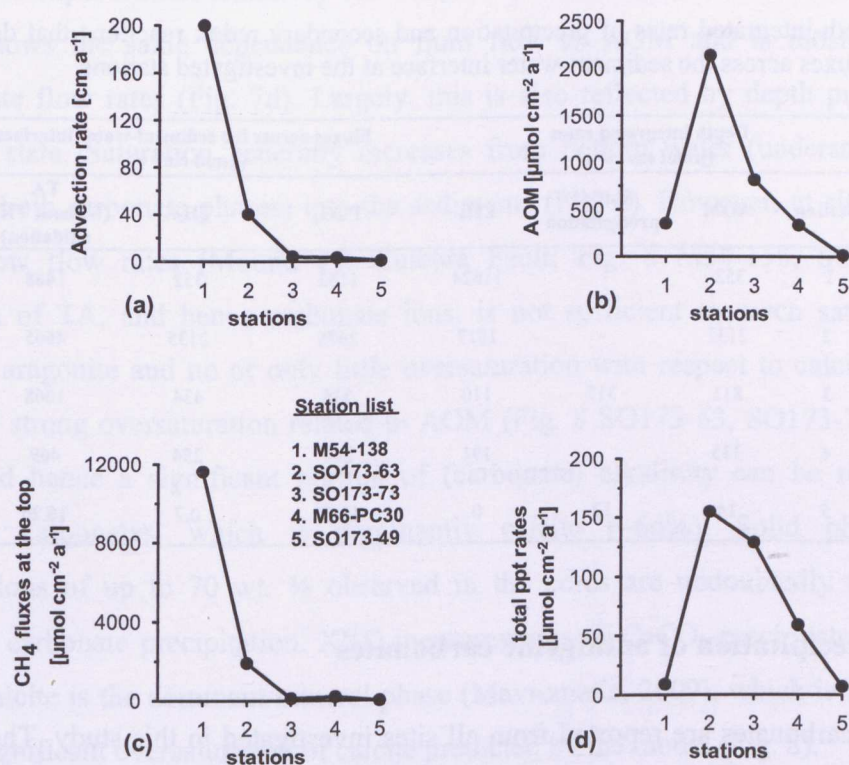


Figure 7. Advection rate (a) and depth integrated rates of (b) AOM, (c) CH_4 fluxes across the sediment-water interface, and (d) depth-integrated precipitation rates of CaCO_3 at all stations numbered from 1 to 5 according to listing in Table 1.

High flow rates ($>40 \text{ cm a}^{-1}$) reduce the efficiency of AOM in oxidizing methane (Fig. 7b) and cause an increased efflux of dissolved methane into the water column (Fig. 7c; Tab. 4). AOM is most efficient at intermediate rates ($1\text{-}40 \text{ cm a}^{-1}$) where methane supply is sufficiently high to enhance microbial activity, but still low enough to prevent significant

bypassing of the microbial filter and release into the water column (Fig. 7c). Our model results show that ascending methane is not escaping into the bottom water at very low fluid flow rates ($<1 \text{ cm a}^{-1}$), whereas 40 % and 98 % of the ascending methane is released into the bottom water at advection velocities of 40 cm a^{-1} and 200 cm a^{-1} , respectively (Fig. 7; Tab. 4). The model-derived methane flux to the water column at the low advection sites (stations 3, 4, 5) are in agreement with the range of fluxes ($0.4\text{-}3.1 \text{ mol m}^{-2} \text{ a}^{-1}$, $\sim 40\text{-}310 \mu\text{mol cm}^{-2} \text{ a}^{-1}$) reported by Mau et al. (2006), who investigated methane emissions at four mound shape structures at continental margin off Costa Rica (Mound 11, Mound 12, Mound 10 and Mound Culebra) by sampling methane plumes situated above the mounds. Hence, lower advection rates seem to be more representative to quantify regional average fluxes of methane from the mounds (cf. Ranero et al., 2008).

Table 4. Depth-integrated rates of precipitation and secondary redox reactions that dominate the system and fluxes across the sediment-water interface at the investigated stations.

Core / site	Station	Depth integrated rates ($\mu\text{mol cm}^{-2} \text{ a}^{-1}$)			Fluxes across the sediment-water interface ($\mu\text{mol cm}^{-2} \text{ a}^{-1}$)			
		AOM	Sulfide precipitation	CH_4	TCO_2	TH_2S	TA (without TH_2S oxidation)	TA (TH_2S oxidation)
Mound 11 (M54-138)	1	352	-	11624	1162	352	1488	785
Quepos Slide (TVMUC-63)	2	2132	-	1917	2676	2135	4665	397
Quepos Slide (TVMUC-73)	3	811	317	110	738	434	1068	200
Pockmark (M66-PC30)	4	335	-	191	249	254	469	-39
Culebra Fault (SO173-49)	5	14	13	0	13.52	0.7	16.26	14.86

II.5.1.2. Precipitation of authigenic carbonates

Authigenic carbonates are reported from all sites investigated in this study. The depletion of calcium corresponding to peak concentrations of TA within the AOM zone is indicative for active CaCO_3 precipitation. Peaks of TA and TH_2S are located very close to the sediment surface at high flow rates of $40\text{-}200 \text{ cm a}^{-1}$ (Quepos Slide-TVMUC-63 and Mound 11; Figs. 2, 3) whereas more prominent peaks occur at greater sediment depth when advection is lower (Figs. 4-6). At Mound 11, Quepos Slide (SO173-63), and Pockmark, TH_2S -profiles could readily be modeled by AOM and solute transport (advection and diffusion), only. At Quepos Slide (SO173-73) and Culebra Fault, however,

standard simulations revealed H_2S -production in excess to the measured profiles suggesting precipitation of iron sulfides (Hensen et al., 2003; Wallmann et al., 2008). In order to fit the observed profiles, precipitation of iron sulfides was considered by application of Equation 13 (Wallmann et al., 2008; Tab. 4), hence reducing the overall flux of TH_2S towards the sediment surface. The trends in TA and dissolved Ca are well reproduced in the model simulations applying the appropriate choice of reaction constants with respect to aragonite and calcite precipitation (Figs. 2-6; Tab 3). The combination of kinetic constants for calcite and aragonite are either 1 and 10 $\text{mmol cm}^{-3} \text{a}^{-1}$ (slow precipitation) or 10 and 100 $\text{mmol cm}^{-3} \text{a}^{-1}$ (fast precipitation), respectively, in order to obtain the best fit to the data. The difference of one order of magnitude between the kinetic constants for calcite and aragonite was used as suggested by Luff and Wallmann (2003) according to experimental results by Burton (1987). Total calcium carbonate precipitation thereby shows the same dependence on fluid flow as AOM and is most effective at intermediate flow rates (Fig. 7d). Largely, this is also reflected by depth profiles of the saturation state. Saturation generally increases from bottom water (undersaturated with respect to both carbonate phases) into the sediments (Fig. 8). However, at sites with very high or low flow rates (Mound 11, Culebra Fault; Fig. 8 M54-138, SO173-49) the production of TA, and hence carbonate ions, is not sufficient to reach saturation with respect to aragonite and no or only little oversaturation with respect to calcite. All other sites show strong oversaturation related to AOM (Fig. 8 SO173-63, SO173-73 and M66-PC30), and hence a significant portion of (carbonate) alkalinity can be removed into authigenic carbonates, which is dominantly calcite (~66%). Solid phase CaCO_3 concentrations of up to 70 wt. % observed in the cores are undoubtedly the result of authigenic carbonate precipitation. XRD-measurements of CaCO_3 -precipitates reveal that Mg-rich calcite is the dominant mineral phase (Mavromatis, 2009), which is in agreement with the significant oversaturation of calcite predicted by the model (Fig. 8).

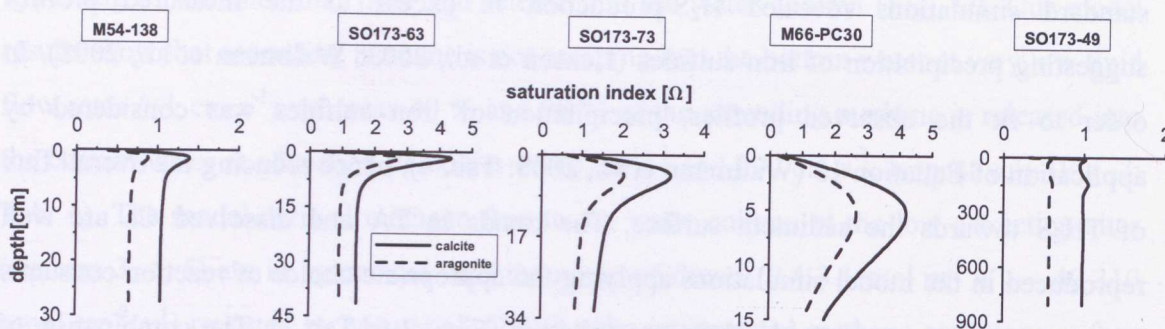


Figure 8. Down-core distribution of saturation state for calcite (solid lines) and aragonite (dashed lines) at all investigated stations.

However, in contrast to pore water calcium and TA profiles, modeled solid phase CaCO_3 profiles only show reasonable fits to the average CaCO_3 content at the Quepos Slide sites (Figs. 3, 4). At all other stations, both absolute concentrations and depth trends obtained in the model do not match the observations. Two general factors can be inferred to explain the observed discrepancy: (1) change of the sedimentary environment (sedimentation rate, mudflows, erosion) or (2) variations in the rate of upward fluid flow as previously observed at various locations (e.g. Tryon et al., 2002; Brown et al., 2005, La Bonte et al., 2007). Since modeled CaCO_3 -profiles reflect steady-state conditions based on recent turnover rates they most likely cannot adequately reflect the dynamic history of the past thousands of years recorded in the succession of authigenic carbonates. In the case of the station at Mound 11 (Fig. 2) an alternative model scenario has been set up, where the system has been calculated in steady-state at a flow velocity of only 50 cm a^{-1} . The result is not in accordance with measured pore water profiles, but reproduces well the overall CaCO_3 content of about 20 wt.%, suggesting that the average advective flow velocity has been lower at this site in the past.

Table 5. Depth integrated CaCO_3 precipitation, dissolution and net production rates within sediment and Ca fluxes across the sediment-water interface and bottom of the sediment at the investigated stations.

Core / site	Depth integrated CaCO_3 rates ($\mu\text{mol cm}^{-2} \text{a}^{-1}$)			Ca fluxes across the sediment-water interface and bottom of the sediment ($\mu\text{mol cm}^{-2} \text{a}^{-1}$)	
	Precipitation	Dissolution	Net precipitation	Sediment water-interface	Bottom
Mound 11 (M54-138)	9	4	5	1608	1613
Quepos Slide (TVMUC-63)	155	23	132	50	182
Quepos Slide (TVMUC-73)	129	18	111	-76	35
Pockmark (M66-PC30)	59	1	58	68	126
Culebra Fault (SO173-49)	7	5.85	1.15	-3	4.15

Our model study indicates that the advective Ca influx across the base of the model column is almost as large as the Ca flux into the bottom water at very high flow velocities (Mound 11) and consequently most of the deeply mobilized Ca escapes precipitation. Overall, there is a net transport of Ca out of the sediment at the Mound 11, Quepos Slide (TVMUC-63) and Pockmark sites (Tab 5). This is caused by high fluid flow velocities at Mound 11 and Quepos Slide (TVMUC-63) and, in contrast, by Ca-enriched fluids at Pockmark. At the Quepos Slide station TVMUC 73 and the Culebra fault sites featuring moderate to low fluid flow rates, a large fraction of Ca from the ascending fluid is fixed in authigenic carbonates. This relation is further illustrated in Figure 9, where the efficiency of CaCO_3 precipitation is plotted as a function of Ca-influx through the lower boundary. Note that values $>100\%$ indicate precipitation of Ca diffusing into the sediment from the overlying bottom water. For the sites Quepos Slide (TVMUC-63) and Pockmark up to 70% of the Ca from deep sources are precipitated while the rest is expelled into the bottom water. At Quepos Slide (TVMUC-73) and Culebra Fault between 30 and 70% of the Ca precipitated as CaCO_3 is derived from the bottom water. It should be noted that the considerably higher Ca fluxes at Pockmark compared to Quepos Slide (TVMUC-73) are caused by high Ca concentrations in the deep fluid while upward flow velocity is about the same at both sites. Ca is significantly enriched above seawater levels in the fluids at the Pockmark and Culebra Fault sites. Such high concentrations of Ca have been frequently observed in ODP (Ocean Drilling Program) drill cores and interpreted to be the result of low temperature alteration of basalt and volcanic material (Gieskes and Lawrence, 1981; Gieskes et al. 1990). As indicated specifically for the Pockmark site, this additional source

of deeply mobilized Ca has a significant impact on precipitation rates of CaCO_3 , and hence may be an important factor for the widespread occurrence of carbonate-paved mounds off Costa Rica. In order to test this hypothesis further systematic model runs with varying boundary conditions and calcium fluxes were performed as described below.

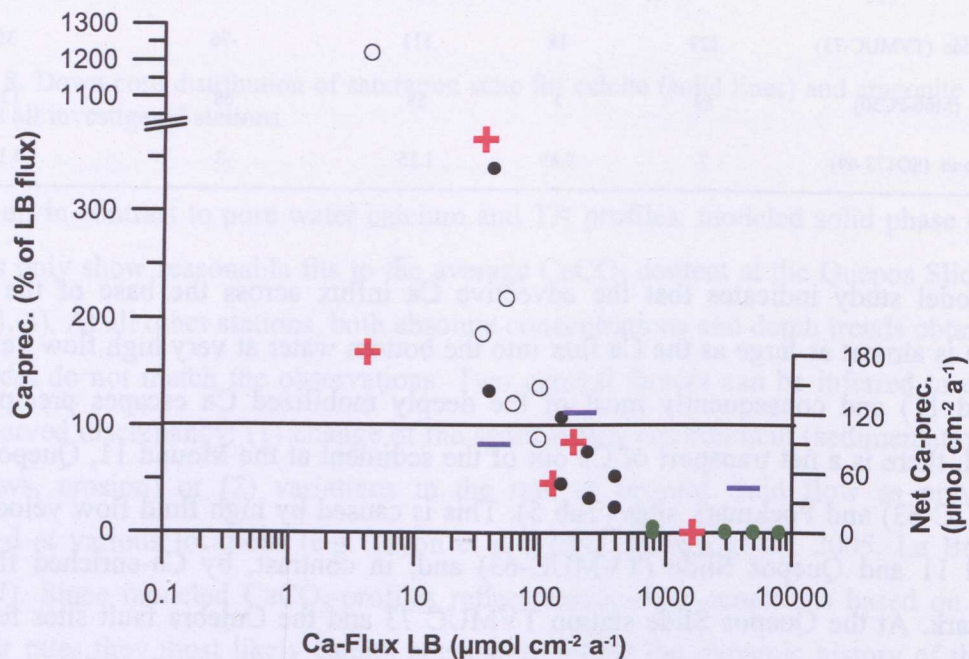


Figure 9. Depth-integrated net CaCO_3 precipitation rates (precipitation-dissolution) as percent of the Ca-influx through the lower boundary. Red crosses indicate model results based on core data. Dots indicate results of systematic runs with variable advection rates (open: 1 cm a^{-1} ; black: 10 cm a^{-1} ; green: 200 cm a^{-1}). Blue horizontal bars indicate depth-integrated net CaCO_3 -precipitation rates averaged for the groups with the same upward advection rates (1, 10, and 200). Note that x-axis is in logarithmic scale.

II.5.2. Systematics of calcium carbonate precipitation

For the systematic model runs, we chose a model column of 50 cm length with a depth resolution of 0.05 cm. All simulations were run into steady-state which on average was reached after $\sim 100,000$ years. Vertical fluid flow velocity, AOM rate and carbonate precipitation rates were simulated based on the general model set-up outlined in section 5.1. As for the site-specific model runs, we assumed calcite saturation and methane levels equal to solubility in equilibrium with gas hydrates in the upward migrating fluids. The

complete set of values and boundary conditions used to define the standard case for systematic parameter variations is given in Table 6.

Table 6. Parameter values applied for model runs with systematic variations of calcium concentrations in the deep fluid and upward fluid velocities. The bold numbers indicate different values for upward flow velocity, calcium concentration, TCO_2 and kinetic constants used in the various model runs.

Parameter	Value	Unit
Model parameter values		
Length of simulated core	50	cm
Number of model layers	1000	
Temperature	9.59	°C
Salinity	34.69	PSU
Pressure	39.54	atm
Sedimentation rate	0.03	cm a^{-1}
Porosity at sediment surface	0.911	
Porosity at great sediment depth	0.730	
Bioturbation coefficient at the sediment surface	0.01	$\text{cm}^2 \text{a}^{-1}$
Depth where bioturbation coefficient is zero	3	cm
Upward fluid velocity	1;10;200	cm a^{-1}
Pore water concentration		
upper / lower boundary		
BW Cl / BS Cl	522/321	mM
BW SO_4 / BS SO_4	28.19/0	mM
Calcium concentrations at the bottom of the sediment column for different model runs	4; 15; 25; 40	mM
BW CH_4 / BS CH_4	0/68	mM
TCO_2 at the bottom of the sediment column for different model runs	10;5;3;2	mM
BW TH_2S / BS TH_2S	0/0	mM
Solid phase concentrations		
upper boundary		
Calcium carbonate	4.24	% wt
Kinetic constants		
Kinetic constant of aragonite dissolution	0.01	a^{-1}
Kinetic constant of aragonite precipitation	10;100	$\text{mmol cm}^{-3} \text{a}^{-1}$
Kinetic constant of calcite dissolution	0.01	a^{-1}
Kinetic constant of calcite precipitation	1;10	$\text{mmol cm}^{-3} \text{a}^{-1}$
Kinetic constant for anaerobic methane oxidation	5	$\text{cm}^3 \text{mmol}^{-1} \text{a}^{-1}$

In total, we performed 24 model runs using four different Ca^{2+} concentrations at the lower boundary (4, 15, 25 and 40 mM) and three different upward advection rates (1, 10, and 200 cm a^{-1}) in order to impose variable Ca-fluxes into the model area. This range of parameter values was selected to cover the variations observed at the investigated stations. Again, all model runs were conducted applying different kinetic constants for calcite (1 and 10 $\text{mmol cm}^{-3} \text{a}^{-1}$) and aragonite (10 and 100 $\text{mmol cm}^{-3} \text{a}^{-1}$), respectively.

Overall, the model runs indicate that increasing calcium concentrations in the migrating fluids significantly enhance precipitation rates of authigenic carbonates (Fig. 10a, b). This finding suggests that precipitation related to AOM is limited by the availability of Ca in a purely diffusive system. The additional (deep) source enables a more efficient removal of carbonate ions produced by AOM and, as noticed before, this effect is most pronounced at moderate upward flow velocities (up to 10 cm a^{-1}).

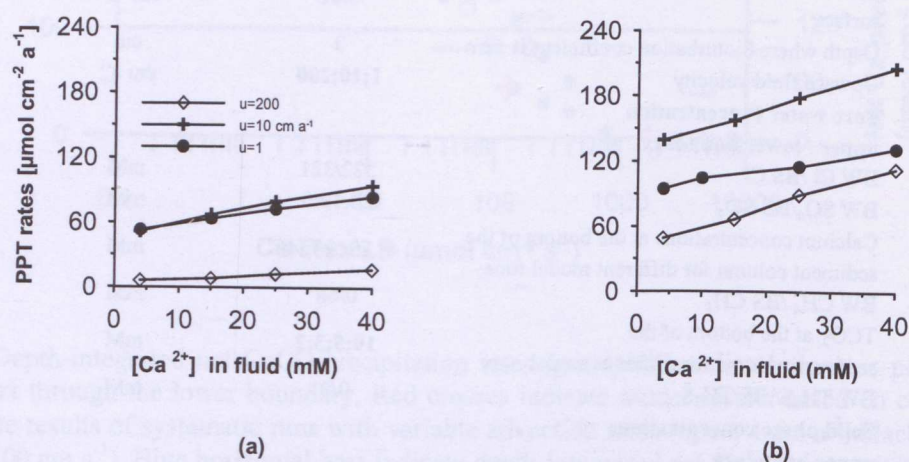


Figure 10. Depth-integrated rates of net CaCO_3 precipitation as a result of systematic model runs for various upward fluid velocities and calcium concentrations at the lower boundary. Plots (a) and (b) show the difference of using low (1, 10 $\text{mmol cm}^{-3} \text{a}^{-1}$) and high (10, 100 $\text{mmol cm}^{-3} \text{a}^{-1}$) kinetic precipitation constants for calcite and aragonite, respectively.

In order to elucidate this relation, the results of the systematic runs are included in Fig.9. It is obvious that (i) at high flow velocities (green dots) much of the Ca in the deep fluid is expelled into the water column, (ii) at moderate flow velocities (black dots) precipitation efficiency is highest and coincides with highest averaged precipitation rates (blue bars), and (iii) at low flow velocities (open dots) increasing amounts of precipitated Ca are

derived from bottom water. Consequently, the highest precipitation rates result from high Ca concentration in the deep fluid at moderate advection velocities. One exception to this systematic relationship is found at the Culebra Fault site, where intense subsurface dissolution of aragonite is predicted due to undersaturated bottom water and very low advection rates.

As for the site-specific model runs the dominant CaCO_3 -phase precipitated is calcite. The higher kinetic constant for calcite precipitation ($k_{\text{PPT-calcite}} = 10 \text{ mmol cm}^{-3} \text{ a}^{-1}$), which had to be used at most of the sites to obtain good fits to measured calcium and TA profiles (Figs. 2-6), results in clearly enhanced carbonate precipitation rates, on average by a factor of 2 (Fig. 10). In summary, this modeling experiment shows that the influx of dissolved Ca from deeper sedimentary strata is a significant Ca source for authigenic carbonate precipitation in addition to Ca diffusing into the sediment from the overlying bottom water. This fact has not been explored in most previous studies. Especially the availability of Ca-enriched fluids, which has been reported from various ODP drill sites (Moore et al., 1988; Kimura et al., 1997; Zahn et al., 1999), may need to be considered to explain the abundance and distribution of authigenic carbonates at cold seep sites.

II.5.3. Quantification of CaCO_3 accumulation at cold seeps

Formation of authigenic carbonates in cold seep environments is a worldwide phenomenon and hence, contributes to the sedimentary calcium sink and acts as an important factor in biogeochemical element recycling as suggested by an earlier study of Han and Suess (1989). Unfortunately, the quantification of this process is still essentially unconstrained, which is mainly due to the lack of quantitative, numerical studies and the heterogeneity of seep environments over space and time (e.g. Tryon et al., 2002; Brown et al., 2005; Solomon et al., 2008). However, extensive studies of fluid expulsion at the seafloor at the Central-American fore arc (Sahling et al., 2008; Ranero et al., 2008), increasing knowledge of the abundance of submarine seeps and mud volcanoes (Judd et al., 2002; Milkov, 2000) as well as the quantification of fluxes and flow velocities (e.g. Wallmann et al., 2006b; Hensen et al., 2007) provide sufficient information for a preliminary estimate.

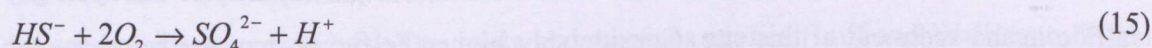
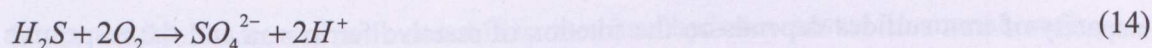
Calcium carbonate precipitation rates for low Ca concentrations in the deep fluid and low advection rates are on average $80 \mu\text{mol cm}^{-2} \text{a}^{-1}$ (Fig. 10). This magnitude is in agreement with previous studies at Hydrate Ridge (Luff and Wallmann, 2003; Luff et al., 2004) and indicates that AOM-induced carbonate formation occurs at similar rates under comparable environmental conditions along continental margins. As outlined above, fluid expulsion off Central America predominantly occurs at mounds (mud volcano-like structures ranging from 0.4-2 km in diameter) showing pronounced variations in flow rates between the hot spots (bacterial mats; $>10 \text{ cm a}^{-1}$) and the normal background ($<5 \text{ cm a}^{-1}$). Since the total area of the hot spots is typically very small, we assume that a conservative (minimum) estimate of about 1 cm a^{-1} is most realistic to represent the overall mean of a typical mound (Ranero et al., 2008). Given that focused seepage occurs at more than >120 sites with a diameter of 1 km along a ~ 500 km long section of the continental margin (Sahling et al., 2008; Ranero et al., 2008) and applying appropriate precipitation rates results in a total Ca-fixation of $7.5 \cdot 10^7 \text{ mol Ca a}^{-1}$ for the entire region. Assuming that this value is representative for the global margin length of about 150,000 km (Jarrard, 2003; Bradley, 2008) irrespective of the difference between active and passive margins, the global Ca-fixation at cold seeps sums up to about $2.2 \cdot 10^{10} \text{ mol Ca a}^{-1}$. As noted above, this estimate suffers from numerous uncertainties, and hence it must be regarded only as a first-order approximation. The highest uncertainty can probably be ascribed to the lack of knowledge of the total number and the seafloor area covered by cold seep sites. In contrast, variations of the fluid velocity may only affect calcium carbonate precipitation by a factor of 2-3 (Fig. 10), but not change the order of magnitude of the estimate. Interestingly, assuming the same average size of a cold seep structure as above ($\sim 0.8 \text{ km}^2$) the same value of about $2.2 \cdot 10^{10} \text{ mol Ca a}^{-1}$ can be obtained when assuming the existence of about 30,000 seep sites at continental margins, which is within the estimated range (1000-100,000) of total deep-water mud volcanoes reported by Milkov (2000).

In contrast, Wallmann et al. (2008) estimated the total AOM-related CaCO_3 precipitation and burial at the seafloor (not seep related) to be in the order of $1.7\text{-}6.7 \cdot 10^{12} \text{ mol a}^{-1}$. This estimate is based on the assumption that the methane formed in anoxic marine sediments ($5\text{-}20 \cdot 10^{12} \text{ mol a}^{-1}$; Reeburgh et al., 1993; Hinrichs and Boetius, 2002) is completely oxidized by AOM and about one third of the DIC formed during this reaction precipitated as authigenic CaCO_3 .

Considering additional effects of silicate weathering and sulfide burial this value may even increase up to $3.3\text{-}13.3 \cdot 10^{12} \text{ mol a}^{-1}$ (Wallmann et al., 2008). Hence, on a global scale authigenic precipitation of CaCO_3 in marine sediments seems to be a significant sink for calcium. It is comparable in magnitude to other processes governing the global Ca-cycle, such as the uptake of Ca during alteration of oceanic crust ($1.5\text{-}2.4 \cdot 10^{12} \text{ mol Ca a}^{-1}$; Alt and Teagle, 1999) or the subduction flux of Ca ($2.2 \cdot 10^{12} \text{ mol Ca a}^{-1}$; Rea and Ruff, 1996). On the other hand, our estimate for cold seeps is about two orders of magnitude lower, which suggests that cold seeps are not as significant in terms of Ca cycling in the oceans as it has been suspected previously (Han and Suess 1989).

II.5.4. Fluxes of TCO_2 and TA across the sediment-water interface

The C.CANDI model applied in this study calculates the depth profiles of the carbonate (CO_3^{2-} , HCO_3^- , CO_2) and hydrogen sulfide (HS^- , H_2S) species dissolved in pore water. Benthic fluxes of the sum of these constituents expressed as TCO_2 , TA and TH_2S are presented in Table 4. The aerobic oxidation of TH_2S and methane at the sediment water interface are not included in the model. As a result, the model predicts that most of the methane converts into bicarbonate at low and moderate fluid flow velocities. We expanded our model using a simple mass balance approach to further study the fate of methane at cold seep sites. Except for the Culebra Fault site (where no video observations are available and fluid flow is very low), the sediments investigated in this study were covered by mats of sulfide-oxidizing bacteria. Those bacteria rely on H_2S being produced in the underlying sediments by AOM. During oxidation, TH_2S is first transformed into elemental sulfur and ultimately into dissolved sulfate using oxygen as electron acceptor (Nelson et al., 1989):



The total alkalinity (TA), if simplified as $\text{TA} = \text{HS}^- + \text{HCO}_3^- + 2 \text{CO}_3^{2-}$, is reduced by 2 equivalents by the release of protons and the removal of HS^- for each mol of HS^- and H_2S being oxidized within such a mat. The TA flux from the sediment is thus reduced by the

aerobic oxidation of TH_2S , whereas HCO_3^- formed through AOM is converted into CO_2 before it enters the ocean.

In Table 4, we corrected the TA flux calculated by the model considering the stoichiometry of aerobic sulfide oxidation and assuming that TH_2S is oxidized completely into dissolved sulfate at the sediment/water interface. Prior to this correction, the TA fluxes were higher than the TCO_2 fluxes at stations where HS^- contributed significantly to the TA flux (Fig. 11). The corrected TA fluxes are much smaller than the TCO_2 fluxes due to the oxidation of HS^- and the proton production during aerobic sulfide oxidation at Mound 11 and Quepos Slide. At Pockmark the corrected TA flux is negative indicating the diffusion of TA from the overlying water into the sediment. The TA flux into the sediment is caused by aerobic sulfide oxidation and the precipitation of authigenic carbonates in the underlying AOM zone removing TA from the deep pore fluids. The fraction of DIC formed by AOM being removed by carbonate precipitation is much higher at the Pockmark station than at the other locations. Hence, the negative TA flux at Pockmark is related to the enhanced efficiency of TA removal by carbonate precipitation. Only at Culebra Fault the corrected TA flux is similar to the TCO_2 flux. At this station, dissolved TH_2S produced by AOM is almost completely removed from the pore water by sulfide precipitation within deeper sediment layers. Consequently, only a small fraction of TA is consumed by aerobic sulfide oxidation. This station features the lowest fluid rise velocity (0.1 cm a^{-1}) among all stations investigated in this study. Moreover, methane is oxidized almost completely at this station already at large sediment depth.

Interestingly, the Fe-flux in this region is about $22 \mu\text{mol cm}^{-2} \text{ a}^{-1}$ (calculated from surface concentrations of total iron of 5.8 wt.% at the reference station), which is similar in magnitude to the total SO_4 -consumption in the sediment. Although the actual binding capacity of iron sulfides depends on the fraction of reactive ferric iron and the respective reaction kinetics, the Fe-flux given above defines the maximum capacity to fix hydrogen sulfide in the sediment at this site. Considerably higher Fe-fluxes than predicted for the Costa Rica margin are generally unlikely for most continental margin environments since the surface Fe-concentrations here are well above the average shale value of 4.72 wt.% (Martin and Meybeck, 1979). For example, Fe-deposition rates are between $6\text{-}14 \mu\text{mol cm}^{-2} \text{ a}^{-1}$ in the Skagerrak Region (North Sea) and $5.1 \mu\text{mol cm}^{-2} \text{ a}^{-1}$ at the continental slope off Chile (Canfield et al., 1993; Thamdrup and Canfield, 1996). Hence, upward fluid flow

velocities $>0.2 \text{ cm a}^{-1}$ will usually result in H_2S -efflux and oxidation. This is supported by the results of the systematic runs that show an average TH_2S -flux across the sediment-water interface of $45 \mu\text{mol cm}^{-2} \text{ a}^{-1}$ for the low advection case of 1 cm a^{-1} .

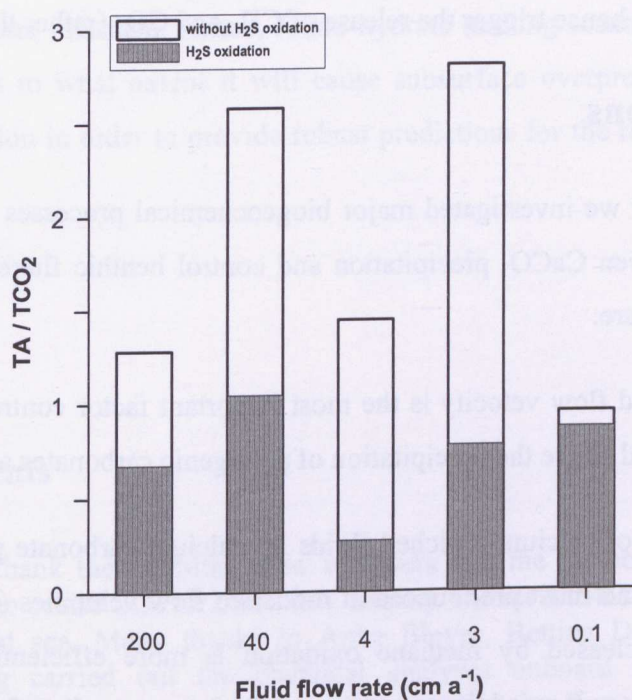


Figure 11. Ratio of TA (total alkalinity) to TCO_2 (total dissolved inorganic carbon) in response to variations of fluid flow rates. Full bars represent corrected ratios considering aerobic sulfide oxidation at the sediment/water interface whereas blank bars represent uncorrected ratios.

Dissociation events of methane hydrates have been suspected to be an important climate factor in the past, particularly during warm periods such as at the Paleocene-Eocene Thermal Maximum (PETM) (Dickens et al. 2003; Zachos et al., 2005), by enhancing CH_4 and CO_2 emissions into the ocean and the atmosphere. Moreover, models predict that future seafloor warming will destabilize methane hydrates hosted in marine sediments (Buffett and Archer, 2004; Archer et al., 2008). The fate of the released methane is, however, quite unconstrained. Our study and previous studies (Luff and Wallmann, 2003) showed that most of the dissolved methane ascending to the sediment surface at cold seep systems is oxidized by AOM consortia and converted into bicarbonate (HCO_3^-) at low fluid flow rates, hence neither the CH_4 nor the CO_2 contents of oceans and atmosphere would be affected. Only at elevated fluid flow velocities, methane release from deep sediments could potentially induce greenhouse gas emissions, and hence ocean acidification and global

warming in a positive feed-back loop. Considering the present day situation, the contribution of the very limited sea floor area of cold seeps seems to be negligible compared to other sources of greenhouse gases. However, substantial melting of global gas hydrate inventories could enhance methane fluxes to the seafloor above the required threshold value, and hence trigger the release of CH_4 and CO_2 (rather than HCO_3^-).

II.6. Conclusions

In the present study we investigated major biogeochemical processes and key parameters that affect vent driven CaCO_3 precipitation and control benthic fluxes at cold vent sites. Our major findings are:

- (1) Upward fluid flow velocity is the most important factor controlling the efficiency of AOM, and hence the precipitation of authigenic carbonates at cold vents.
- (2) The impact of calcium-enriched fluids on calcium carbonate precipitation rates is significant and most pronounced at moderate flow velocities ($\sim 10 \text{ cm a}^{-1}$). Hence, carbonate released by methane oxidation is more efficiently transformed into CaCO_3 , if there is an additional source of Ca from ascending fluids.
- (3) Authigenic carbonate formation induced by AOM has been shown to be an important process with respect to carbon and calcium burial in marine sediments (Wallmann et al., 2008). Although AOM-rates and consequently CaCO_3 precipitation rates are enhanced at cold seeps, a preliminary extrapolation and global estimate suggests that these sites do not significantly affect the calcium cycling in the ocean because of the comparatively small seafloor area.
- (4) The release of dissolved greenhouse gases (CH_4 , CO_2) is only relevant at moderate to high fluid advection rates. Methane ascent from deep sedimentary sources does not induce greenhouse gas emissions at the seafloor at low fluid rise velocities ($\leq 0.1 \text{ cm a}^{-1}$). Under these conditions, methane is completely oxidized by AOM within deeper sediment layers while sulfide being produced by AOM is largely removed by the precipitation of sulfide minerals and sulfide oxidation at the seafloor is negligible.

- (5) Enhanced fluid flow promotes the aerobic oxidation of methane and sulfide and the conversion of methane into CO₂. Sedimentary methane fluxes caused by the dissociation of gas hydrates or other processes are thus only potential climate drivers, if fluid flow accelerates the upward transport of methane towards the sediment-water interface. Hence, future hydrate melting scenarios need to address the question to what extent it will cause subsurface overpressuring and upward fluid advection in order to provide robust predictions for the release of greenhouse gases.

Acknowledgements

We would like to thank the captains, crew members and the members of the scientific parties of R/V Sonne cruise SO173/2 and R/V Meteor cruises M54/2 and M66/2 for their helpful assistance at sea. Many thanks to Anke Bleyer, Bettina Domeyer and Regina Surberg for having carried out the chemical analyses onboard and at shore-based laboratories. We also appreciate the indispensable support by Roger Luff and Matthias Haeckel concerning the handling of C.CANDI. The helpful comments of two anonymous reviewers and the associated editor are greatly appreciated. This work was funded by the German Science Foundation (DFG). It is contribution 197 of the Sonderforschungsbereich 574 "Volatiles and Fluids in Subduction Zones" at Kiel University.

References

- Aloisi, G., M. Drews, K. Wallmann, and G. Bohrmann (2004), Fluid expulsion from the Dvurechenskii mud volcano (Black Sea) - Part I. Fluid sources and relevance to Li, B, Sr, I and dissolved inorganic nitrogen cycles, *Earth and Planetary Science Letters*, 225(3-4), 347-363.
- Alt, J. C., and D. A. H. Teagle (1999), The uptake of carbon during alteration of oceanic crust, *Geochim. Cosmochim. Acta*, 63(10), 1527-1535.
- Archer, D., B. Buffett., V. Brovkin (2008), Ocean methane hydrates as a slow tipping point in the global carbon cycle, *Proceedings of the National Academy of Sciences.*, 106, 20596-20601, doi:10.1073/pnas.0800885105.
- Berner, R. A. (1980), *Early diagenesis. A theoretical approach*, Princeton University Press, 241 pp., New York.
- Boetius, A., K. Ravensschlag, C. J. Schubert, D. Rickert, F. Widdel, A. Giesecke, R. Amann, B. B. Jørgensen, U. Witte, and O. Pfannkuche (2000), A marine microbial consortium apparently mediating anaerobic oxidation of methane, *Nature*, 407, 623-626.
- Boetius, A., and E. Suess (2004), Hydrate Ridge: a natural laboratory for the study of microbial life fueled by methane from near-surface gas hydrates, *Chemical Geology*, 205, 291 - 310.
- Bohrmann, G., K. Heeschen, C. Jung, W. Weinrebe, B. Baranov, B. Cailleau, R. Heath, V. Hühnerbach, M. Hort, D. Masson, and I. Trummer (2002), Widespread fluid expulsion along the seafloor of the Costa Rica convergent margin, *Terra Nova*, 14, 69-79.
- Borowski, W. S., C. K. Paull, and W. Ussler III (1996), Marine pore-water sulfate profiles indicate in situ methane flux from underlying gas hydrate, *Geology*, 24(7), 655-658.
- Boudreau, B. P. (1997), *Diagenetic models and their implementation: modeling transport and reactions in aquatic sediments*, 414 pp., Springer, Berlin, Heidelberg, New York.
- Bradley, D. C. (2008), Passive margins through earth history, *Earth-Science Reviews*, 91(1-4), 1-26.
- Brown, K. M., M. D. Tryon, H. R. DeShon, L. M. Dorman, S. Y. Schwartz (2005), Correlated transient fluid pulsing and seismic tremor in the Costa Rica subduction zone. *Earth and Planetary Science Letters*, 238, 189-203.
- Brückmann, W., M. Rhein, G. Rehder, J. Bialas, and A. Kopf (2009), SUBFLUX, *Cruise No.66*, 158 pp, METEOR-Berichte 09-2, Universität Hamburg, August 12 - December 22, 2005.
- Buffett, B., and D. Archer (2004), Global inventory of methane clathrate: sensitivity to changes in the deep ocean, *Earth and Planetary Science Letters*, 227, 185-199.

- Burton, E. A., and L. M. Walter (1987), Relative Precipitation Rates of Aragonite and Mg Calcite from Seawater - Temperature or Carbonate Ion Control, *Geology*, 15(2), 111-114.
- Canfield, D. E., B. Thamdrup, J. W. Hansen (1993), the anaerobic degradation of organic matter in Danish coastal sediments: Iron reduction, manganese reduction, and sulfate reduction, *Geochimica Et. Cosmochimica. Acta*, 57, 3867-3883.
- Dickens, G. R. (2003), Rethinking the global carbon cycle with a large, dynamic and microbially mediated gas hydrate capacitor, *Earth and Planetary Science Letters*, 213(3-4), 169-183.
- Gieskes, J. M., G. Blanc, P. Vrolijk, H. Elderfield, and R. Barnes (1990), Interstitial water chemistry - major constituents, *Proceedings of ODP*, Scientific Results.
- Gieskes, J. M., and J. R. Lawrence (1981), Alteration of Volcanic Matter in Deep-Sea Sediments - Evidence from the Chemical-Composition of Interstitial Waters from Deep-Sea Drilling Cores, *Geochimica Et Cosmochimica Acta*, 45(10), 1687-1703.
- Grasshoff, K., K. Kremling, and M. Ehrhardt (1997), *Methods of seawater analysis*, 419 pp, Verlag Chemie, Weinheim.
- Han, M. W., and E. Suess (1989), Subduction-induced pore fluid venting and the formation of authigenic carbonates along the cascadia continental margin: implications for the global Ca-cycle, *Palaeogeography, Palaeoclimatology, Palaeoecology*, 71, 97-118.
- Han, X. Q., E. Suess, H. Sahling, and K. Wallmann (2004), Fluid venting activity on the Costa Rica margin: new results from authigenic carbonates, *International Journal of Earth Sciences*, 93(4), 596-611.
- Hensen, C., M. Zabel, K. Pfeifer, T. Schwenk, S. Kasten, N. Riedinger, H. D. Schulz, and A. Boettius (2003), Control of sulfate pore-water profiles by sedimentary events and the significance of anaerobic oxidation of methane for the burial of sulfur in marine sediments, *Geochim. Cosmochim. Acta*, 67(14), 2631-2647.
- Hensen, C., and K. Wallmann, M. Schmidt, C.R. Ranero, E. Suess (2004), Fluid expulsion related to mud extrusion off Costa Rica continental margin - a window to the subducting slab, *Geology*, 32, 201-204.
- Hensen, C., and K. Wallmann (2005), Methane formation at Costa Rica continental margin - constraints for gas hydrate inventories and cross-decollement fluid flow, *Earth and Planetary Science Letters*, 236(1-2), 41-60.
- Hensen, C., M. Nuzzo, E. Hornibrook, L. M. Pinheiro, B. Bock, V. H. Magalhães, and W. Brückmann (2007), Sources of mud volcano fluids in the Gulf of Cadiz - indications for hydrothermal imprint, *Geochim. Cosmochim. Acta*, 71, 1232-1248.

- Hinrichs, K. U. and A. Boetius, (2002), The anaerobic oxidation of methane: new insights in microbial ecology and biogeochemistry. In *Ocean Margin Systems*. Wefer, G., Billett, D., Hebbeln, D., Jørgensen, B.B., Schlüter, M., and van Weering, T. (eds), 457-477, Heidelberg: Springer-Verlag.
- Ivanenkov, V. N., and Y. I. Lyakhin (Eds.) (1978), *Determination of total alkalinity in seawater*, 110-114 pp., Nauka Publ. House, Moscow.
- Jarrard, R. D. (2003), Subduction fluxes of water, carbon dioxide, chlorine, and potassium, *Geochemistry Geophysics Geosystems*, 4(5), 50.
- Judd, A. G., M. Hovland, L. I. Dimitrov, S. G. Gil, and V. Jukes (2002), The geological methane budget at continental margins and its influence on climate change, *Geofluids*, 2, 109-126.
- Kimura, G., E. Silver, P. Blum, and participants (1997), *Proc. ODP, Init. Repts.*, 170, 458 pp, College Station, TX (Ocean Drilling Program).
- Kutterolf, S., A. Freundt, W. Pérez, T. Mörz, U. Schacht, H. Wehrmann, and H.-U. Schmincke (2008), Pacific offshore record of plinian arc volcanism in Central America: 1. Along-arc correlations, *G-cubed*, 9(2), doi:10.1029/2007GC001631.
- LaBonte, A.L., K.M. Brown, M.D. Tryon (2007). Monitoring periodic and episodic flow events at Monterey Bay seeps using a new optical flow meter, *J. Geophys. Res.* 112.
- Linke, P., K. Wallmann, E. Suess, C. Hensen, and G. Rehder (2005), In-situ benthic fluxes from an intermittently active mud volcano at the Costa Rica convergent margin, *Earth Planet. Sci. Lett.*, 235, 79-95.
- Lu, Z., C. Hensen, U. Fehn, and K. Wallmann (2007), Old iodine in fluids venting along the Central American convergent margin, *Geophysical Research Letters*, 34(22).
- Luff, R., K. Wallmann, S. Grandel, and M. Schlüter (2000), Numerical modelling of benthic processes in the deep Arabian Sea, *Deep-Sea Res. II*, 47(14), 3039-3072.
- Luff, R., and K. Wallmann (2003), Fluid flow, methane fluxes, carbonate precipitation and biogeochemical turnover in gas hydrate-bearing sediments at Hydrate Ridge, Cascadia Margin: Numerical modeling and mass balances, *Geochim. Cosmochim. Acta*, 67(18), 3403-3421.
- Luff, R., K. Wallmann, and G. Aloisi (2004), Numerical modeling of carbonate crust formation at cold vent sites: significance for fluid and methane budgets and chemosynthetic biological communities, *Earth Planet. Sci. Lett.*, 221, 337-353.
- Martin, J. B., M. Kastner, P. Henry, X. Le Pichon, and S. Lallement (1996), Chemical and isotopic evidence for sources of fluids in a mud volcano field seaward of the Barbados accretionary wedge, *J. Geophys. Res.*, 101(B9), 20325-20345.

- Martin, J. M., M. Meybeck (1979), Elemental Mass-Balance of Material Carried by Major World Rivers, *Marine Chemistry*, 7, 173-206.
- Mau, S., H. Sahling, G. Rehder, E. Suess, P. Linke, and E. Soeding (2006), Estimates of methane output from mud extrusions at the erosive convergent margin off Costa Rica., *Marine Geology*, 225, 129-144.
- Mavromatis, V. (2009), Mineralogical and isotope geochemical investigations of high Mg-calcites: Laboratory and field studies *P.hD. Thesis*, 96 pp, University of Kiel, Kiel.
- Milkov, A. V. (2000), Worldwide distribution of submarine mud volcanoes and associated gas hydrates, *Mar. Geol.*, 167, 29-42.
- Moore, J. C. et al. (1988), Tectonics and Hydrogeology of the Northern Barbados Ridge - Results from Ocean Drilling Program Leg-110, *Geological Society of America Bulletin*, 100(10), 1578-1593.
- Mörz, T., Kopf, A., Brückmann, W., Fekete, N., Hühnerbach, V., Masson, D., Hepp, D.A., Suess, E., Weinrebe, W. (2005a), Styles and productivity of mud diapirism along the Middle American Margin / Part 1: Margin Evolution, Segmentation, Dewatering and Mud Diapirism, In: *Mud volcanoes, geodynamics and seismicity, ATO Sci. Ser. IV*, Martinelli G, Panahi B (eds) 51: 35-48, Kluwer Academic Publishers Dordrecht/Boston/London.
- Mörz, T. et al. (2005b), Styles and productivity of mud diapirism along the Middle American Margin / Part 2: Mound Culebra and Mounds 11, and 12. In: *Mud volcanoes, geodynamics and seismicity, ATO Sci. Ser. IV*, Martinelli G, Panahi B (eds) 51: 49-76, Kluwer Academic Publishers Dordrecht/Boston/London.
- Nelson, D. C., C. O. Wirsen, and H. W. Jannasch (1989), Characterization of Large, Autotrophic *Beggiatoa* Spp Abundant at Hydrothermal Vents of the Guaymas Basin, *Applied and Environmental Microbiology*, 55(11), 2909-2917.
- Ranero, C. R., and R. Von Huene (2000), Subduction erosion along the Middle America convergent margin, *Nature*, 404, 748-752.
- Ranero, C. R., I. Grevemeyer, H. Sahling, U. Barckhausen, C. Hensen, K. Wallmann, W. Weinrebe, P. Vannucchi, R. von Huene, and K. McIntosh (2008), Hydrogeological system of erosional convergent margins and its influence on tectonics and interplate seismogenesis, *G-cubed*, 9(3), doi:10.1029/2007GC001679.
- Rea, D. K. and L. J. Ruff, (1996), Composition and mass flux of sediment entering the world's subduction zones: Implications for global sediment budgets, great earthquakes, and volcanism. *Earth and Planetary Science Letters*, 140, 1-12.
- Reeburgh, W. S., S. C. Whalen, M. J. Alperin (1993), The role of methylotrophy in the global methane budget, In: *Murrell, J.C. and Kelly, D.P. (eds.)*, 1-14, Seventh Int. Symp. Microb. Growth on C1 Compounds, Intercept Ltd., Andover.

- Sahling, H., D. G. Masson, C. R. Ranero, V. Hühnerbach, W. Weinrebe, I. Klauke, D. Bürk, W. Brückmann, and E. Suess, (2008), Fluid seepage at the continental margin offshore Costa Rica and southern Nicaragua, *G-cubed*, 9. doi:10.1029/2008GC001978.
- Schmidt, M., C. Hensen, T. Morz, C. Muller, I. Grevemeyer, K. Wallmann, S. Mau, and N. Kaul (2005), Methane hydrate accumulation in "Mound 11" mud volcano, Costa Rica forearc, *Marine Geology*, 216(1-2), 83-100.
- Solomon, E. A., M. Kastner, H. Jannasch, G. Robertson, Y. Weinstein, (2008), Dynamic fluid flow and chemical fluxes associated with a seafloor gas hydrate deposit on the northern Gulf of Mexico slope, *Earth and Planetary Science Letters*, 270, 95-10.
- Thamdrup B. and D. E. Canfield (1996), Pathways of carbon oxidation in continental margin sediments off central Chile, *Limnology and Oceanography*, 41, 1629-1650.
- Tishchenko, P., C. Hensen, K. Wallmann, and C. S. Wong (2005), Calculation of the stability and solubility of methane hydrate in seawater, *Chemical Geology*, 219(1-4), 37-52.
- Tryon, M.D., K. M Brown, M. E. Torres (2002), Fluid and chemical flux in and out of sediments hosting methane hydrate deposits on Hydrate Ridge, Or, II: Hydrological Processes. *Earth and Planetary Science Letters*, 201, 541-557.
- Vannucchi, P., C. R. Ranero, S. Galeotti, S. M. Straub, D. W. Scholl, and K. McDougall-Ried (2003), Fast rates of subducting erosion along the Costa Rica Pacific margin: Implications for nonsteady rates of crustal recycling at subduction zones, *Journal of Geophysical Research*, 108, doi: 10.1029/2002JB002207.
- Wallmann, K., P. Linke, E. Suess, G. Bohrmann, H. Sahling, M. Schlüter, A. Dählmann, S. Lammers, J. Greinert, and N. v. Mirbach (1997), Quantifying fluid flow, solute mixing, and biogeochemical turnover at cold vents of the eastern Aleutian subduction zone, *Geochim. Cosmochim. Acta*, 61(24), 5209-5219.
- Wallmann, K., G. Aloisi, M. Haeckel, A. Obzhairov, G. Pavlova, and P. Tishchenko (2006a), Kinetics of organic matter degradation, microbial methane generation, and gas hydrate formation in anoxic marine sediments, *Geochim. Cosmochim. Acta*, 70, 3905-3927.
- Wallmann, K., M. Drews, G. Aloisi, and G. Bohrmann (2006b), Methane discharge into the Black Sea and the global ocean fluxes via fluid flow through submarine mud volcanoes, *Earth Planet. Sci. Lett.*, 248, 545-560.
- Wallmann, K., G. Aloisi, M. Haeckel, P. Tishchenko, G. Pavlova, J. Greinert, S. Kutterolf, and A. Eisenhauer (2008), Silicate weathering in anoxic marine sediments, *Geochimica et Cosmochimica Acta*, 72(12), 2895-2918.
- Zachos, J. C., U. Röhl, S. A. Schellenberg, A. Sluijs, D. A. Hodell, D. C. Kelly, E. Thomas, M. Nicolo, I. Raffi, L. J. Lurens, H. McCarren, and D. Kroon (2005), Rapid

Acidification of the Ocean During the Paleocene-Eocene Thermal Maximum, *Science*, 308, 1611-1615.

Zahn, R., Comas, M. C., and Klaus, A. (Eds.), (1999), *Proc. ODP, Init. Repts.*, 161: College Station, TX (Ocean Drilling Program).

Quantification of dissolved methane discharge at mud mounds offshore Costa Rica

Deniz Karac¹, Tina Schirmer², Christina Hensen^{1,3}, Ingo Klauke², Klaus Wallmann¹

¹ Sonderforschungsbereich 374, University of Kiel, Wobbeplatz 1-3, D-24108 Kiel, Germany
² Department of Biomineralogy, University of Wuerzburg, Am Hubland, D-97074, Wuerzburg, Germany
³ Leibniz-Institut of Marine Science, IFM-GEOMAR, Wustrowerde 1-3, D-24108 Kiel, Germany

To be submitted to *Global Biogeochemical Cycles*

Abstract

Dissolved methane fluxes from two mud mounds (Mound 11 and Mound 12) at the submarine seafloor of the Costa Rica fore arc have been estimated by combining geochemical and geoscientific data analysis. The study is supported by 30 kHz sidescan sonar data, pore-water analysis and visual seafloor observations by remotely operated vehicle, ROV deployments at the mud mounds. Our study shows that bacterial mats occur in patches at Mound 11, whereas they appear to be distributed at Mound 12 covering about 25% of the entire mound. A numerical transport reaction model was applied to determine dissolved methane fluxes considering advective migration of methane (ADM) and upward fluid flow. At bacterial mat sites at Mound 11, ADM consumes on average 8% of the methane flux from depth due to high advection rates (average 10 cm d^{-1}) allowing for significant methane discharge into the water column ($15.7 \text{ mmol m}^{-2} \text{ d}^{-1}$ in comparison, ADM consumes on average 20% of the methane flux from depth at Mound 12. Lower

- Barth, W., Brückmann, and E. Suck (2003). Fluid escape at the active Costa Rica subduction zone. *Journal of Geophysical Research*, 108, doi:10.1029/2002JB001978.
- Barth, W., Conrad, M. C., and Klaus, A. (Eds.) (1999). *Proc. IAGLR, Costa Rica*, 144.
- Schmidt, M., C. Hensen, J. Munn, C. Muehlenberg, and M. N. Kaul (2005). Methane hydrate accumulation in "Mound 11" mud volcano, Costa Rica forearc. *Marine Geology*, 216(1-2), 63-100.
- Solomon, E. A., M. Karter, H. Jannach, G. Robertson, Y. Weinstein (2003). Dynamic fluid flow and chemical fluxes associated with a seafloor gas hydrate deposit on the northern Gulf of Mexico slope. *Earth and Planetary Science Letters*, 210, 95-10.
- Thamdrup H. and D. E. Canfield (1991). Pathways of carbon oxidation in continental margin sediments of central Chile. *Geology and Geochemistry*, 47, 1629-1650.
- Tishchenko, P., C. Hensen, K. Wallmann, and C. S. Wong (2005). Calculation of the stability and solubility of methane hydrate in seawater. *Chemical Geology*, 219(1-4), 37-52.
- Tryon, M.D., K. M. Hovens, M. E. Torres (2002). Fluid and chemical flux in and out of sediments hosting methane hydrate deposits on Hydrate Ridge, Or. II: Hydrological Processes. *Earth and Planetary Science Letters*, 201, 543-557.
- Vannucchi, P., C. R. Ranero, S. Galotti, S. M. Straub, D. W. Scholl, and K. McDougall-Ried (2003). Fast rates of subsiding erosion along the Costa Rica Pacific margin: implications for porosity index of crustal recycling at subduction zones. *Journal of Geophysical Research*, 108, doi:10.1029/2002JB002407.
- Wallmann, K., P. Link, F. Sachs, G. Bohrmann, H. Sahling, M. Schäfer, A. Dahmann, S. Lammert, J. Greiner, and N. V. Mikhalch (1997). Quantifying fluid flow, solute mixing, and biogeochemical turnover at cold vents of the eastern Aleutian subduction zone. *Geochimica Cosmochimica Acta*, 61(24), 5209-5219.
- Wallmann, K., G. Altsi, M. Haeckel, A. Obzinov, G. Pavlova, and P. Tishchenko (2006a). Kinetics of organic matter degradation, microbial methane generation, and gas hydrate formation in exotic marine sediments. *Geochimica Cosmochimica Acta*, 70, 3905-3927.
- Wallmann, K., M. Drews, G. Altsi, and G. Bohrmann (2006b). Methane discharge into the Black Sea and the global ocean through 96 fluid flow through submarine mud volcanoes. *Earth Planetary Sci. Lett.*, 248, 349-360.
- Wallmann, K., G. Altsi, M. Haeckel, P. Tishchenko, J. Pavlov, J. Greiner, S. Kutterolf, and A. Eisenhauer (2005). Silicate weathering in exotic marine sediments. *Geochimica et Cosmochimica Acta*, 72(12), 2895-2918.
- Zachos, J. C., U. Röhl, S. A. McInerney, A. Stouffer, D. A. Hodell, D. G. Kelly, E. Thomas, M. Niemi, I. Raff, L. J. Linsley, H. McCann, and D. Wright (2005). Rapid

Chapter III

Quantification of dissolved methane discharge at mud mounds offshore Costa Rica

Deniz Karaca^{1*}, Tina Schleicher², Christian Hensen^{1,3}, Ingo Klaucke³, Klaus Wallmann^{1,3}

¹Sonderforschungsbereich 574, University of Kiel, Wischhofstraße 1-3, D-24148 Kiel, Germany

²Department of Bioinformatics, University of Würzburg, Am Hubland, D-97074, Würzburg Germany

³Leibniz-Institute of Marine Sciences, IFM-GEOMAR, Wischhofstraße 1-3, D-24148 Kiel, Germany

To be submitted to Global Biogeochemical Cycles

Abstract

Dissolved methane fluxes from two mud mounds (Mound 11 and Mound 12) at the submarine section of the Costa Rica fore arc have been estimated by combining geochemical and geoacoustic data analysis. The study is supported by 75 kHz sidescan sonar data, pore-water analysis and visual sea-floor observations by remotely operated vehicle. ROV deployments at the most active sites show that bacterial mats occur as patches at Mound 11, whereas they appear in a distinct zone at Mound 12 covering about 25% of the entire mound. A numerical transport reaction model was applied to determine dissolved methane fluxes considering anaerobic oxidation of methane (AOM) and upward fluid flow. At bacterial mat sites of Mound 11, AOM consumes on average 8% of the methane flux from depth due to high advection rates (average 60 cm a⁻¹) allowing for significant methane discharge into the water column (2557 $\mu\text{mol cm}^{-2} \text{a}^{-1}$). In comparison, AOM consumes on average 20% of the methane flux from depth at Mound 12. Lower

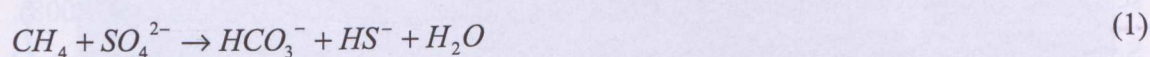
advection rates at this mound (average 29 cm a^{-1}) lead to reduced methane output of $1146 \mu\text{mol cm}^{-2} \text{ a}^{-1}$. Consequently, Mound 11 is a younger and more active feature while Mound 12 is older as increased age and lower activity allows for more methane oxidation at Mound 12. The overall amount of dissolved methane released from the entire mud mounds into the water column was moderate with a discharge of $0.36 \cdot 10^6 \text{ mol a}^{-1}$ at Mound 11, whereas it was calculated as $0.58 \cdot 10^6 \text{ mol a}^{-1}$ at Mound 12, suggesting that mud mounds at the submarine section of the Costa Rica fore arc do not represent a pathway for significant methane discharge from the seafloor.

* Corresponding author (D. Karaca). Fax: +49 431 6002928. E-mail address: dkaraca@ifm-geomar.de

III.1. Introduction

Mud volcanism is an important natural source of the greenhouse gas methane to the hydrosphere and atmosphere (Kopf, 2002; Milkov et al., 2003, Solomon et al., 2009). Recent investigations (e.g. Bohrmann et al., 2003; Pinheiro et al., 2003, Loncke et al., 2004) show that the number of active submarine mud volcanoes might be much higher than previously estimated (ranging from 10^3 to 10^5 ; Milkov, 2000; Milkov et al., 2003) and the gas emitted from deep-sea seeps might reach the upper ocean (Mac Donald et al., 2002; Rehder et al., 2002; Sauter et al., 2006). A number of considerable research efforts have been contributed to the global atmospheric methane budget (e.g. Hovland et al., 1993; Dimitrov, 2002; Etiope, 2004; Judd, 2004; Kvenvolden and Rogers, 2005). However, the quantification of global methane emission from active submarine mud volcanoes and the fate of this discharge remain poorly constrained because of the uncertainties associated with the number of active volcanoes and their gas release (Kopf, 2003; Vogt et al., 1999).

Modern marine sediments, however, account for only 3% of the global methane flux to the atmosphere (Reeburgh, 2003) since much of the dissolved methane ascending to the surface is consumed before reaching the seafloor through anaerobic oxidation of methane (AOM). This process is performed by a consortium of bacteria and archaea, which gain energy by the following reaction:



The methane flux into the water column has been investigated in detail at only a few mud volcanoes such as Håkon Mosby (Sauter et al., 2006), Dvurechenskii (Wallmann et al., 2006; Lichtschlag et al., 2010), Atlante and Cyclope (Henry et al., 1996) and mud mounds off Costa Rica (Mau et al., 2006) based on direct flux measurements or geochemical modeling. However, flux measurements are spatially limited which is the main obstacle for establishing reliable estimates for regional methane fluxes.

Here, we present quantitative estimates of dissolved methane discharge from well-studied mound-shaped structures (Mound 11 and Mound 12) at the submarine segment of the Costa Rica fore-arc margin. Our study is based on (1) fauna distribution mapping related to methane emission by remotely operated vehicle (ROV) Quest; (2) application of numerical

model C.CANDI (Luff et al., 2000) to estimate the amount of methane that is transported into the bottom water considering AOM, molecular diffusion and upward advection; (3) 75-kHz sidescan sonar data for extrapolation of flux measurements taking into account previous estimates of area covered by seabed fauna (Mau et al., 2006). Our model allows for the spatial variability of the seepage and dissolution of methane into seawater. The combination of these geochemical and geoaoustic data via a geographical information system (GIS) provides a novel and systematic approach to estimate methane fluxes compared to other geochemically and hydroacoustically determined fluxes.

III.2. Study Area

The morphology and structure of the continental margin offshore Central America is controlled by the subduction of the Cocos Plate beneath the Caribbean Plate. Subduction erosion is believed to be the dominant process that controls the tectonic evolution of the overriding plate along the Costa Rica Pacific margin at least since ~16Ma (Vannucchi et al., 2003; Ranero & Von Huene, 2000; von Huene, 2004). Those processes provide pathways for fluid circulation at the Costa Rica margin and a great number of dewatering features have been clearly identified on the subducting plate covered by numerous mound-like structures (Sahling et al., 2008; Bohrmann et al., 2002). It has been hypothesized that overpressuring of subducted sediments due to clay mineral dehydration and subsequent upward migration of released fluids significantly affects fluid flow in upper plate sediments, and hence the formation of cold seeps (Hensen et al., 2004; Ranero et al. 2008). Several of these cold seeps have been sampled and show indications for active fluid seepage and emission of methane-rich fluids (Hensen et al., 2004; Linke et al., 2005; Mau et al., 2006; Karaca et al., 2010) and the occurrence of authigenic carbonates and chemosynthetic communities (Sahling et al., 2008).

In our study, we focus particularly on two cold seep sites, Mound 11 and Mound 12, which are referred to geomorphologically as mounds since no clear categorization into structural types has been accomplished (Fig.1). Two mounds are only slightly more than 1 km apart and located 30 km arcward from the trench on the mid slope off Costa Rica at around 1000 m water depth. Mound 11 consists of two distinct summits reaching up to 25 m above the surrounding sea floor whereas Mound 12 has only one cone-shaped summit with 30 m in relief (Klaucke et al., 2008; Schmidt et al., 2005).

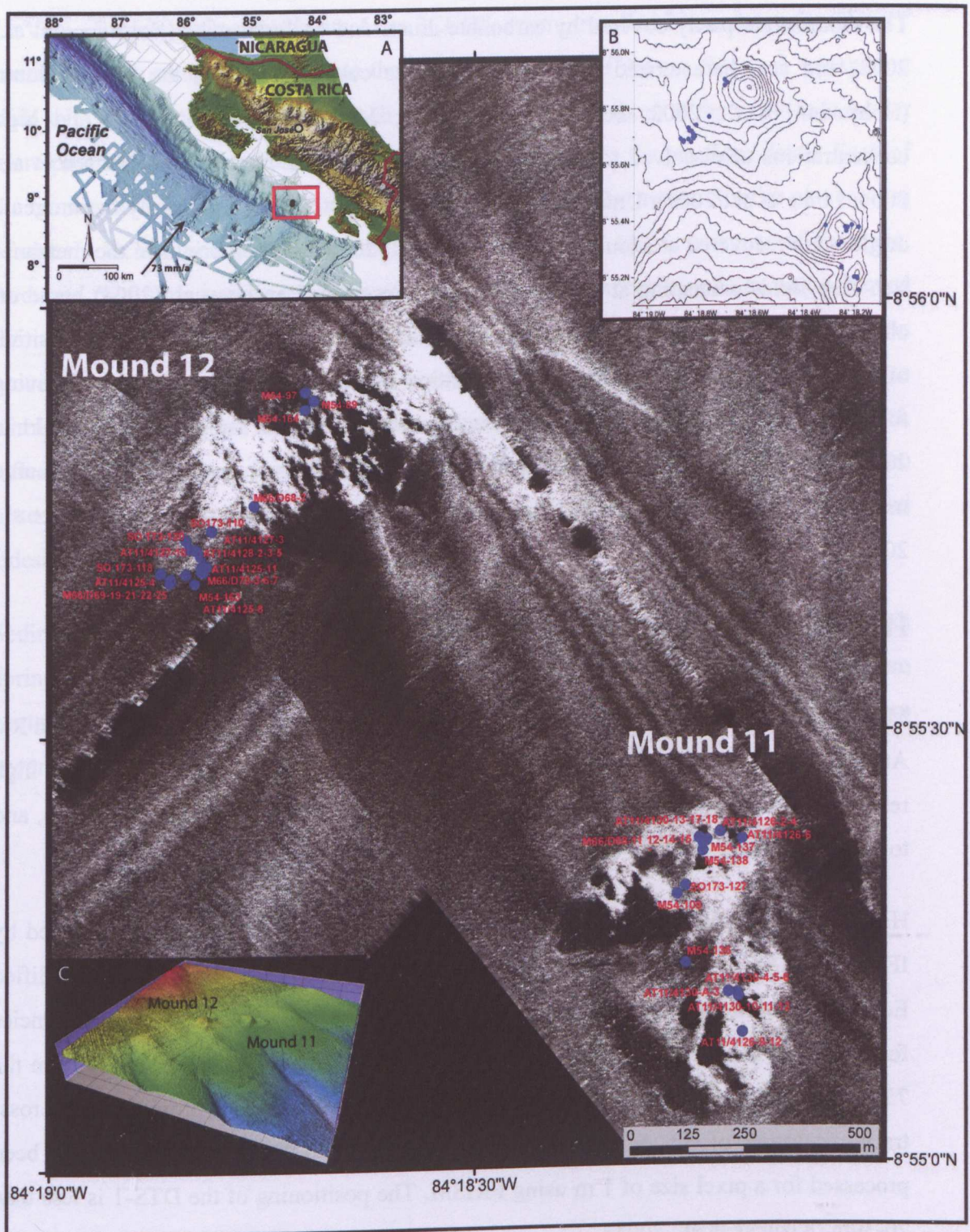


Figure 1. Mosaic of 75 kHz sidescan sonar data of study area at continental margin off Costa Rica with indication for station locations (blue dots); high backscatter intensity is shown in light tones. Insets show overview maps of (A) location, (B) regional bathymetric contours (100 m contours) and (C) 3D view of study area.

The mounds are partly covered by carbonate crusts and bacterial mats (Bohrmann et al., 2002) and are characterized by elevated methane concentrations in the water column (Bohrmann et al., 2002; Schmidt et al., 2005; Mau et al., 2006, 2007) and high concentrations of dissolved methane and sulfide in sediment pore waters (Hensen et al., 2004; Linke et al., 2005). Uniquely, gas hydrates and methane of a primarily thermogenic origin were recovered at Mound 11 (Schmidt et al., 2005). A deep origin of the methane-rich seep fluids emanating at Mound 11 was proposed by Hensen et al. (2004) based on observed chlorinity depletion and boron enrichment, combined with isotopic composition of the fluids, suggesting that fresh water addition by clay mineral dewatering is a driving force of overpressuring and fluid advection. However, seep fluid sampling at Mound 11 in 2005–2006 revealed an unusually high B/Li ratio of the fluids, suggesting that the source may be a mixture of subducted sediment and eroded upper plate material (Tryon et al., 2010).

III.3. Material and Methods

Mound 11 and 12 have been surveyed on expeditions with RV Meteor, RV Sonne and RV Atlantis between 2002 and 2005 (M54; M66; SO173, AT11-28) in order to obtain high resolution side-scan sonar data as well as visual observations from underwater video, and to collect sediment cores.

High resolution side-scan sonar data were obtained using the DTS-1 system operated by IFM-GEOMAR during RV Sonne cruise SO173. The DTS-1 system is a modified EdgeTech dual frequency chirp system working with 75 and 410 kHz centre frequencies for maximum ranges of 750 and 150 m, respectively. Data presented herein are from the 75 kHz signal, which is a 14 ms long pulse of 7.5 kHz bandwidth providing an across-track resolution of 5.6 cm. Towing speed averaged 2.5 kn and the data have been processed for a pixel size of 1 m using PRISM. The positioning of the DTS-1 is less than 20-30m (Klaucke et al., 2008).

Video observations of the seafloor along three tracks (68, 69, and 70; Fig. 2a) of ROV QUEST (Schilling Robotics, model “Quest 5 electric workclass ROV”, based at Marum, Bremen, Germany) during RV Meteor cruise M66 revealed areas with distinct lithologic features and fauna related to seabed methane emission. Recorded video material (camera:

1x Video Broadcast Quality "Insite Atlas 3CCD", zoom, installed 20cm above the QUEST basement) was analysed to estimate the relative coverage of the sea floor. A transparent slide with a 4*5 box raster (where each box counts 5%) was fixed to the monitor to render more precisely the estimation of fauna distribution relative to the sea floor detail. Each of the consecutive freeze images was analysed along each of the tracks. Similar percentages of closely located positions were summarized and assigned to one category of coverage. Accurate positioning and navigation of the ROV with an accuracy of 2m was achieved through the use of an ultra-short baseline positioning system (IXSEA GAPS). Navigation processing of ROV data was achieved according to the method of Schleicher (2006) to eliminate a number of outliers which could result from inaccurate measurements, reflexions at boundary layers of different water bodies or bottom structures. Video observations were exported to ArcGIS 9.3 for analysis in relation to georeferenced sidescan sonar image of the area.

Sediment cores were taken by TV guided multi-corer (TV-MUC), ROV-directed push coring (ROV) and gravity corer (GC). Multi-cores and push core were collected from bacterial mat sites (Tab.1). Flux measurements from individual seeps have been accomplished by the application of the numerical model (Section 4).

Table 1. Details of sampling sites included in this study.

Location	Site description	Core	Gear	Latitude (°N)	Longitude (°W)	Research vessel	Water Depth (cm)
Mound 11	Background	M54-109	GC	8° 55.31'	84° 18.26'	R/V Meteor	1000
		M54-136	GC	8° 55.23'	84° 18.25'	R/V Meteor	1023
		AT11-4130-A	PC	8° 55.19'	84° 18.20'	R/V Atlantis	~1000
	Bacterial Mat	AT11-4130-3	PC	8° 55.19'	84° 18.20'	R/V Atlantis	~1000
		M54-137	TV-MUC	8° 55.37'	84° 18.23'	R/V Meteor	1024
		M54-138	TV-MUC	8° 55.36'	84° 18.23'	R/V Meteor	10 24
		SO173-127	TV-MUC	8° 55.32'	84° 18.25'	R/V Sonne	1 012
		M66-D68/11	PC	8° 55.78'	84° 18.66'	R/V Meteor	105 1
		M66-D68/12	PC	8° 55.78'	84° 18.66'	R/V Meteor	105 1
		M66-D68/14	PC	8° 55.78'	84° 18.66'	R/V Meteor	105 1
		M66-D68/15	PC	8° 55.78'	84° 18.66'	R/V Meteor	105 1
		AT11-4126-2	PC	8° 55.38'	84° 18.20'	R/V Atlantis	~1000
		AT11-4126-4	PC	8° 55.38'	84° 18.20'	R/V Atlantis	~1000
		AT11-4126-6	PC	8° 55.37'	84° 18.18'	R/V Atlantis	~1000
		AT11-4126-9	PC	8° 55.14'	84° 18.18'	R/V Atlantis	~1000
		AT11-4126-12	PC	8° 55.14'	84° 18.18'	R/V Atlantis	~1000
		AT11-4130-4	PC	8° 55.19'	84° 18.18'	R/V Atlantis	~1000
		AT11-4130-5	PC	8° 55.19'	84° 18.18'	R/V Atlantis	~1000
		AT11-4130-6	PC	8° 55.19'	84° 18.18'	R/V Atlantis	~1000
		AT11-4130-10	PC	8° 55.19'	84° 18.18'	R/V Atlantis	~1000
AT11-4130-11	PC	8° 55.19'	84° 18.18'	R/V Atlantis	~1000		
AT11-4130-12	PC	8° 55.19'	84° 18.18'	R/V Atlantis	~1000		
AT11-4130-13	PC	8° 55.37'	84° 18.22'	R/V Atlantis	~1000		
AT11-4130-17	PC	8° 55.37'	84° 18.22'	R/V Atlantis	~1000		
AT11-4130-18	PC	8° 55.37'	84° 18.22'	R/V Atlantis	~1000		
Mound 12	Background	M54-89	GC	8° 55.89'	84° 18.69'	R/V Meteor	997
		M54-97-2	GC	8° 55.90'	84° 18.70'	R/V Meteor	1001
		M54-164	GC	8° 55.88'	84° 18.70'	R/V Meteor	1022
	Bacterial Mat	SO173/118	TV-MUC	8° 55.69'	84° 18.84'	R/V Sonne	1018
		SO173/120	TV-MUC	8° 55.73'	84° 18.84'	R/V Sonne	1 011
		M54-163-3	TV-MUC	8° 55.68'	84° 18.83'	R/V Meteor	1024
		M66-D58/2	PC	8° 55.78'	84° 18.66'	R/V Meteor	1051
		M66-D69/19	PC	8° 55.74'	84° 18.82'	R/V Meteor	102 0
		M66-D69/22	PC	8° 55.74'	84° 18.82'	R/V Meteor	102 0
		M66-D69/25	PC	8° 55.74'	84° 18.82'	R/V Meteor	102 0
		M66-D70/3	PC	8° 55.66'	84° 18.79'	R/V Meteor	1022
		M66-D70/6	PC	8° 55.66'	84° 18.79'	R/V Meteor	1022
		M66-D70/7	PC	8° 55.66'	84° 18.79'	R/V Meteor	1022
		AT11-4125-4	PC	8° 55.69'	84° 18.87'	R/V Atlantis	~1000
		AT11-4125-8	PC	8° 55.69'	84° 18.82'	R/V Atlantis	~1003
		AT11-4125-11	PC	8° 55.72'	84° 18.81'	R/V Atlantis	~1005
		AT11-4127-3	PC	8° 55.72'	84° 18.83'	R/V Atlantis	~1007
		AT11-4127-10	PC	8° 55.72'	84° 18.83'	R/V Atlantis	~1008
		AT11-4128-2	PC	8° 55.71'	84° 18.82'	R/V Atlantis	~1009
		AT11-4128-3	PC	8° 55.71'	84° 18.82'	R/V Atlantis	~1010
AT11-4128-5	PC	8° 55.71'	84° 18.82'	R/V Atlantis	~1011		

III.4. Model set-up

The reactive-transport model C.CANDI (Luff et al., 2000) was applied to investigate rates of upward fluid flow and CH₄ turnover at sampled locations. The model describes transport process for 5 dissolved species in the pore water (SO₄, CH₄, HS, H₂S, Cl) forced by advection and molecular diffusion (see Luff et al., 2000 and Luff and Wallmann, 2003 for a more detailed model description).

The model considers molecular diffusion and advection based on the following differential equation (after Berner, 1980):

$$\phi \frac{\partial C_w}{\partial t} = \frac{\partial}{\partial x} \left(\phi(x) D(x) \frac{\partial C_w}{\partial x} \right) - \frac{\partial}{\partial x} (v(x) \phi(x) C_w) + \phi(x) \sum R_w \quad (2)$$

where C_w is the concentration of dissolved species (mmol cm⁻³), $D(x)$ is the molecular diffusion coefficient corrected for tortuosity (cm² a⁻¹), $v(x)$ is the pore water velocity (cm a⁻¹), Φ is the porosity, and $\sum R_w$ (μmol cm⁻³ a⁻¹) is the rate of all diagenetic reactions affecting dissolved species.

Sediment porosity changes with depth due to sediment compaction. The depth profile is approximated by fitting the measured data with:

$$\phi = (\phi_0 - \phi_\infty) * \text{Exp}(-const \cdot x) + \phi_\infty \quad (3)$$

where ϕ_∞ and ϕ_0 are the porosity at infinite depth and at sediment surface, and $const$ is the attenuation coefficient for the exponential decrease of porosity with depth.

The upward flow velocity v_0 was determined by fitting the model to the dissolved chloride profiles. The upward directed pore water flux is composed of the downward burial component modified by compaction and the upward fluid advection:

$$v(x) = \frac{\omega_\infty \cdot \phi_\infty - v_0 \cdot \phi_0}{\phi(x)} \quad (4)$$

where $v(x)$ represents the depth-dependent fluid flow velocity (cm a^{-1}) and v_0 is the surface value of the fluid flow velocity (cm a^{-1}).

Temperature-dependent molecular diffusion coefficients of dissolved species were calculated after Boudreau (1997) and corrected for porosity decrease:

$$D_s(x) = \frac{D_0(x)}{1 - \ln(\phi(x))^2} \quad (5)$$

where D_0 is the molecular diffusion coefficient in seawater ($\text{cm}^2 \text{a}^{-1}$).

The kinetic constant of AOM (k_{AOM}) determined by fitting the pore water profiles of sulfate, and hydrogen sulfide is applied to define the rate of anaerobic methane oxidation (R_{AOM}) considering second order kinetics:

$$R_{AOM} = k_{AOM} [CH_4] [SO_4^{2-}] \quad (6)$$

Constant concentrations were prescribed at the upper and lower boundary of the model column (Dirichlet boundary conditions). In general, upper boundary conditions were chosen to represent regional seawater composition while lower boundary values reflect the composition of the deep fluid. All simulations were performed assuming steady state conditions ($dc/dt \approx 0$). The vertical resolution of the model grid was set to 1000 layers in order to resolve the steep pore water gradients for the overall simulation time of 100,000 years. Parameter values chosen for each model run are listed in Table 2.

Table 2. Summary of parameter values used for the steady state simulations at all seep locations. Temperature (4.72°C), salinity (34.57 PSU) and pressure (100.61 atm) values applied for all seeps were taken from CTD measurements. Methane concentration of 68 mM applied for all seeps represent methane hydrate saturation (Tishchenko et al., 2005) at the lower boundary. BW indicates concentrations of dissolved species at the upper boundary of the model column; whereas BS indicates concentrations of dissolved species at the bottom of the sediment column.

* $BWCH_4/BSCH_4$ is applied as 0/68 mM at all stations.

Stations	Model parameters values				Porewater concentrations*			
	Length of simulated core (cm)	Porosity at sediment surface	Porosity at large sediment depth	Maximum depth of bioirrigation	Bioirrigation coefficient	BW Cl/BS Cl (mM)	BWSO ₄ /BS SO ₄ (mM)	BWTH ₂ S/BSTH ₂ S (mM)
Mound 11								
M54-109	230	0.738	0.620	130	1	548/204	28.43/0	0/0.5
M54-136	205	0.754	0.705	50	2	551/263	27.40/0	0/0.6
AT11-4130-A	40	0.727	0.536	15	35	528/501	27.12/0	0/0
AT11-4130-3	30	0.627	0.565	9	30	529/500	27.01/0	0/0
M54-137	22	0.834	0.709	-	-	550/397	28.2/0	0.01/6
M54-138	27.5	0.872	0.726	-	-	551/210	28.19/0	
SO173-127	24.50	0.827	0.695	-	-	553/234	28.36/0	
M66-D68/11	30	0.617	0.502	6	40	563/333	29/0	0.1/7
M66-D68/12	25	0.634	0.540	-	-	557/461	27.70/0	0.3/4.7
M66-D68/14	25	0.626	0.528	6	30	565/421	29/0	0.03/5
M66-D68/15	25	0.633	0.497	10	19	563/451	29.10/0	0.01/10
AT11-4126-2	30	0.731	0.580	10	20	540/404	28.03/0	0/3.82
AT11-4126-4	30	0.731	0.576	-	-	540/225	28.03/0	0/0
AT11-4126-6	35	0.731	0.558	15	20	534/457	27.64/0	0/3
AT11-4126-9	30	0.731	0.576	-	-	540/480	28.43/0	0/9.5
AT11-4126-12	30	0.768	0.573	-	-	522/464	28.23/0	0/8
AT11-4130-4	24.50	0.627	0.565	-	-	550/219	28.69/0	0/0
AT11-4130-5	22	0.627	0.565	-	-	550/200	29.79/0	0/0
AT11-4130-6	22	0.627	0.565	-	-	540/210	28.13/0	0/0
AT11-4130-10	25	0.627	0.589	-	-	545/193	28.41/0	0/0
AT11-4130-11	20	0.627	0.528	-	-	550/217	28.01/0	0/0
AT11-4130-12	25	0.615	0.627	3	60	511/180	28.06/0	0/0.009
AT11-4130-13	26	0.649	0.529	-	-	5511/259	28.93/0	0/0
AT11-4130-17	20	0.627	0.528	-	-	542/244	28.29/0	0.002/0
AT11-4130-18	22	0.627	0.565	-	-	528/300	28.06/0	0.003/0.002
Mound 12								
M54-89	500	0.659	0.665	100	100	545/491	28.17/0	0.003/4.11
M54-97-2	370	0.732	0.642	150	9	552/360	28.39/0	0/0.2
M54-164	285	0.728	0.690	170	150	558/560	28.71/0	0.003/6
SO173-118	32	0.858	0.729	-	-	555/558	28.72/0	0.1/12
SO173-120	31.50	0.860	0.699	14	10	554/559	29.31/0	0.01/13.32
M54-163-3	30	0.847	0.755	18	20	549/558	27.83/0	
M66-D58/2	20	0.674	0.502	-	-	566/566	28.90/0	0.1/15
M66-D69/19	25	0.657	0.534	-	-	557/563	28.50/0	0/16
M66-D69/22	25	0.616	0.521	5	1	552/567	28.30/0	0.06/15.11
M66-D69/25	25	0.579	0.527	-	-	557/562	28/0	0/15.13
M66-D70/3	25	0.639	0.521	-	-	549/547	28.22/0	0.6/17
M66-D70/6	25	0.615	0.484	-	-	549/556	28.06/0	1/17.60
M66-D70/7	25	0.610	0.529	8	1	548/553	28.47/0	0.2/22.18
AT11-4125/4	30	0.787	0.602	8	1	529/530	28.25/0	1.39/11
AT11-4125-8	50	0.787	0.590	15	1	531/529	28.53/0	0/0.73
AT11-4125-11	25	0.702	0.528	-	-	526/528	28.98/0	0.09/10
AT11-4127-3	35	0.758	0.561	3	2	532/532	28.45/0	0.2/3.69
AT11-4127-10	35	0.755	0.579	3	2	526/531	28/0	0/3.61
AT11-4128-2	30	0.663	0.557	-	-	528/528	28.71/0	0.003/10.90
AT11-4128-3	30	0.668	0.557	-	-	528/531	28/0	6.52/12.50
AT11-4128-5	30	0.675	0.545	-	-	530/530	28.95/0	0.001/10.60

III.5. Results

III.5.1. Seafloor observations

Using ROV Quest, large parts of Mound 12 and a part of the NW cone of Mound 11 were surveyed along three tracks (68, 69, and 70) (Fig. 2a). Video observations of Mound 11 and Mound 12 showed carbonate coverage at each mound through the areas represented by high backscatter intensity in the sidescan sonar image (Fig.2b). More abundant carbonate coverage was observed at Mound 12 (50-100%) than Mound 11 (<10%), although the extent of video transects at Mound 11 is limited.

Bacterial mats observed at Mound 12 are not widespread along the tracks but are abundant around the active seep sites at the western flank of the mound corresponding to a moderate backscatter area (Fig.2c). ROV dives showed that the mat had an elongated shape stretching over tens of metres. It was probably aligned along a fracture where methane-charged fluids and/or methane gas bubbles ascend to the surface. Distribution of bacterial mats at Mound 11 is within the limit of the track and densely populated at across the NW cone. A large bacterial mat located close to the top of mound had an elongated shape with a length of approximately 3 m while the width of the mat varied in between 0.2 and 1.5 m (Brückmann et al., 2009).

Extensive areas of *Calypptogena* sp in association with *Bathymodiolus* sp and Vestimentiferan tube worms were also observed at NW cone of Mound 11. No bubble-releasing seeps were observed during ROV surveys. Molluscs of *Calypptogena* sp. are widespread at each mound, but no live clams or mussels were observed (Fig.2d). At the western flank of Mound 12, the seafloor morphology is relatively uniform with large platform-like structures. These structures are associated with Vestimentiferan tube worms and large amounts of dead bivalves of *Bathymodiolus* sp.

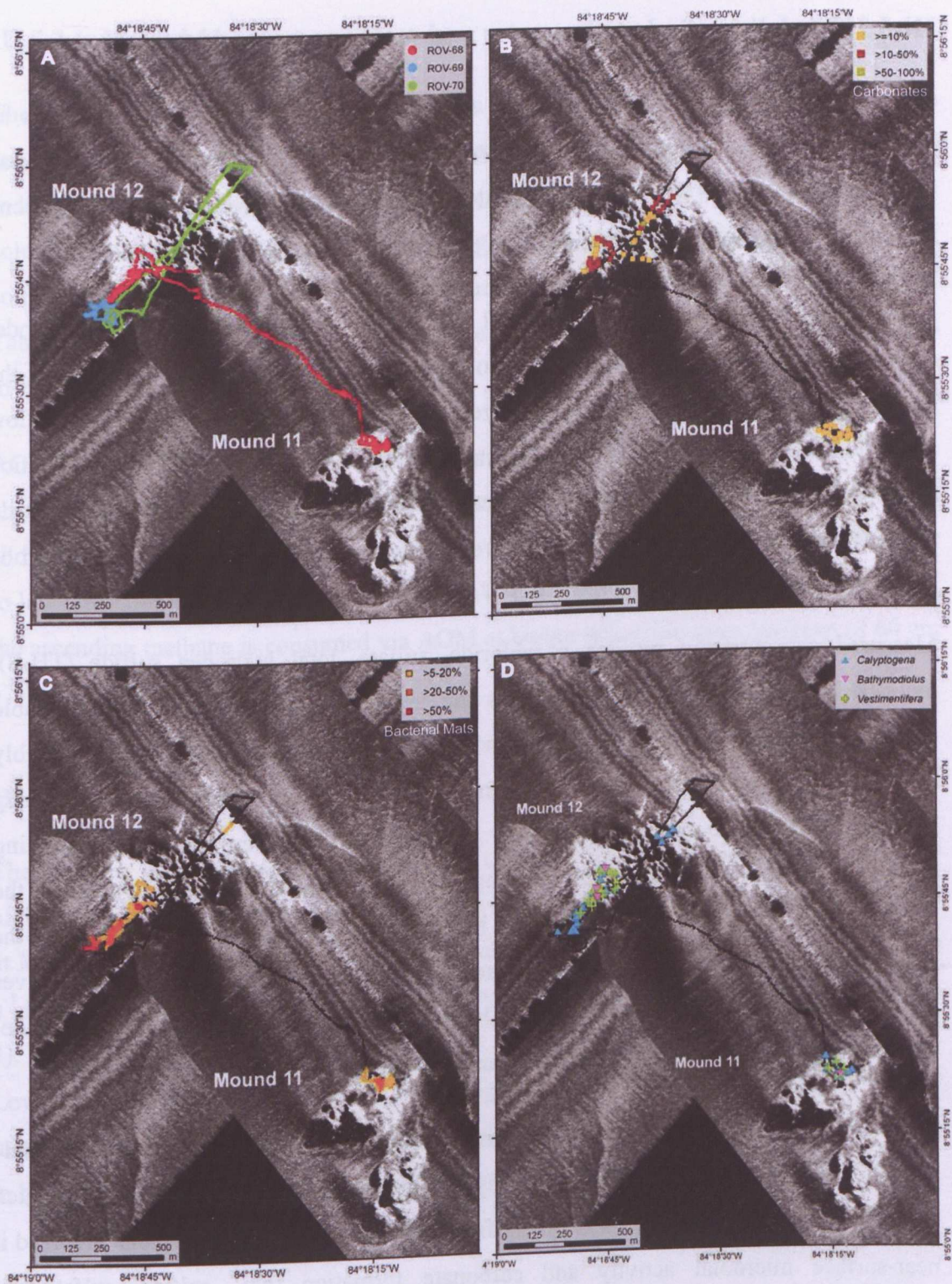


Figure 2. Sea-floor observation maps of study area overlain with sidescan sonar image as background showing (A) positions of ROV tracks, (B) distribution of authigenic carbonates, (C) distribution of bacterial mats, (D) other seep related fauna biota.

III.5.2. Modeling of advection rates and methane turnover

A total of 21 push and TV-guided multi cores were taken from bacterial mat sites at Mound 11, whereas 18 push and TV-guided multi cores were collected from bacterial mats at Mound 12 (Tab. 1). Additional push and gravity cores were taken from background sediments on both mounds. No cores were collected from clam fields.

Using the model presented in section 4, all cores were simulated into steady state. Model runs showed that the best steady state fit to the measured data was obtained applying the combination of parameter values summarized in Table 2. The rates for upward fluid flow and AOM were determined by fitting the model to the data. POC-based sulfate reduction was considered to be negligible at cold seeps at the Costa Rican margin (Karaca et al., 2010). Previous studies showed that the overall biogeochemical turnover is dominated by AOM and associated processes (Luff and Wallmann 2003).

Measured concentration profiles of chloride, sulfate, total hydrogen sulfide (TH₂S), methane and alkalinity of selected cores are presented in Figures 3-4. Considerable deviations exist only for methane profiles where measured concentrations are considerably lower than simulated values. This discrepancy is due to the loss of methane via degassing from the sediment during core recovery. Methane profiles were simulated assuming methane saturation of the upward migrating fluid with respect to methane hydrate at the lower boundary (Tishchenko et al., 2005). Methane flux calculations does not include the release of gaseous methane and the methane fluxes during peak discharges, it rather gives the methane discharge into the overlying bottom water during the current period of dewatering considering both fluid advection and molecular diffusion.

There are significant differences in the fluid composition of pore waters from Mound 11 and Mound 12 (Figures 3 and 4, respectively). For instance, the composition of pore waters from Mound 12 are only slightly different from seawater, except for those ions involved in near-surface microbial activity and carbonate formation (e.g., sulfide, sulfate and alkalinity). In comparison, fluids from Mound 11 deviate significantly from seawater showing a general trend of freshening indicated by low Cl concentrations (Hensen et al., 2004). In general, dissolved hydrogen sulfide and alkalinity profiles display maxima within the sulfate-methane transition zone indicating the predominance of AOM for the depletion of sulfate at bacterial mats at both mounds.

III.5.2.1. Mound 11

The advection rates of the pore fluid ranges in total from 0.1 to 200 cm a⁻¹ (Tab. 3), with an average of 60 cm a⁻¹ in bacterial mats compared to only 2 cm a⁻¹ in surrounding sediments (Tab. 3). High flow rates at bacterial mats cause an increased influx of all solutes into shallow subsurface sediments (Fig. 3) and reduce the efficiency of the AOM so that higher amounts of dissolved methane are emanating into the water column (Fig. 5; Tab. 4). Methane fluxes range from an average of 2557 $\mu\text{mol cm}^{-2} \text{a}^{-1}$ in the bacterial mats to 100 $\mu\text{mol cm}^{-2} \text{a}^{-1}$ in background sediments.

AOM is most efficient at low and intermediate flow rates and acts as a filter to reduce the amount of methane which is released into the water column (Fig. 5). Our model results show that AOM consumes an average of 58% of the methane flux from greater depth due to low advection rates (average of 2 cm a⁻¹) in background sediments, whereas only 8% of the ascending methane is consumed via AOM at higher advection rates (average of 60 cm a⁻¹) in bacterial mat fields.

III.5.2.2. Mound 12

The resulting pore fluid advection at Mound 12 varies between 0.1 and 100 cm a⁻¹. The highest advection of 100 cm a⁻¹ at Mound 12 is lower than the calculated highest advection at Mound 11. Similarly, average advection rates of 29 cm a⁻¹ in bacterial mats and 0.4 cm a⁻¹ in background sediments are much lower than the rates calculated for Mound 11 (Tab. 4).

Lower fluid flow rates at this mound cause higher efficiencies of AOM and decrease the methane discharge into the water column ranging from an average of 1146 $\mu\text{mol cm}^{-2} \text{a}^{-1}$ in bacterial mats to 9.7 $\mu\text{mol cm}^{-2} \text{a}^{-1}$ in background sediments (Fig. 5; Tab. 4).

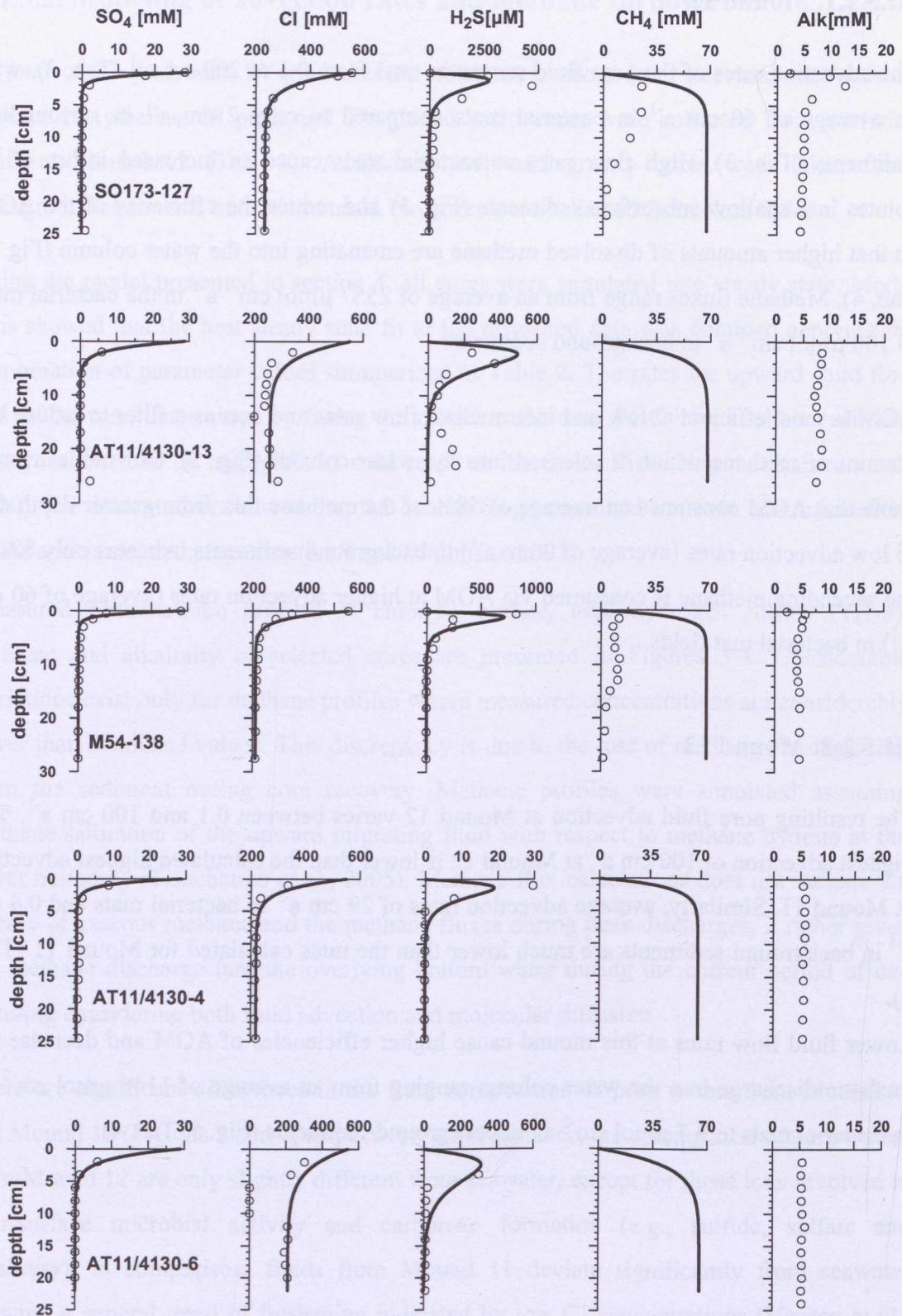


Figure 3. Measured (dots) and simulated (solid lines) concentration profiles of sulfate, chloride, total hydrogen sulfide (TH₂S), methane and alkalinity in selected stations at Mound 11.

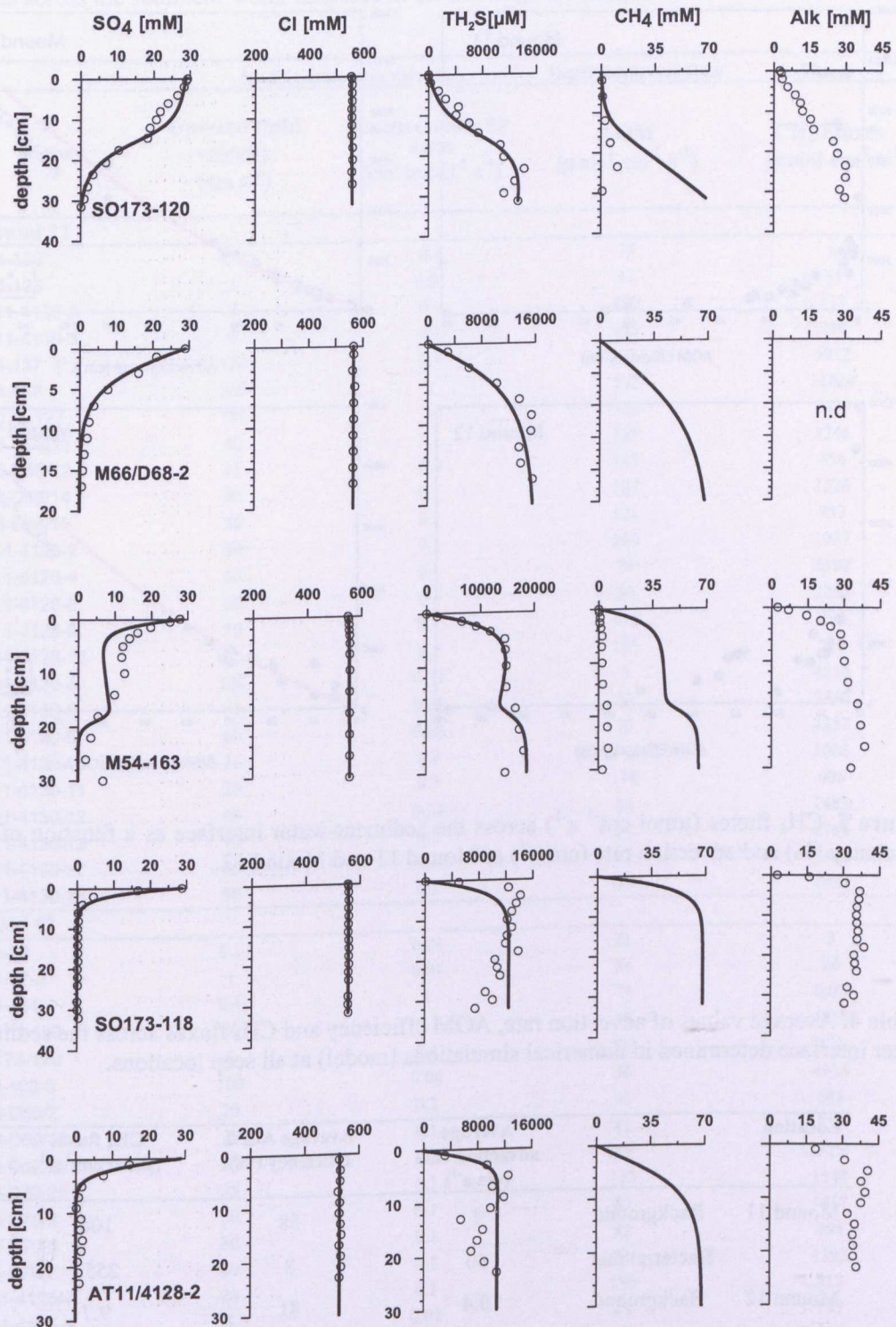


Figure 4. Measured (dots) and simulated (solid lines) concentration profiles of sulfate, chloride, total hydrogen sulfide (TH_2S), methane and alkalinity in selected stations at Mound 12.

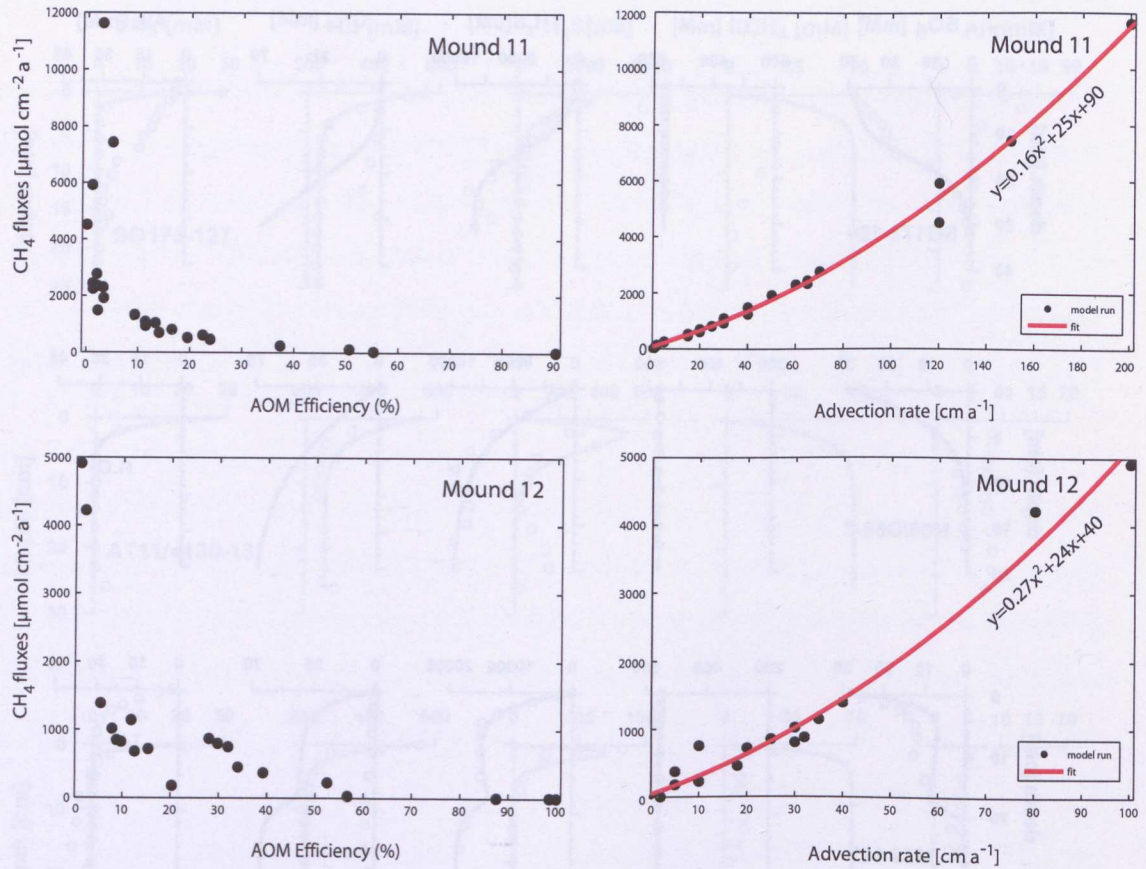


Figure 5. CH_4 fluxes ($\mu\text{mol cm}^{-2} \text{a}^{-1}$) across the sediment-water interface as a function of AOM efficiency (%) and advection rate (cm a^{-1}) at Mound 11 and Mound 12.

Table 4. Average values of advection rate, AOM efficiency and CH_4 fluxes across the sediment-water interface determined in numerical simulations (model) at all seep locations.

Location		Average advection rate (cm a^{-1})	Average AOM efficiency (%)	CH_4 fluxes ($\mu\text{mol cm}^{-2} \text{a}^{-1}$)
Mound 11	Background	2	58	100
	Bacterial mat	60	8	2557
Mound 12	Background	0.4	81	9.7
	Bacterial mat	29	20	1146

Table 3. Summary of parameter values determined by fitting the steady state simulations to measured data (upward fluid velocity and k_{AOM}) and depth integrated rate of AOM and methane fluxes across the sediment-water interface at the investigated stations.

Stations	Model parameters values		Depth integrated Rate	Fluxes
	Upward fluid velocity (cm a^{-1})	Kinetic constant for AOM ($\text{cm}^3 \text{mmol}^{-1} \text{a}^{-1}$)	AOM ($\mu\text{mol cm}^{-2} \text{a}^{-1}$)	CH_4 Fluxes ($\mu\text{mol cm}^{-2} \text{a}^{-1}$)
Mound 11				
M54-109	0.1	0.1	75	8
M54-136	1	0.01	42	34
AT11-4130-A	2	0.1	120	117
AT11-4130-3	5	0.1	143	240
M54-137	120	0.1	62	5912
M54-138	200	1	352	11624
SO173-127	150	1	385	7429
M66-D68/11	40	0.1	125	1246
M66-D68/12	15	0.2	143	456
M66-D68/14	40	0.1	137	1326
M66-D68/15	30	0.1	121	932
AT11-4126-2	30	0.1	160	1037
AT11-4126-4	60	0.1	78	2300
AT11-4126-6	60	0.1	30	2252
AT11-4126-9	20	0.1	113	690
AT11-4126-12	15	0.1	126	519
AT11-4130-4	120	0.01	3	4516
AT11-4130-5	65	0.05	31	2440
AT11-4130-6	60	0.05	30	2252
AT11-4130-10	30	0.2	140	1085
AT11-4130-11	20	0.3	176	606
AT11-4130-12	40	0.02	34	1483
AT11-4130-13	70	0.1	57	2765
AT11-4130-17	65	0.1	51	2347
AT11-4130-18	50	0.1	67	1922
Mound 12				
M54-89	0.1	0.01	21	3
M54-97-2	1	0.01	34	26
M54-164	0.1	1	79	0.07
SO173-118	80	0.1	92	4218
SO173-120	5	0.1	239	371
M54-163-3	100	0.06	56	4916
M66-D58/2	20	0.1	98	683
M66-D69/19	25	0.1	82	851
M66-D69/22	25	0.1	89	825
M66-D69/25	35	0.3	153	1143
M66-D70/3	30	0.1	87	1017
M66-D70/6	30	0.1	82	994
M66-D70/7	40	0.1	81	1392
AT11-4125/4	20	0.1	130	717
AT11-4125-8	5	0.01	45	177
AT11-4125-11	10	1	354	755
AT11-4127-3	10	0.5	247	224
AT11-4127-10	10	0.5	247	224
AT11-4128-2	30	1	340	802
AT11-4128-3	32	1	339	874
AT11-4128-5	18	0.5	233	454

III.5.3. Estimation of regional methane release

To estimate the amount of methane emitted from each of the studied mounds, the total area covered by the prevailing type of vent fauna (bacterial mats) and background sediments were multiplied by average methane fluxes at the sediment/water interface. The area estimates are based on seafloor observations and side scan sonar mapping wherein video control of the sampling site is a prerequisite, but the area to which the measurements can be extrapolated requires mapping with geoacoustic tools.

Side scan sonar images indicate that the backscatter intensity of the southern and northern flanks of Mound 12 are similar to the surrounding sediment, while the backscatter intensity of the summit and western flank are higher (Fig. 6). The central mound is covered by a few meters of sediment on the northern and southern flanks, but only a very thin sediment layer on the western flank (Klaucke et al., 2008). This western flank is bounded by a 0.05 km² zone of medium backscatter intensity corresponding very well to the distribution of bacterial mats (Fig. 2c). No bacterial mats occur within the high backscatter intensity on side scan sonar records.

To estimate the validity of point flux measurements in a regional context and to extrapolate to regional flux values, the region of medium backscatter intensity (Fig. 6) covering of about 25% of the total mound was assumed to be representative for bacterial mats, whereas the rest of the mound (75 %) was considered as background sediments. It should be noted that 80% of all seeps occur in the moderate backscatter areas but only a few (20%) are found in the high backscatter areas.

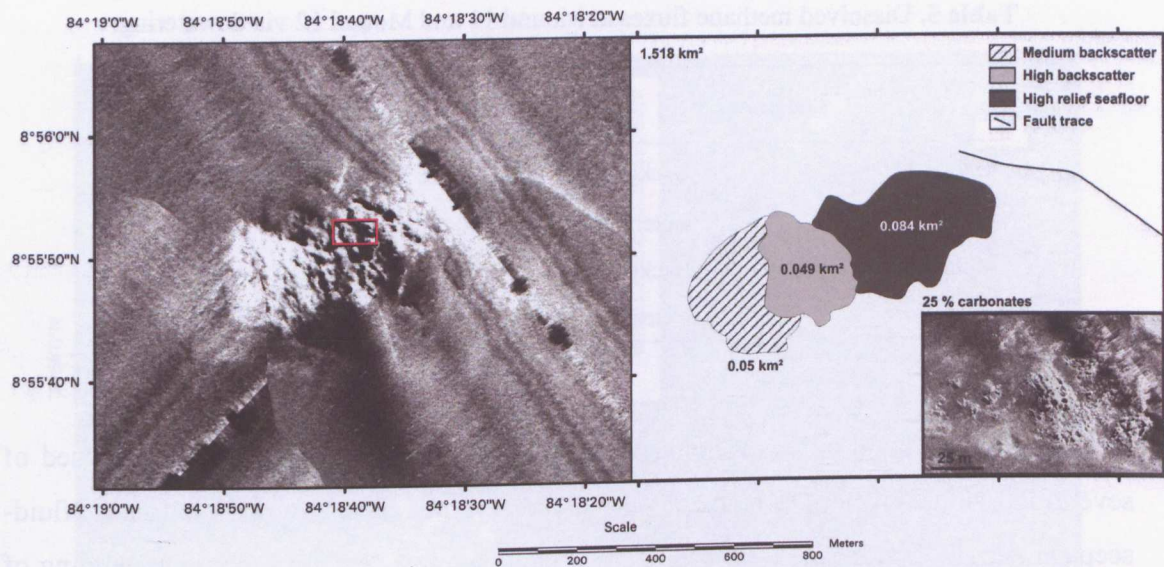


Figure 6. Map of interpolation of 75 kHz sidescan sonar data of Mound 12 and calculated surface extension for different areas. The inset shows details from the high relief seafloor area.

Backscatter intensity of the area covered by bacterial mats at Mound 12 is well correlated with classification of the side scan sonar mosaic map (Fig. 7). Based on the number of backscatter values, three backscatter classes via GIS were created; areas with low backscatter (class 1), areas with medium backscatter (class 2) and areas with high backscatter (class 3; Fig. 7). This approach uses only image grayscale values as representation of backscatter strength, rather than any detailed characteristics of the backscatter signal itself. However, it reveals a good correlation with high methane fluxes observed in the field of bacterial mats. Highest methane fluxes intersect with the medium backscatter intensity corresponding to a backscatter class of 2. In this regard, the average methane flux of $1146 \mu\text{mol cm}^{-2} \text{a}^{-1}$ in the field of bacterial mats is, thus, assumed to be typical for that habitat and used to extrapolate to total emission of dissolved methane to $0.57 \cdot 10^6 \text{ mol a}^{-1}$ (Tab. 5). The methane emission in background sediments, calculated by multiplying the average methane flux of $9.7 \mu\text{mol cm}^{-2} \text{a}^{-1}$ and area occupied (0.133 km^2) results in $0.01 \cdot 10^6 \text{ mol a}^{-1}$.

Table 5. Dissolved methane fluxes at Mound 11 and Mound 12 via dewatering.

Location		Total area (km ²)	CH ₄ fluxes (in 10 ⁶ mol a ⁻¹)
Mound 11	Background	0.167	0.17
	Bacterial mat	0.0074	0.19
Mound 12	Background	0.133	0.01
	Bacterial mat	0.05	0.57

In the case of Mound 11, morphology is rugged on two distinct summits composed of several individual edifices (Klaucke et al., 2008; Tryon et al., 2010). In addition, all fluid-seepage activity is concentrated within the double summit area that prevents mapping of different backscatter intensities on side scan sonar images and consequently estimating the area covered by bacterial mats with a good accuracy. We derived the total methane emission output in bacterial mats using the first order estimates for the total area covered by bacterial mats (max. 1700 m²) reported by Mau et al. (2006). Their estimate is based on the total surveyed area of 0.04 km² which is one fourth of the total area of Mound 11 calculated as 0.175 km² in this study. For the total area estimate of 0.175 km² at Mound 11, we calculated a total methane emission output of 0.19·10⁶ mol a⁻¹ in bacterial mats based on average methane flux of 2557 μmol cm⁻² a⁻¹ (Tab. 5) and area occupied (4x1700m²). This value falls to 0.17·10⁶ mol a⁻¹ in background sediments calculated by multiplying the average methane flux of 100μmol cm⁻² a⁻¹ and area occupied (0.167 km²).

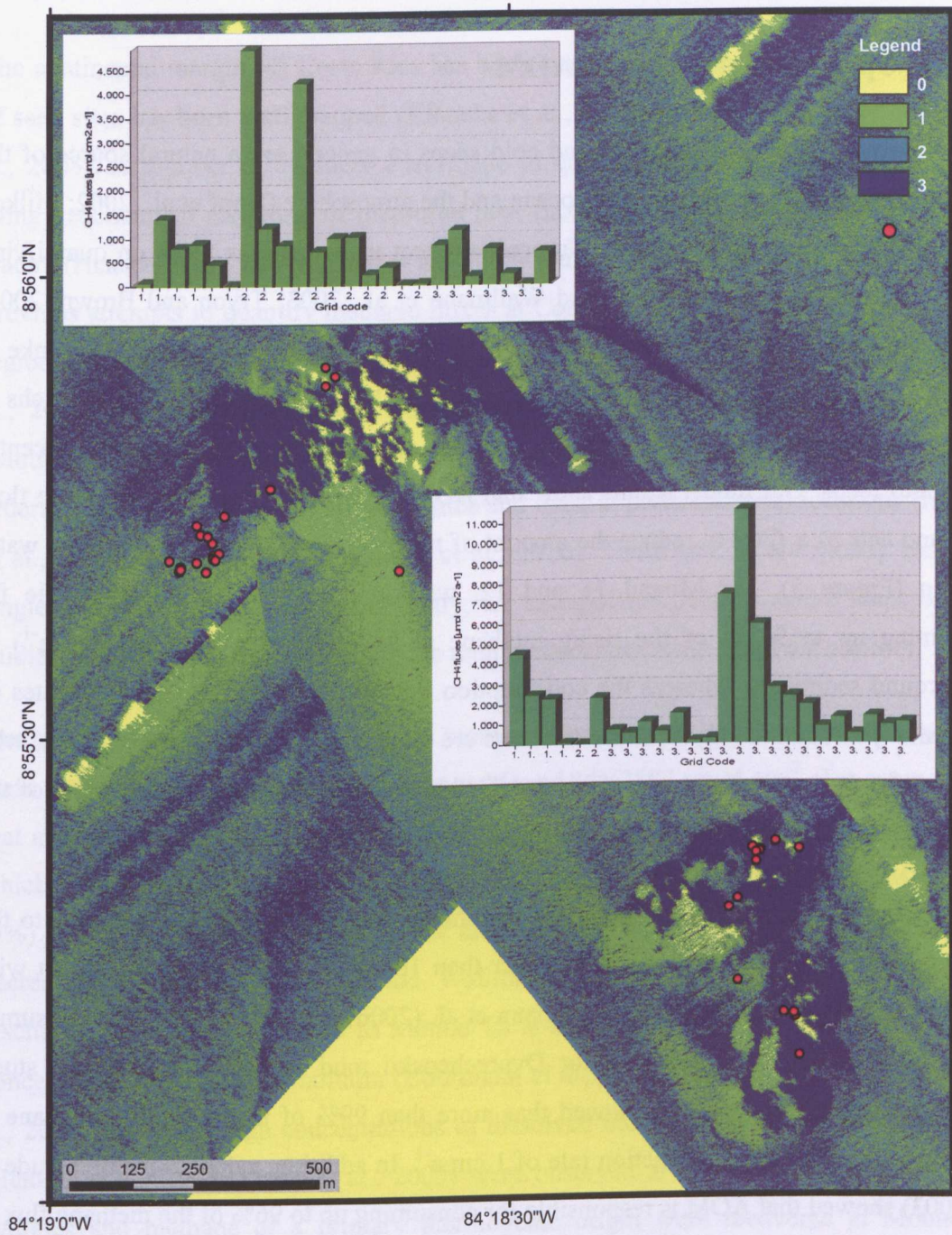


Figure 7. Classified sidescan sonar mosaic map of Mound 11 and Mound 12, including intersection with geochemical methane point sources (red dots).

III.6. Discussion

III.6.1. Upward advection and AOM

Mud volcanoes, hydrocarbon seeps and cold seeps in general are a natural source of the greenhouse gas methane fluxes to the ocean and the atmosphere (Kopf et al., 2002; Milkov et al., 2003; Solomon et al., 2009). Numerous recent investigations focus on quantifying CH_4 flux from the sea floor (Luff and Wallmann et al., 2003; Tryon and Brown, 2001; Wallmann et al., 2006; Torres et al., 2002; Mau et al., 2006; Haese et al., 2003; Linke et al., 2005; Sommer et al., 2006) and mechanism of AOM (Boetius et al., 2000, Hinrichs et al., 1999). However, the effect of fluid flow rate on AOM efficiency has only recently come into focus. Our model results show that AOM is most efficient at intermediate flow rates and acts as a filter to reduce the amount of methane which is released into the water column (Figure 5). For Mound 11 and 12, we found that AOM is responsible for consuming up to 95 % of the rising methane at low advection rates ($<1 \text{ cm a}^{-1}$) in background sediments, whereas the consumption falls to 1% at higher advection rates ($>100 \text{ cm a}^{-1}$) in bacterial mats. Those numbers are confirmed by Karaca et al. (2010), who reported for at bacterial mat site of Mound 11 that AOM consumes about only 2% of the ascending methane at a high advection rate of 200 cm a^{-1} .

Overall, our simulation results show that significant amounts of methane escape into the bottom water only at fluid flow rates higher than 10 cm a^{-1} , which is in agreement with results from other seep locations. Wallmann et al. (2006) calculated that AOM consumes about 80% of the rising methane for Dvurechenskii mud volcano. Their model study presented systematic runs and showed that more than 99% of the ascending methane is consumed by AOM at an advection rate of 1 cm a^{-1} . In addition, calculations of Treude et al (2003) showed that AOM is responsible for consuming up to 96% of the methane flux at an advection rate of 10 cm a^{-1} . Furthermore, Haese et al. (2003) calculated that 100% of the ascending methane is anaerobically oxidized within surface sediments at fluid flow rates of $3\text{-}5 \text{ cm a}^{-1}$ at the Kazan mud volcano confirming that methane is only released into the bottom water at high fluid flow velocities.

III.6.2 Estimation of methane emission at Mound 11 and Mound 12

The continental margin off Costa Rica has been extensively surveyed and the distribution of seep sites has been well mapped (Klaucke et al., 2008; Ranero et al., 2008; Sahling et al., 2008). A number of attempts were made to quantify the fluid fluxes in this region using geochemical modeling of measured heat fluxes and concentration profiles in pore waters (Hensen et al., 2004; Linke et al., 2005; Ranero et al., 2008, Karaca et al., 2010). Previous attempts to quantify methane fluxes at Costa Rican mounds in the outer fore-arc region were based on observed methane concentrations in the near-bottom water (Mau et al., 2006). However, published fluid flux estimates for five of the major cold vents (Mound Culebra, Mound 10, Mound 11, Mound 12, Quepos Slide) vary over several orders of magnitude between different sites and even at particular seep locations (Hensen et al., 2004; Mau et al., 2006, Karaca et al., 2010). These studies are mostly based on single seep flux estimations. In our study, we extrapolated over 25 active seeps of each studied mound that allows estimating the total methane discharge from the seafloor.

Our calculations show that the average methane flux into the overlying bottom water in areas covered by bacterial mats is higher at Mound 11 ($2557 \mu\text{mol cm}^{-2} \text{a}^{-1}$) compared to that at Mound 12 ($1146 \mu\text{mol cm}^{-2} \text{a}^{-1}$). Furthermore, the average proportion of methane which is oxidized by AOM is much higher at Mound 12 (20%) compared to Mound 11 (8%). Since an increasing portion of the deep methane flux is consumed by AOM, with decreasing advection rate (Luff and Wallmann, 2003), higher amounts of methane discharge at Mound 11 relative to Mound 12 is expected. Previously, elevated methane concentrations in the water column (Bohrmann et al., 2002; Schmidt et al., 2005; Mau et al., 2006, 2007) and high concentrations of dissolved methane and sulfide in pore waters (Hensen et al., 2004; Linke et al., 2005) were observed at both mounds. Likewise, gas hydrates and methane of a primary thermogenic origin were recovered at Mound 11 (Schmidt et al., 2005). In line with this finding, Hensen et al. (2004) and Ranero et al. (2008) proposed a deep origin of methane rich fluids emanating at Mound 11 based on chloride depletion and boron enrichment in the fluids combined with an isotopic composition of water that is consistent with a source from clay mineral dehydration. On the other hand, Tryon et al. (2010) proposed that both mounds have a common source which may be a mixture of subducted sediments and eroded upper plate material due to high B/Li ratio of the fluids; however differences in fluid composition point to a relatively

near-surface origin. Carbon isotopic composition of total dissolved inorganic carbon (TCO_2) has been found to be much lower at Mound 12 ($\delta^{13}\text{C}_{\Sigma\text{TCO}_2} = -60$ to -68%) than at Mound 11 ($\delta^{13}\text{C}_{\Sigma\text{TCO}_2} = -11$ to -23% ; Fűri et al., 2010). Very low $\delta^{13}\text{C}_{\Sigma\text{TCO}_2}$ values in such environments are a clear geochemical signature of dissolved inorganic carbon production from AOM process. Taken together, these observations and our results indicate that Mound 11 is a younger and more active feature while Mound 12 is older as previously reported by Tryon et al. (2010). The increased age and lower activity allows for more methane oxidation at Mound 12, confirming our observation of high AOM efficiency at this mound.

Mau et al. (2006) estimated the methane output at Mound 11 and Mound 12 by mapping the methane plume located above the mounds and by measuring the bottom current velocities. They determined the methane inventory in the plume as well as a clearance time from the current measurements to derive the methane emission into the water column. The largest methane flux was found at Mound 12 ($0.4 \cdot 10^6 \text{ mol a}^{-1}$), whereas lower emissions were calculated for Mound 11 ($0.07 \cdot 10^6 \text{ mol a}^{-1}$). These values are small compared to our estimations which range from $0.36 \cdot 10^6 \text{ mol a}^{-1}$ at Mound 11 to $0.58 \cdot 10^6 \text{ mol a}^{-1}$ at Mound 12. The benthic output calculations of Mau et al. (2006) were based on the area covered by bacterial mats and dominant chemosynthetic communities. However, we considered a large amount of additional methane discharge from background sediments in addition to that from sites covered by bacterial mats to derive the overall methane release from the sea floor.

As outlined above, we found lower advection rates as well as lower methane fluxes from single locations into the overlying bottom water at Mound 12 compared to Mound 11 (see Tab. 4). As the fluid flow velocity increases, methane emission should become elevated as well. We calculated the total methane discharge in areas covered by bacterial mats at Mound 11 (see section 5.3) based on first-order estimates of the total area covered by bacteria (Mau et al. 2006). Our calculations resulted in a lower methane emission at Mound 11 compared to Mound 12 although calculated methane fluxes are higher. The total area of Mound 11 (0.175 km^2) is almost as large as the one of Mound 12 (0.183 km^2) and the dominant chemosynthetic communities do not differ. Seafloor observations with a video sledge (OFOS) recorded at Mound 11 showed that fluid flow occurred only within small patches of bacterial mats and clam communities while most of the remaining mound

surface was inactive (Mau et al., 2006). However, areal coverage of OFOS surveys at Mound 11 investigated by Mau et al. (2006) might be insufficient to do an appropriate estimate of the fraction of seafloor covered by bacterial mats and thus, the areal extent might have been largely underestimated. On the other hand, Mound 11 does not appear to be clogged in large parts by carbonate precipitations (Klaucke et al., 2008) and is highly active (Hensen et al., 2004; Schmidt et al., 2005, Karaca et al., 2010). Overall, these findings suggest either that Mound 11 is still a younger and more active mound with a smaller venting area or a much larger area of Mound 11 is covered by bacterial mats than that estimated previously.

III.6.3 Methane emission compared to other mud volcanoes

To date, methane discharge has been quantified at very few mud volcanoes using a variety of methods, such as pore-water modeling (Wallmann et al., 2006; Haese et al., 2003), video analysis, in-situ measurements obtained by benthic flux chambers (Lichtsschlag et al., 2010; Sommer et al., 2009; Sauter et al., 2006) and water column methane budgets (Mau et al., 2006).

Gaseous methane fluxes shown in Table 6 range between 0.9 and $6.3 \cdot 10^6$ mol a⁻¹ and are close to the flux of dissolved methane indicating that gas bubbling is a significant transport pathway for the emission of methane through mud volcanoes. Acoustic measurements indicate that submarine mud volcanoes located on the continental shelf may emit free gas into the overlying water (Holland et al., 2003). However, the absence of acoustic “flares” at many other mud volcanoes located at larger water depth and the high solubility of methane in the ascending fluids (60–160 mM) suggest that methane is usually released as dissolved rather than gaseous methane in the deep marine environment and does not reach the atmosphere.

Table 6. Methane fluxes at mud volcanoes reported so far. Methane emanates as bubbles (gaseous) or dissolved within advecting pore water (dissolved).

Methane flux in 10^6 mol a^{-1}	Type	Area	Reference
0.36	Dissolved	Mound 11	This study
0.58	Dissolved	Mound 12	This study
0.07	Dissolved	Mound 11	Mau et al., 2006
0.4	Dissolved	Mound 12	Mau et al., 2006
13	Dissolved	Dvurechenskii mud volcano, Black Sea	Lichtschlag et al., 2010
1.9	Dissolved	Dvurechenskii mud volcano, Black Sea	Wallmann et al., 2006
0.006-0.6	Dissolved	Captain Arutyunov mud volcano, Gulf of Cadiz	Sommer et al., 2009
0.04-0.66	Dissolved	Håkon Mosby mud volcano, Norwegian Sea	Sauter et al., 2006
185	Dissolved	Atalante, offshore Barbados	Henry et al., 1996
6.5	Dissolved	Atalante, offshore Barbados	Recalculated by Wallmann et al., 2006
14	Dissolved	Cyclope, offshore Barbados	Henry et al., 1996
0.6	Dissolved	Cyclope, offshore Barbados	Recalculated by Wallmann et al., 2006
0.6	Dissolved	Mound Culebra, offshore Costa Rica	Mau et al., 2006
0.9 (0.4-1.3)	Gaseous	Vodyanitskii mud volcano, Black Sea	Sahling et al., 2009
6.3 (2.5-11.4)	Gaseous	Håkon Mosby mud volcano, Norwegian Sea	Sauter et al., 2006

Dissolved methane discharge estimated in this study ($0.36 - 0.58 \cdot 10^6 \text{ mol a}^{-1}$) is a low to moderate methane flux compared to the overall methane release from other mud volcanoes which range between 0.006 and $185 \cdot 10^6 \text{ mol a}^{-1}$ (Tab. 6). Henry et al. (1996) calculated large methane emissions at mud volcanoes offshore Barbados ($14 - 185 \cdot 10^6 \text{ mol a}^{-1}$ per structure). However, the upper values of dissolved methane flux have been adjusted downward by Wallmann et al. (2006) applying more appropriate boundary conditions ($0.6 - 6.5 \cdot 10^6 \text{ mol a}^{-1}$). Lichtschlag et al. (2010) calculated the methane discharge at Dvurechenskii Mud Volcano as $13 \cdot 10^6 \text{ mol a}^{-1}$, which is about an order of magnitude higher than the previous estimate of $1.9 \cdot 10^6 \text{ mol a}^{-1}$ (Wallmann et al., 2006). At Håkon Mosby Mud Volcano, up to $5.4 \cdot 10^6 \text{ mol a}^{-1}$ methane discharge was estimated by Ginsburg et al. (1999). Very active systems like Håkon Mosby, Dvurechenskii, Atlante and Cyclops Mud Volcanoes are characterized by high fluid flow rates. Wallmann et al. (2006) argued that high methane emission rates are associated with high rates of fluid flow and water discharge and extended areas with active mud extrusions where microbial activity is low. At mud volcanoes and mud extrusions with low emission rates (Captain Arutyunov, Kazan, Culebra, Mound 11, Mound 12) methane discharge is focussed at small active patches, and diffusive discharge is not significant since methane is almost completely oxidized within the surface sediments.

Füri et al. (2010) calculated a total methane output of $3.1 \cdot 10^7 \text{ mol a}^{-1}$ for the latest estimate of 77 mounds observed along a $\sim 460 \text{ km}$ long stretch of the continental slope at the Central America margin (Klaucke et al., 2008; Ranero et al., 2008; Sahling et al., 2008). Our methane flux values at Mound 11 and Mound 12 ($0.36 - 0.58 \cdot 10^6 \text{ mol a}^{-1}$) agree well with the average flux according to Füri et al. (2010; 0.4 mol a^{-1} per mound) and represents only $\sim 1 \%$ of the total amount of methane output from mounds at the Central America margin. Moreover, an average submarine mud volcano thought to be emitted about $2 \cdot 10^6 \text{ mol CH}_4 \text{ a}^{-1}$ into the ocean via dewatering (Wallmann et al., 2006) which is four times higher than our study estimates, suggesting that mud mounds at the submarine section of the Costa Rica fore arc do not represent a pathway for significant methane discharge from the seafloor.

III.7. Conclusions

We estimated dissolved methane discharge from well-studied mud mounds (Mound 11 and Mound 12) at the submarine segment of the Costa Rica fore-arc margin. This study offers a second order approximation approach for estimating the methane output and is subject to errors. Our calculations of flux rates into the overlying bottom water are rather straight forward based on modelling of real pore water data. Limited observation is a very common source of uncertainty in such studies while a larger database of seafloor observations or a higher resolution of geoaoustic data would surely improve the areal estimates of areas covered by seep colonies. All in all the following conclusions are drawn:

1. 80 % of all seeps occur at areas of moderate backscatter intensity at Mound 12.
2. High methane fluxes occur within moderate backscatter areas, which coincides with active vent sites (bacterial mats).
3. At bacterial mat sites of Mound 11, AOM consumes on average 8% of the methane flux from depth due to high advection rates (average 60 cm a^{-1}), so that $2557 \mu\text{mol cm}^{-2} \text{ a}^{-1}$ of methane is discharged into the overlying bottom water. In comparison, AOM consumes on average 20% of the methane flux from depth at Mound 12. Lower advection rates at this mound (average 29 cm a^{-1}) lead to a reduce methane output of $1146 \mu\text{mol cm}^{-2} \text{ a}^{-1}$.
4. We proposed that Mound 11 is a younger and more active feature while Mound 12 is older as previously reported by Tryon et al. (2010). The increased age and lower activity allows more methane oxidation at Mound 12, confirming our observation of high AOM efficiency at this mound.
5. The overall methane release from the entire mound structures range from $0.36 \cdot 10^6 \text{ mol a}^{-1}$ at Mound 11 to $0.58 \cdot 10^6 \text{ mol a}^{-1}$ at Mound 12.
6. We suggest either that Mound 11 is still a younger and more active mound with a smaller venting area, or a much larger area of Mound 11 is covered by bacterial mats than that previously estimated (Mau et al., 2006).
7. Our results suggest that mud mounds at the submarine section of the Costa Rica fore arc do not represent a major pathway for methane discharge from the seafloor.

References

- Aloisi, G., Drews, M., Wallmann, K., Bohrmann, G., 2004, Fluid expulsion from the Dvurechenskii mud volcano (Black Sea) - Part I. Fluid sources and relevance to Li, B, Sr, I and dissolved inorganic nitrogen cycles, *Earth and Planetary Science Letters*, 225, 347-363.
- Berner, R. A., 1980, *Early diagenesis. A theoretical approach*, Princeton University Press, 241pp., New York
- Boetius, A., Ravensschlag, K., Schubert, C. J., Rickert, D., Widdel, F., Giesecke, A., Amann, R., Jørgensen, B. B., Witte, U., and Pfannkuche, O., 2000, A marine microbial consortium apparently mediating anaerobic oxidation of methane, *Nature*, 407, 623-626.
- Bohrmann, G., Heeschen, K., Jung, C., Weinrebe W., Baranov, B., Cailleau, B., Heath R., Hühnerbach, V., Hort, M., Masson, D., Trummer I., 2002, Widespread fluid expulsion along the seafloor of the Costa Rica convergent margin, *Terra Nova*, 14, 69-79.
- Bohrmann, G., et al. 2003, Mud volcanoes and gas hydrates in the Black Sea: new data from Dvurechenskii and Odessa mud volcanoes, *Geo-Marine Letters*, 23, 239-249.
- Boudreau, B. P., 1997, *Diagenetic models and their implementation: modelling transport and reactions in aquatic sediments*, 414 pp., Springer, Berlin, Heidelberg, Berlin, Heidelberg, New York.
- Brückmann, W., Rhein, M., Rehder, G., Bialas, J., and Kopf A., 2009, SUBFLUX, *Cruise No.66*, 158 pp, METEOR-Berichte 09-2, Universität Hamburg, August 12 - December 22, 2005.
- Dimitrov, L. I., 2002, Mud volcanoes - the most important pathway for degassing deeply buried sediments, *Earth-Sci. Rev.*, 59, 49-76.
- Etioppe, G., 2004, New directions: GEM - Geologic emissions of methane, the missing source in the atmospheric methane budget, *Atmospheric Environment*, 38, 3099-3100.
- Füri, E., Hilton, D.R., Tryon, M.D., Brown, K.M., McMurtry, G. M., Bruckmann, W., Wheat, C. G., 2010, Carbon release from submarine seeps at the Costa Rica fore arc: Implications for the volatile cycle at the Central America convergent margin, *Geochemistry Geophysics Geosystems*, 11.
- Ginsburg, G. D., Milkov, A.V., Soloviev, V.A., Egorov, A.V., Cherkashev, G.A., Vogt, P.R., Crane, K., Lorenson, T.D., Khutorskoy, M.D., 1999, Gas hydrate accumulation at the Haakon Mosby Mud Volcano, *Geo-Marine Lett.*, 19, 57-67.
- Haese, R. R., Meile, C., Van Cappellen, P., De Lange, G. J., 2003, Carbon geochemistry of cold seeps: methane fluxes and transformation in sediments from Kazan mud volcano, eastern Mediterranean Sea, *Earth Planet. Sci. Lett.*, 212, 361-375.

- Henry, P., et al., 1996, Fluid flow in and around a mud volcano field seaward of the Barbados accretionary wedge: results from Manon cruise, *J. Geophys. Res.*, 101, 20,297-220,323.
- Hensen, C., and K. Wallmann, 2004, Methane fluxes and gas hydrate reservoirs in slope sediments along Costa Rica continental margin, paper presented at EGU, Nice, France.
- Hinrichs, K. U., Hayes, J.M., Sylva, S.P., Brewer, P.G., DeLong, E.F., 1999, Methane-consuming archaea bacteria in marine sediments, *Nature*, 398, 802-805.
- Holland, C. W., G. Etiope, et al., 2003, Mud volcanoes discovered offshore Sicily, *Marine Geology* 199: 1-6.
- Hovland, M., Judd, A. G., Burke, Jr. R. A., 1993, The global flux of methane from shallow submarine sediments, *Chemosphere*, 26, 559-578.
- Judd, A. G., 2004, Natural seabed gas seeps as sources of atmospheric methane, *Environmental Geology*, 46, 988-996.
- Karaca, D., Hensen, C., Wallmann, K., 2010, Controls on authigenic carbonate precipitation at cold seeps along the convergent margin off Costa Rica, *Geochemistry. Geophysics Geosystems*, 11, Q08S27, doi:10.1029/2010GC003062.
- Klaucke, I., Masson, D. G., Petersen, C. J., Weinrebe, W., Ranero, C. R., 2008, Multifrequency geoacoustic imaging of fluid escape structures offshore Costa Rica: Implications for the quantification of seep processes, *Geochemistry Geophysics Geosystems*, 9, Q0401010.1029/2007gc001708
- Kopf, A., 2002, Significance of mud volcanism, *Rev. Geophys.*, 40, 1-52.
- Kvenvolden, K. A., and B. W. Rogers, 2005, Gaia's breath - global methane exhalations, *Marine and Petroleum Geology*, 22, 579-590.
- Lichtschlag, A., Felden, J., Wenzhofer, F., Schubotz, F., Ertefai, T. F., Boetius, A., de Beer, D., 2010, Methane and sulfide fluxes in permanent anoxia: In situ studies at the Dvurechenskii mud volcano (Sorokin Trough, Black Sea), *Geochimica Et Cosmochimica Acta*, 74, 5002-5018.
- Linke, P., Wallmann, K., Suess, E., Hensen, C., and Rehder, G., 2005, In-situ benthic fluxes from an intermittently active mud volcano at the Costa Rica convergent margin, *Earth Planet. Sci. Lett.*, 235, 79-95.
- Loncke, L., and J. Mascle, 2004, Mud volcanoes, gas chimneys, pockmarks and mounds in the Nile deep-sea fan (Eastern Mediterranean): geophysical evidences, *Marine and Petroleum Geology*, 21, 669-689.

- Luff, R., and K. Wallmann, 2003, Fluid flow, methane fluxes, carbonate precipitation and biogeochemical turnover in gas hydrate-bearing sediments at Hydrate Ridge, Cascadia Margin: Numerical modeling and mass balances, *Geochim. Cosmochim. Acta*, 67, 3403–3421.
- Luff, R., Wallmann, K., Grandel, S., Schlüter, M., 2000, Numerical modeling of benthic processes in the deep Arabian Sea, *Deep-Sea Res. II*, 47(14), 3039-3072.
- MacDonald, I. R., Leifer, I., Sassen, R., Stine, P., Mitchell, R., Guinasso, N., 2002, Transfer of hydrocarbons from natural seeps to the water column and atmosphere, *Geofluids*, 2, 95-107.
- Martin, J. B., M. Kastner, P. Henry, X. Le Pichon, and S. Lallement (1996), Chemical and isotopic evidence for sources of fluids in a mud volcano field seaward of the Barbados accretionary wedge, *J. Geophys. Res.*, 101(B9), 20325-20345.
- Mau, S., Sahling, H., Rehder, G., Suess, E., Linke, P., and Soeding E., 2006, Estimates of methane output from mud extrusions at the erosive convergent margin off Costa Rica., *Marine Geology*, 225, 129-144.
- Milkov, A. V., Sassen, R., Apanasovich, T.V., Dadashev, F.G., 2003, Global gas flux from mud volcanoes: a significant source of fossil methane in the atmosphere and the ocean, *Geophys. Res. Lett.*, 30, 1037, doi: 10.1029/2002GL016358.
- Pinheiro, L. M., et al., 2003, Mud volcanism in the Gulf of Cadiz: results from the TTR-10 cruise, *Marine Geology*, 195, 131-151.
- Ranero, C. R., Grevenmeyer, I., Sahling, H., Barckhausen, U., Hensen, C., Wallmann, K., Weinrebe, W., Vannucchi, P., von Huene, R., McIntosh, K., 2008, Hydrogeological system of erosional convergent margins and its influence on tectonics and interplate seismogenesis, *G-cubed*, 9(3), doi:10.1029/2007GC001679.
- Ranero, C. R., and R. Von Huene, 2000, Subduction erosion along the Middle America convergent margin, *Nature*, 404, 748-752.
- Reeburgh, W.S. (2003), Global methane biogeochemistry. In: Hollan, H.D., Turekian, K.K. (Eds), *Treatise on Geochemistry*, vol.4, Elsevier, pp.65-89.
- Sahling, H., Masson, D. G., Ranero, C. R., Hühnerbach, V., Weinrebe, W., Klauke, I., Bürk, D., Brückmann, W., Suess, E., 2008, Fluid seepage at the continental margin offshore Costa Rica and southern Nicaragua, *G-cubed*, 9. doi:10.1029/2008GC001978.
- Sauter, E. J., et al., 2006, Methane discharge from a deep-sea submarine mud volcano into the upper water column by gas hydrate-coated methane bubbles, *Earth and Planetary Science Letters*, 243, 354-365.
- Schleicher, 2006, Bestimmung von ventspezifischen Faunenvergesellschaftungen am mittelamerikanischen Kontinentalrand mit Hilfe quantitativer Videoauswertung, Diploma Thesis, 68pp, University of Kiel, Kiel.

- Schmidt, M., Hensen, C., Morz, T., Muller, C., Grevenmeyer, I., Wallmann, K., Mau, S., Kaul N., 2005, Methane hydrate accumulation in "Mound 11" mud volcano, Costa Rica forearc, *Marine Geology*, 216(1-2), 83-100.
- Solomon, E. A., Kastner, M., MacDonald, I. R., Leifer, I., 2009, Considerable methane fluxes to the atmosphere from hydrocarbon seeps in the Gulf of Mexico, *Nature Geoscience*, 2, 561-565.
- Sommer, S., et al., 2009, Seabed methane emissions and the habitat of frenulate tubeworms on the Captain Arutyunov mud volcano (Gulf of Cadiz), *Marine Ecology-Progress Series*, 382, 69-86.
- Tishchenko, P., Hensen, C., Wallmann, K., Wong, C. S., 2005, Calculation of the stability and solubility of methane hydrate in seawater, *Chemical Geology*, 219, 37-52.
- Torres, M. E., et al., 2002, Fluid and chemical fluxes in and out of sediments hosting methane hydrate deposits on Hydrate Ridge, OR, I: Hydrological provinces, *Earth and Planetary Science Letters*, 201, 525-540.
- Treude, T., Boetius, A., Knittel, K., Wallmann, K., Jørgensen, B.B., 2003, Anaerobic oxidation of methane above gas hydrates, *Mar. Ecol., Prog. Ser.* 264, 1-14.
- Tryon, M. D., and K. M. Brown (2001), Complex flow patterns through Hydrate Ridge and their impact on seep biota, *Geophysical Research Letters*, 28, 2863-2866.
- Tryon, M. D., Wheat, C. G., Hilton, D. R., 2010, Fluid sources and pathways of the Costa Rica erosional convergent margin, *Geochemistry Geophysics Geosystems*, 11.
- Vannucchi, P., C. R. Ranero, S. Galeotti, S. M. Straub, D. W. Scholl, and K. McDougall-Ried, 2003, Fast rates of subducting erosion along the Costa Rica Pacific margin: Implications for nonsteady rates of crustal recycling at subduction zones, *Journal of Geophysical Research*, 108, doi: 10.1029/2002JB002207.
- von Huene, R., Ranero, C. R., Watts, P., 2004, Tsunamigenic slope failure along the Middle America Trench in two tectonic settings, *Marine Geology*, 203, 303-317.
- Wallmann, K., Drews, M., Aloisi, G., Bohrmann, G., 2006, Fluid expulsion from the Dvurechenskii mud volcano (Black Sea): Part II. Methane fluxes and new estimates of global methane discharge into the ocean via submarine mud volcanism, *Earth and Planetary Science Letters*, 248, 544-559.

Chapter IV

Quantification of methane emission from bacterial mat sites at Quepos Slide offshore Costa Rica

Deniz Karaca^{1*}, Tina Schleicher², Christian Hensen^{1,3}, Peter Linke^{1,3}, Klaus Wallmann^{1,3}

¹Sonderforschungsbereich 574, University of Kiel, Wischhofstraße 1-3, D-24148 Kiel, Germany

²Department of Bioinformatics, University of Würzburg, Am Hubland, D-97074, Würzburg Germany

³Leibniz-Institute of Marine Sciences, IFM-GEOMAR, Wischhofstraße 1-3, D-24148 Kiel, Germany

To be submitted to Marine Geology

Abstract

Sea floor methane emission from the Quepos Slide bacterial mat sites at the submarine segment of the Costa Rica fore-arc margin was estimated by extrapolating the flux measurements from individual seeps to the total area covered by mat bacterial mats. This approach is based on (i) detailed mapping in order to determine the abundance of seeps, and thus the spatial validity of the flux measurements; and (ii) application of numerical model to estimate the amount of methane that is transported into the bottom water. Model results illustrate that the majority of the studied seeps transport rather limited amount of methane into the water column due to medium to low advection rates (average 10 cm a^{-1}) allowing high methane consumption by AOM from greater depth (average 45%) and limiting the methane discharge into the water column. Consequently, the emission of

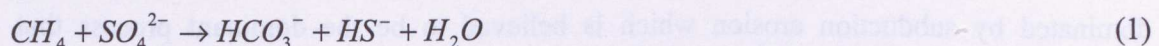
dissolved methane into the water column was moderate, with an average estimated rate of $351 \mu\text{mol cm}^{-2} \text{ a}^{-1}$. Depth-integrated AOM rates ($56 - 1538 \mu\text{mol CH}_4 \text{ cm}^{-2} \text{ a}^{-1}$) are comparable with the values reported at other very active vents sites, suggesting that the Quepos Slide should be regarded as one of the active sites at the seafloor. The overall amount of dissolved methane released from the entire bacterial mat sites of Quepos Slide into the water column is determined as $0.56 \cdot 10^6 \text{ mol a}^{-1}$. This conservative estimate, relying on rather accurate determinations of sea floor methane fluxes out of bacterial mats emphasizes the importance of submarine slides as sites of natural methane seepage, if the methane flux from these structures is similar to the Quepos Slide flux. However, the global extent of methane seepage from submarine slides remains unknown to date, warranting a more extensive monitoring program.

* Corresponding author (D. Karaca). Fax: +49 431 6002928. E-mail address: dkaraca@ifm-geomar.de

IV.1. Introduction

Fluxes of the greenhouse gas methane from many individual sources to the ocean and the atmosphere have attracted considerable interest in recent years. A number of considerable research efforts have been contributed to the global atmospheric methane budget (e.g. Hovland et al., 1993; Dimitrov, 2002; Etiope and Klusman, 2002, Etiope, 2004; Judd, 2004; Kvenvolden and Rogers, 2005; Luyendyk et al., 2005). Current estimates of global methane fluxes from seabed to the atmosphere vary between 0.4 and 48 Tg a⁻¹ (Judd, 2004). Progress in quantifying methane emissions has been restricted by uncertainties regarding the total area involved in active seepage and the temporal variability in seep intensity and activity which are the main obstacles in establishing reliable estimates for regional and global methane fluxes.

Each year, ocean sediments produce a quantity of methane equivalent to about half of the methane emitted to the atmosphere from all natural sources (Reeburgh, 2007). Very little of the methane produced below the sea floor reaches the ocean or the atmosphere, however, since most is consumed by anaerobic microorganisms which control its discharge to the water column (Boetius and Suess, 2004; Niemann et al., 2006). The key process in methane-rich seafloor sediments is the microbially mediated anaerobic oxidation of methane (AOM), which has a major role in regulation of global methane fluxes:



At continental margins, cold seep manifestations of methane seepage may comprise mud volcanoes, mud diapirs, surface gas hydrate deposits and methane-laden pockmarks (Hovland et al., 2005). The amount of methane released from submarine mud volcanoes (Henry et al, 1996; Sauter et al., 2006; Wallmann et al., 2006; de Beer et al., 2006; Feseker et al., 2008; Mau et al, 2006) and from natural gas seeps (Hovland et al., 1993; Dimitrov, 2002; Etiope and Klusman, 2002, Etiope, 2004; Judd, 2004; Kvenvolden and Rogers, 2005, Luyendyk et al., 2005; Kessler et al., 2006; Solomon et al, 2008) into the water column and into the atmosphere is highly variable and remains poorly constrained. The determination of reliable estimates must rely on detailed mapping in order to determine the abundance of seeps and thus the spatial validity of the flux measurements.

In the present study, we aim to estimate the overall emission of dissolved methane at bacterial mats of a submarine slide (Quepos Slide) at the submarine segment of the Costa Rica fore-arc margin. Our study is based on (1) fauna distribution mapping related to methane emission by remotely operated vehicle (ROV) Quest; (2) application of numerical model C.CANDI (Luff et al., 2000) to estimate the amount of methane that is transported into the bottom water considering AOM, molecular diffusion, upward advection and non-local mixing. This approach provides a reliable method for the estimation of methane fluxes on a regional basis as opposed to other methods that determine such fluxes in a spatially limited manner. Our findings show that extrapolation of flux measurements from individual seeps to regional models is only likely to be valid if it is based on detailed mapping of seep fauna distribution.

IV.2. Study Area

The morphology and structure of the continental margin offshore Central America is controlled by the subduction of the Cocos Plate beneath the Caribbean Plate. From north to south, there are four morphologically different segments on the oceanic plate characterizing the forearc area in this region (1) the smooth oceanic crust formed at the East Pacific Rise, (2) the smooth oceanic crust generated at the Cocos-Nazca spreading centre, (3) the seamount segment generated at the Cocos-Nazca spreading centre, and (4) the rough oceanic crust of the Cocos Ridge. (von Huene et al., 2000). The entire section is dominated by subduction erosion which is believed to be the dominant process that controls the tectonic evolution of the overriding plate along the Costa Rica Pacific margin at least since ~16Ma (Vannucchi et al., 2003; Ranero & Von Huene, 2000; von Huene, 2004). Those processes provide pathways for fluid circulation at the Costa Rica margin. Consequently, a great number of dewatering features have been clearly identified on the subducting plate covered by numerous cold seep structures (Sahling et al., 2008; Bohrmann et al., 2002). Several of these cold seeps have been sampled and show indications for active fluid seepage and emission of methane-rich fluids (Hensen et al., 2004; Linke et al., 2005; Mau et al., 2006; Karaca et al., 2010) and the occurrences of authigenic carbonates and chemosynthetic communities (Sahling et al., 2008).

In our study, we visited a cold seep structure, Quepos Slide, which is located at shallow water depth (~400 m) in a very productive upwelling area (Brückmann et al., 2009) (Fig.1).

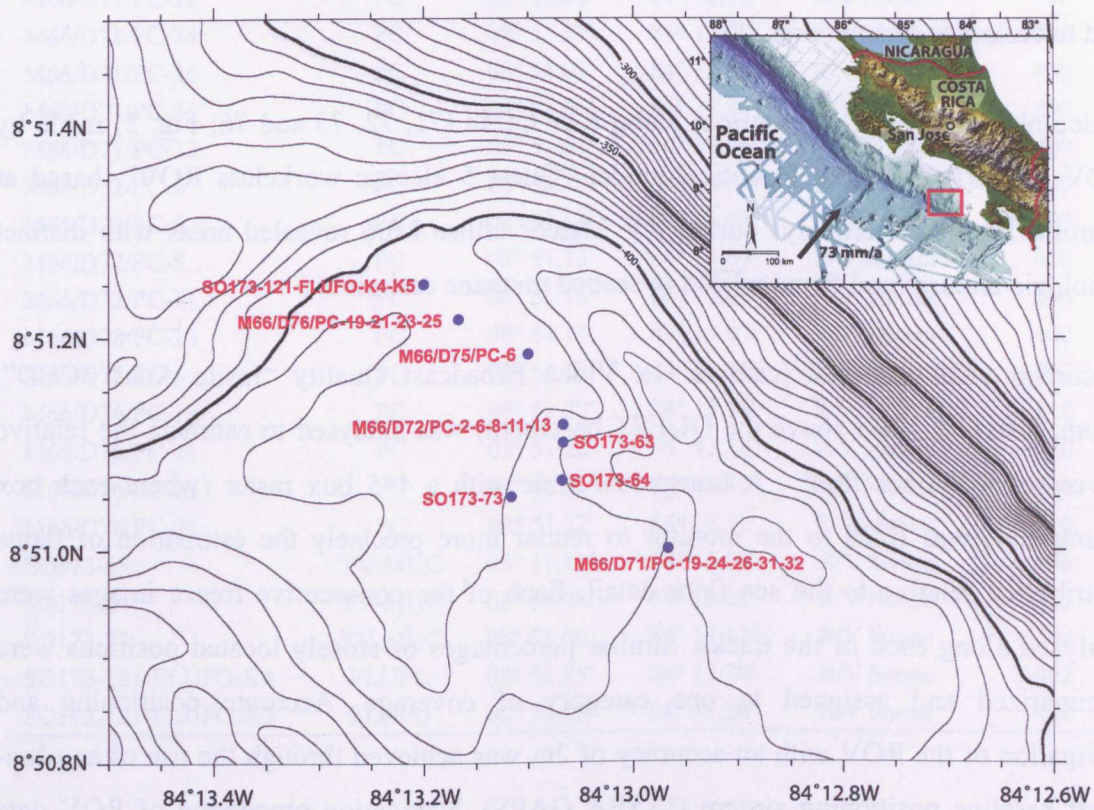


Figure 1. Location of the Quepos Slide, offshore Costa Rica, with coring stations.

Quepos Slide is a submarine slide related to intense fluid emanation wherein much of the area below the head wall is densely covered by bacterial mats. Geochemical and isotopic composition of the fluids (i.e. chlorinity depletion, boron enrichment, $\delta^{18}\text{O}$ and δD isotope composition), suggests that fresh water addition by clay mineral dewatering is a driving force of over-pressuring and fluid advection as a likely source of the fluids (Hensen et al., 2004). However, seep fluid sampling at Mound 11 in 2005–2006 revealed an unusually high B/Li ratio of the fluids, suggesting that the source may be a mixture of subducted sediment and eroded upper plate material (Tryon et al., 2010).

IV.3. Material and Methods

Quepos Slide was surveyed on expeditions M66 (with RV Meteor in 2003) and SO173 (with RV Sonne in 2005) in order to obtain visual observations from underwater video, and to collect sediment cores.

Video observations of the seafloor along four tracks (71, 72, 75 and 76; Fig. 2) made by ROV QUEST (Schilling Robotics, model "Quest 5 electric workclass ROV", based at Marum, Bremen, Germany) during RV Meteor cruise M66 revealed areas with distinct lithologic features and fauna related to seabed methane emission.

Recorded video material (camera: 1x Video Broadcast Quality "Insite Atlas 3CCD", zoom, installed 20cm above the QUEST basement) was analysed to estimate the relative coverage of the sea floor. A transparent slide with a 4*5 box raster (where each box counts 5%) was fixed to the monitor to render more precisely the estimation of fauna distribution relative to the sea floor detail. Each of the consecutive freeze images were analyzed along each of the tracks. Similar percentages of closely located positions were summarized and assigned to one category of coverage. Accurate positioning and navigation of the ROV with an accuracy of 2m was achieved through the use of an ultra-short baseline positioning system (IXSEA GAPS). Navigation processing of ROV data was achieved according to the method of Schleicher (2006) via eliminating a number of outliers that could result from inaccurate measurements, reflexions at boundary layers of different water bodies or bottom structures.

Surface sediment cores were taken with a TV-guided multi-corer (TV-MUC), ROV-directed push coring (ROV) and the FLUFO-lander (FLUFO). All investigated sites were located at bacterial mats at a water depth of about 400 m (Table.1). Flux measurements from individual seeps have been determined by the application of the numerical model (Section 4).

Table 1. Details of sampling sites included in this study.

Core	Gear	Latitude (°N)	Longitude (°W)	Research vessel	Water Depth (cm)
M66/D71/PC-19	PC	08° 51.01'	84° 12.98'	R/V Meteor	400
M66/D71/PC-24	PC	08° 51.01'	84° 12.98'	R/V Meteor	400
M66/D71/PC-26	PC	08° 51.01'	84° 12.98'	R/V Meteor	400
M66/D71/PC-31	PC	08° 51.01'	84° 12.98'	R/V Meteor	400
M66/D71/PC-32	PC	08° 51.01'	84° 12.98'	R/V Meteor	400
M66/D72/PC-2	PC	08° 51.13'	84° 13.07'	R/V Meteor	400
M66/D72/PC-6	PC	08° 51.13'	84° 13.07'	R/V Meteor	400
M66/D72/PC-8	PC	08° 51.13'	84° 13.07'	R/V Meteor	400
M66/D72/PC-11	PC	08° 51.13'	84° 13.07'	R/V Meteor	400
M66/D72/PC-13	PC	08° 51.13'	84° 13.07'	R/V Meteor	400
M66/D75/PC-6	PC	08° 51.19'	84° 13.11'	R/V Meteor	397
M66/D76/PC-19	PC	08° 51.22'	84° 13.18'	R/V Meteor	410
M66/D76/PC-21	PC	08° 51.22'	84° 13.18'	R/V Meteor	410
M66/D76/PC-23	PC	08° 51.22'	84° 13.18'	R/V Meteor	410
M66/D76/PC-25	PC	08° 51.22'	84° 13.18'	R/V Meteor	410
SO173-63	TV-MUC	08° 51.11'	84° 13.08'	R/V Sonne	406
SO173-64	TV-MUC	08° 51.08'	84° 13.08'	R/V Sonne	407
SO173-73	TV-MUC	08° 51.06'	84° 13.12'	R/V Sonne	404
SO173-121-FLUFO-K4	FLUFO	08° 51.25'	84° 13.20'	R/V Sonne	402
SO173-121-FLUFO-K5	FLUFO	08° 51.25'	84° 13.20'	R/V Sonne	402

IV.4. Reaction-transport model

The reactive-transport model C.CANDI (Luff et al., 2000) was applied to investigate rates of upward fluid flow and CH₄ turnover at sampled locations. The model describes transport process for 6 dissolved species in the pore water (SO₄, CH₄, HS, H₂S, Cl, NH₄) forced by advection, molecular diffusion and non-local mixing (see Luff et al., 2000 and Luff and Wallmann, 2003 for a more detailed model description).

The model considers molecular diffusion, non-local mixing and advection based on the following differential equation (after Berner, 1980):

$$\phi \frac{\partial C_w}{\partial t} = \frac{\partial}{\partial x} \left(\phi(x) D(x) \frac{\partial C_w}{\partial x} \right) - \frac{\partial}{\partial x} (v(x) \phi(x) C_w) + \phi(x) \alpha(x) (C_w - C_0) \quad (2)$$

where C_w is the concentration of dissolved species (mmol cm^{-3}), $D(x)$ is the molecular diffusion coefficient corrected for tortuosity ($\text{cm}^2 \text{a}^{-1}$), $v(x)$ is the pore water velocity (cm a^{-1}), ϕ is the porosity, α is the pore water mixing coefficient (a^{-1}), $(C_w - C_0)$ is the difference between the concentration at any depth and in seawater.

Sediment porosity changes with depth due to sediment compaction. The depth profile is approximated by fitting the measured data with:

$$\phi = (\phi_0 - \phi_\infty) * \text{Exp}(-\text{const} \cdot x) + \phi_\infty \quad (3)$$

where ϕ_∞ and ϕ_0 are the porosity at infinite depth and at sediment surface, and const is the attenuation coefficient for the exponential decrease of porosity with depth.

The upward flow velocity v_0 was determined by fitting the model to the dissolved chloride profiles. The upward directed pore water flux is composed of the downward burial component modified by compaction and the upward fluid advection:

$$v(x) = \frac{\omega_\infty \cdot \phi_\infty - v_0 \cdot \phi_0}{\phi(x)} \quad (4)$$

where $v(x)$ represents the depth-dependent fluid flow velocity (cm a^{-1}) and v_0 is the surface value of the fluid flow velocity (cm a^{-1}).

Temperature-dependent molecular diffusion coefficients of dissolved species were calculated after Boudreau (1997) and corrected for porosity decrease:

$$D_s(x) = \frac{D_0(x)}{1 - \ln(\phi(x))^2} \quad (5)$$

where D_0 is the molecular diffusion coefficient in seawater ($\text{cm}^2 \text{a}^{-1}$).

The depth dependent mixing coefficient was approximated by:

$$\alpha(x) = \frac{\alpha'}{(1 + \text{Exp}(x - x_{\text{mix}}) / \sigma)} \quad (6)$$

where α' is the pore water-mixing coefficient (a^{-1}), x_{mix} is the depth of the mixed layer (cm) and σ determines the thickness of the transition layer between the mixed and the non-mixed proportion of the sediment column.

The kinetic constant of AOM (k_{AOM}) which was determined by fitting the pore water profiles of sulfate, and hydrogen sulfide, was applied to define the rate of anaerobic methane oxidation (R_{AOM}) considering second order kinetics:

$$R_{\text{AOM}} = k_{\text{AOM}} [\text{CH}_4] [\text{SO}_4^{2-}] \quad (7)$$

Constant concentrations were prescribed at the upper and lower boundary of the model column (Dirichlet boundary conditions). In general, upper boundary conditions were chosen to represent regional seawater composition while lower boundary values reflect the composition of the deep fluid. All simulations were performed assuming steady state conditions ($dc/dt \approx 0$). The vertical resolution of the model grid was set to 1000 layers in order to resolve the steep pore water gradients for the overall simulation time of 100,000 years. The best steady state fit to the measured data was obtained applying the combination of parameter values summarized in Table 2. POC-based sulfate reduction was considered to be negligible at cold seeps at the Costa Rican margin (Karaca et al., 2010). Previous studies showed that overall biogeochemical turnover is dominated by AOM and associated processes (Luff and Wallmann 2003).

Table 2. Summary of parameter values used for the steady state simulations at all seep locations. Temperature (9.59°C), salinity (34.69 PSU) and pressure (34.59 atm) values applied for all simulations were taken from CTD measurements. Gas hydrates are not stable under the prevailing conditions and solubility of methane in seawater is about 53 mM at the sediment/water interface conditions (Tishchenko et al., 2005). BW indicates concentrations of dissolved species at the upper boundary of the model column; whereas BS indicates concentrations of dissolved species at the bottom of the sediment column.

Stations	Model parameters values				Porewater concentrations*				
	Length of simulated core (cm)	Porosity at sediment surface	Porosity at large sediment depth	Maximm depth of mixing (cm)	Non-local mixing coefficient	BWNH ₄ /BSNH ₄ (mM)	BW Cl/BS Cl (mM)	BWSO ₄ /BS SO ₄ (mM)	BWTH ₂ S/BSTH ₂ S (mM)
M66/D71/PC-19	25	0.77	0.59	6	30	0.04/1.6	561/531	28.7/0	0/5.16
M66/D71/PC-24	20	0.78	0.62	-	-	0.05/1.9	552/518	28.7/0	0/5.12
M66/D71/PC-26	20	0.80	0.59	-	-	0.07/2.8	557/458	28.7/0	0/3.96
M66/D71/PC-31	20	0.78	0.48	-	-	0.09/1.6	560/519	28.7/0	0/5.69
M66/D71/PC-32	25	0.77	0.48	6	13	0.01/2.2	555/516	28.7/0	0/6.30
M66/D72/PC-2	25	0.79	0.53	-	-	0/1.5	560/490	28.7/0	0/6.32
M66/D72/PC-6	30	0.78	0.52	-	-	0/1.5	565/490	28.7/0	0/6.71
M66/D72/PC-8	30	0.79	0.52	6	1	0/1.5	566/505	28.7/0	0/4.10
M66/D72/PC-11	30	0.76	0.63	-	-	0.01/1.5	555/470	28.7/0	0/5.67
M66/D72/PC-13	30	0.79	0.62	-	-	0.02/0.1	555/478	28.7/0	0/3.04
M66/D75/PC-6	30	0.79	0.71	-	-	0.1/1.2	560/466	28.7/0	0/6.47
M66/D76/PC-19	30	0.47	0.47	-	-	0.03/0.5	540/387	28.7/0	0/0
M66/D76/PC-21	30	0.59	0.38	-	-	0/0.5	559/415	28.7/0	0/0
M66/D76/PC-23	20	0.55	0.46	-	-	0.02/0.5	557/421	28.7/0	0/0
M66/D76/PC-25	20	0.50	0.47	-	-	0.01/0.4	555/438	28.7/0	0/0
SO173-63	41.5	0.91	0.73	-	-	0/2.5	552/321	28.7/0	0/0.085
SO173-64	53.5	0.9	0.68	20	10	0.01/2.8	554/324	28.7/0	0/0
SO173-73	32.5	0.91	0.725	-	-	0/2.2	555/324	28.7/0	0/0.09
SO173-121-FLUFO-K4	17	0.90	0.82	-	-	0/1.4	553/380	28.7/0	0/0.3
SO173-121-FLUFO-K5	12	0.92	0.85	-	-	0/0.6	553/437	28.7/0	0/4.36

* BWCH₄/BSCH₄ is applied as 0/53mM at all stations.

IV.5. Results and discussion

IV.5.1. Seafloor observations

At Quepos Slide, an area of approximately 60,000 m² was surveyed with ROV Quest along four tracks (71, 72, 75 and 76; Fig.2). Video observations generally show a rather flat sea floor alternating dome-like structures or outcrops having a relief of a few meters.

The sea floor generally consists of soft sediments with extremely abundant mats of bacteria that are widespread in the entire surveyed area (Fig.3).

Elevated areas in the southern part of the region are entirely populated by thick bacterial mats of white and yellow-orange color as well as grey filamentous mats formed by sulfide-oxidizing bacteria (e.g. *Beggiatoa* sp.), which profit from the high fluxes of sulfide generated by the anaerobic oxidation of methane (AOM) (Boetius et al., 2000; Boetius and Suess, 2004). Transition from yellow to orange in the mat center and bright white in the outer rim were observed, sometimes in association with grey mats. The mats were elongated with a length and width of approximately 10 and 2m. The bright white bacterial mats are widely distributed in low abundance around the southern part of the site stretching over tens of meters with an elongation parallel to the walls of outcropping sediments. Small patches of thick bacterial mats with a circular shape are widespread. During the video observations, no bubbles were detected being released from the bacterial mats.

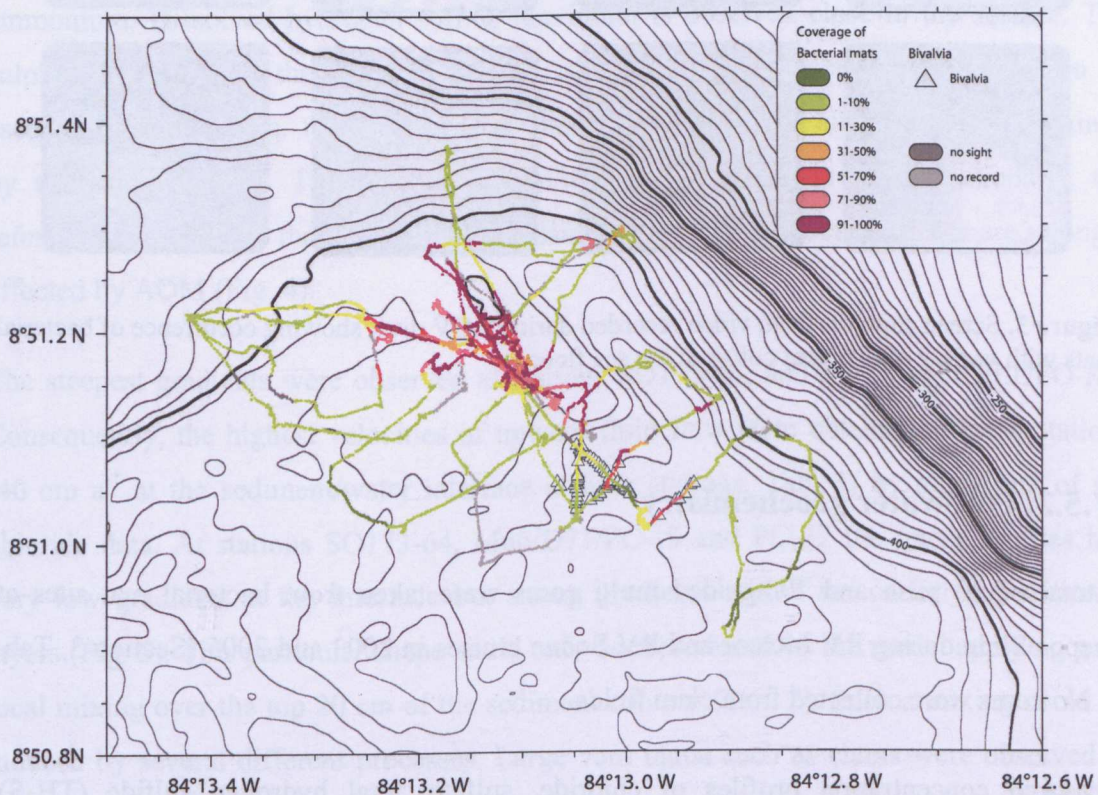


Figure 2. Sea floor observation map showing distribution of bacterial mat along the ROV. Quest dives of track 71, 72, 75 and 76. Color range given in gradients is associated with bacterial mats coverage at the sea floor.

A small amount of shell fragments of bivalves were observed in the southern tail of the elevation (Fig.2). They are assumed to be a member of the genus Thyasiridae or Lucinidae (Heiko Sahling, pers. comm.) living partly buried in the sediment. However species of these families were found harbor to chemoautotroph bacteria (Imhoff et al., 2003). Their coverage of the sea floor is limited to less than 2% within the spotted area, hence we do not report on either their spatial distribution or their influence on methane fluxes.

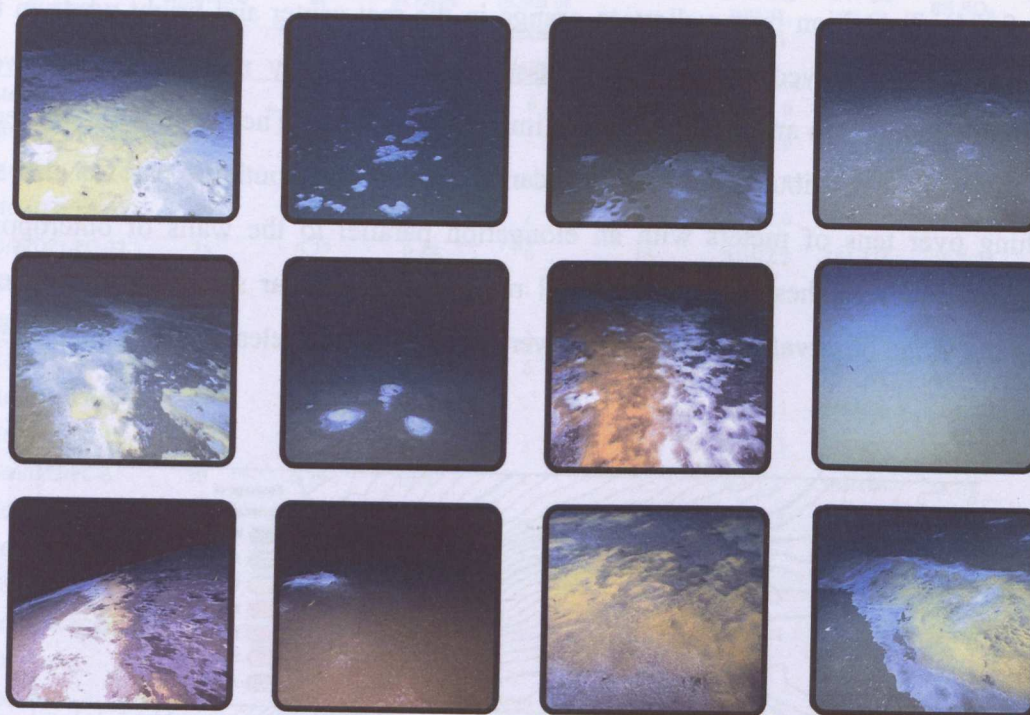


Figure 3. Screen captures from video recorded during ROV dive, showing occurrence of bacterial mats with variety of different colors at the sea floor.

IV.5.2. Porewater geochemistry

A total of 20 push and TV-guided multi cores were taken from bacterial mat sites at Quepos Slide during RV Meteor and RV Sonne cruises in 2003 and 2005 (Section 3, Tab. 1). No cores were collected from clam fields.

Measured concentration profiles of chloride, sulfate, total hydrogen sulfide (TH₂S), ammonium, methane and alkalinity of selected cores are presented in Figures 4-5. Considerable deviations exist only for methane profiles where measured concentrations are considerably lower than simulated values. This discrepancy is due to the loss of methane

via degassing from the sediment during core recovery. The thermodynamic calculations showed that gas hydrates were not stable under the prevailing conditions while the solubility of methane in seawater is about 53 mM at the sediment/water interface (Tishchenko et al., 2005). Methane flux calculations does not include the release of gaseous methane and the methane fluxes during peak discharges, it rather gives the methane discharge into the overlying bottom water during the current period of dewatering considering both fluid advection and molecular diffusion.

IV.5.2.1. Transport of dissolved species

In general, composition of pore fluids deviate significantly from seawater showing a general trend of freshening associated by low Cl concentrations (Hensen et al., 2004) Chloride concentrations which are low at the core base increase towards sea water values at the sediment/water interface. The concentrations measured at the core base reflect the low salinity of the ascending fluids while the curvature of the tracer profiles is induced by upward fluid flow. A general, the decrease in chlorinity is accompanied by an increase in ammonium. Dissolved hydrogen sulfide maximum is observed close to the surface. The sulphide enriched in these surface layers is produced by the anaerobic oxidation of ascending methane (Eq. 1) and the strong interfacial gradients in alkalinity are maintained by the same process. The much lower alkalinity and sulphide concentrations at the reference site confirm that the pore fluids sampled within the bacterial mats are strongly affected by AOM (Fig. 4).

The steepest gradients were observed at stations SO173-63, and SO173-121-FLUFO-K4. Consequently, the highest velocities of upward fluid flow were obtained at these stations (40 cm a^{-1} at the sediment/water interface at both stations, Tab. 3) by modelling of the chloride data. At stations SO173-64, M66/D71/PC-19 and PC-32 the tracer profiles had very low gradients at the interface but strong gradients within the underlying sediment layers (Fig. 5). This particular shape could only be reproduced by the model applying non-local mixing over the top 20 cm of the sediment column (Tab. 2). Such a mixing could be induced by several different processes. Large vent fauna such as clams were observed to pump bottom water into surface sediments at other vent locations (Wallmann et al., 1997). However, this process termed "bioirrigation" is probably not responsible for the mixing at these stations because no large vent fauna were observed at these sites (Fig. 6, green zone).

The mixing may also be induced by shallow convection of bottom waters through surface sediments. The low density fluids at the core base and the high-density bottom waters create an unstable density layering which may induce spontaneous convection (Henry et al., 1992). This process has been shown to occur at other cold vent sites where low-salinity fluids are expelled into the ocean (Henry et al., 1992; Henry et al., 1996; Aloisi et al., 2004). Finally, bottom currents may induce large pressure gradients and seawater advection through surface sediments at vent sites where the seafloor has a rough topography. A strong flow of bottom waters has been observed through sediments at Hydrate Ridge induced by the rapid flow of bottom waters against small mounds ("beaver mounds"; Gubsch, 2010). Modelling showed that small seafloor structures with an elevation of only a few centimetres above the surrounding seafloor may induce bottom water inflow at moderately high permeability of the affected surface sediments (Gubsch, 2010). Further data are needed to reveal the mechanisms responsible for the penetration of bottom waters into the surface sediments collected at sites SO173-64, M66/D71/PC-19 and PC-32. However, the tracer data clearly show that the upper sediment layers were strongly affected by rapid mixing with overlying bottom waters.

Table 3. Summary of parameter values determined by fitting the steady state simulations to measured data (upward fluid velocity and k_{AOM}) and depth integrated rate of AOM and methane fluxes across the sediment-water interface at the investigated stations.

Stations	Model parameters values		Depth integrated Rate	Fluxes
	Upward fluid velocity (cm a^{-1})	Kinetic constant for AOM ($\text{cm}^3 \text{mmol}^{-1} \text{a}^{-1}$)	AOM ($\mu\text{mol cm}^{-2} \text{a}^{-1}$)	CH_4 Fluxes ($\mu\text{mol cm}^{-2} \text{a}^{-1}$)
M66/D71/PC-19	2	0.03	62	212
M66/D71/PC-24	3	0.1	120	205
M66/D71/PC-26	20	2	505	343
M66/D71/PC-31	4	0.1	128	234
M66/D71/PC-32	6	0.04	74	250
M66/D72/PC-2	3	0.2	190	197
M66/D72/PC-6	1	0.05	98	135
M66/D72/PC-8	2	0.02	56	183
M66/D72/PC-11	5	0.1	129	176
M66/D72/PC-13	1	1	87	194
M66/D75/PC-6	3	0.1	177	224
M66/D76/PC-19	20	1	204	308
M66/D76/PC-21	15	0.5	157	200
M66/D76/PC-23	12	0.3	148	279
M66/D76/PC-25	10	0.3	150	240
SO173-63	40	12	1538	816
SO173-64	5	4	180	6
SO173-73	4	5	534	24
SO173-121-FLUFO-K4	40	6	1353	2049
SO173-121-FLUFO-K5	2	4	1159	415

IV.5.2.2. Upward fluid flow velocities

The upward fluid velocity of the porewater was determined by fitting the model to the measured data (Tab. 3). These velocities do not match the range of previously reported values for Quepos Slide in the field of $0.1 - 40 \text{ cm a}^{-1}$ (Lorenson et al., 2010), which they indicate low to moderate values, but appear comparable to other cold vents with sediment velocities of $0.1 - 300 \text{ cm a}^{-1}$ were observed at other cold vents with sediment porewater velocities of $0.1 - 300 \text{ cm a}^{-1}$ (Lorenson et al., 2010). The upward fluid flow velocities of the bacterial mats on Hydrothermal Slide average 20 cm a^{-1} (Lorenson et al., 2010) with a range of 10 to 250 cm a^{-1} (Lorenson et al., 2010). The rate of fluid flow at the 121m Westside Mid-Venture was observed to be as high as 600 cm a^{-1} and was found to decrease to $30 - 60 \text{ cm a}^{-1}$ (Lorenson et al., 2010).

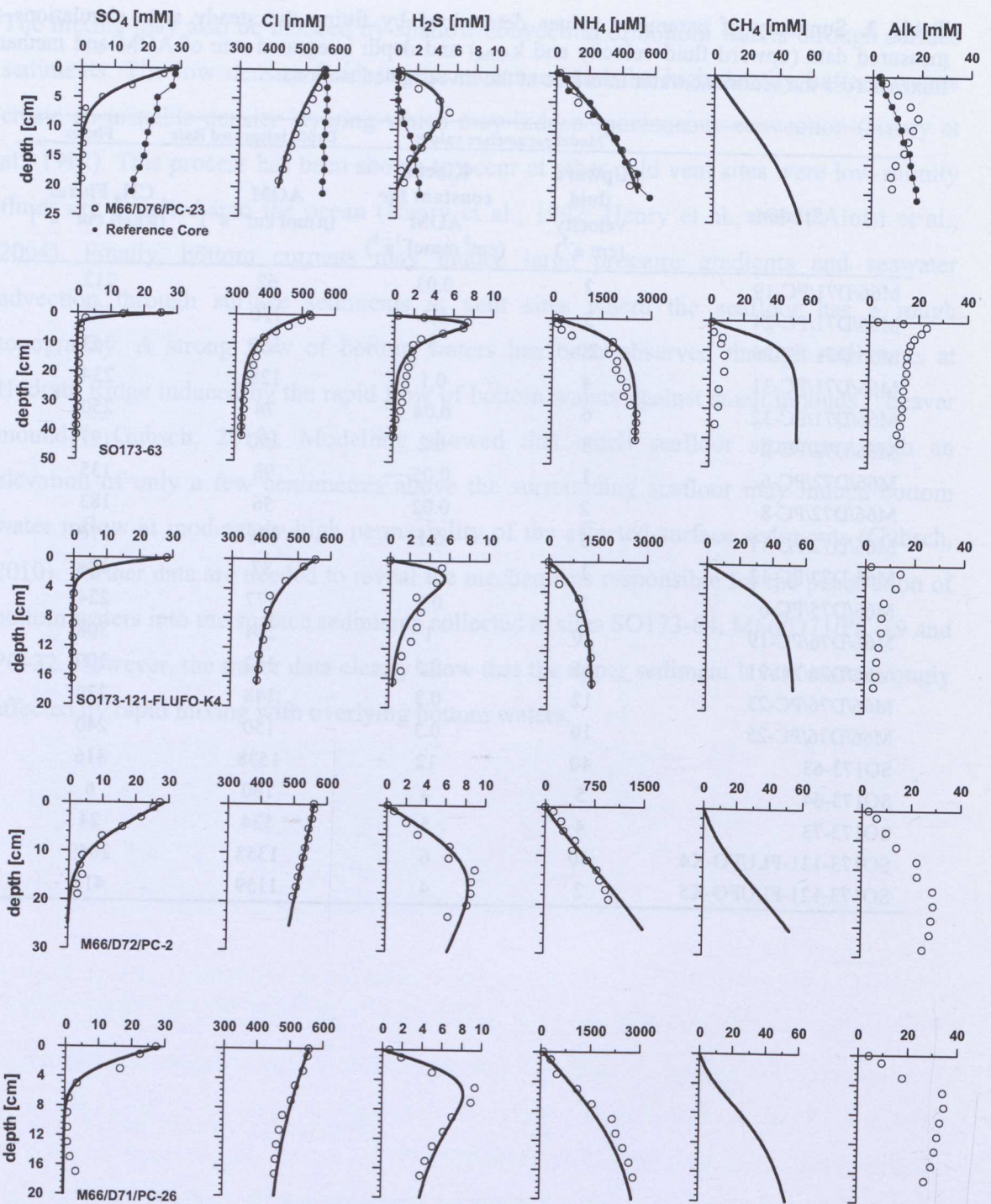


Figure 4. Measured (dots) and simulated (solid lines) concentration profiles of sulfate, chloride, total hydrogen sulfide (TH_2S), ammonium, methane and alkalinity in selected stations at Quepos Slide.

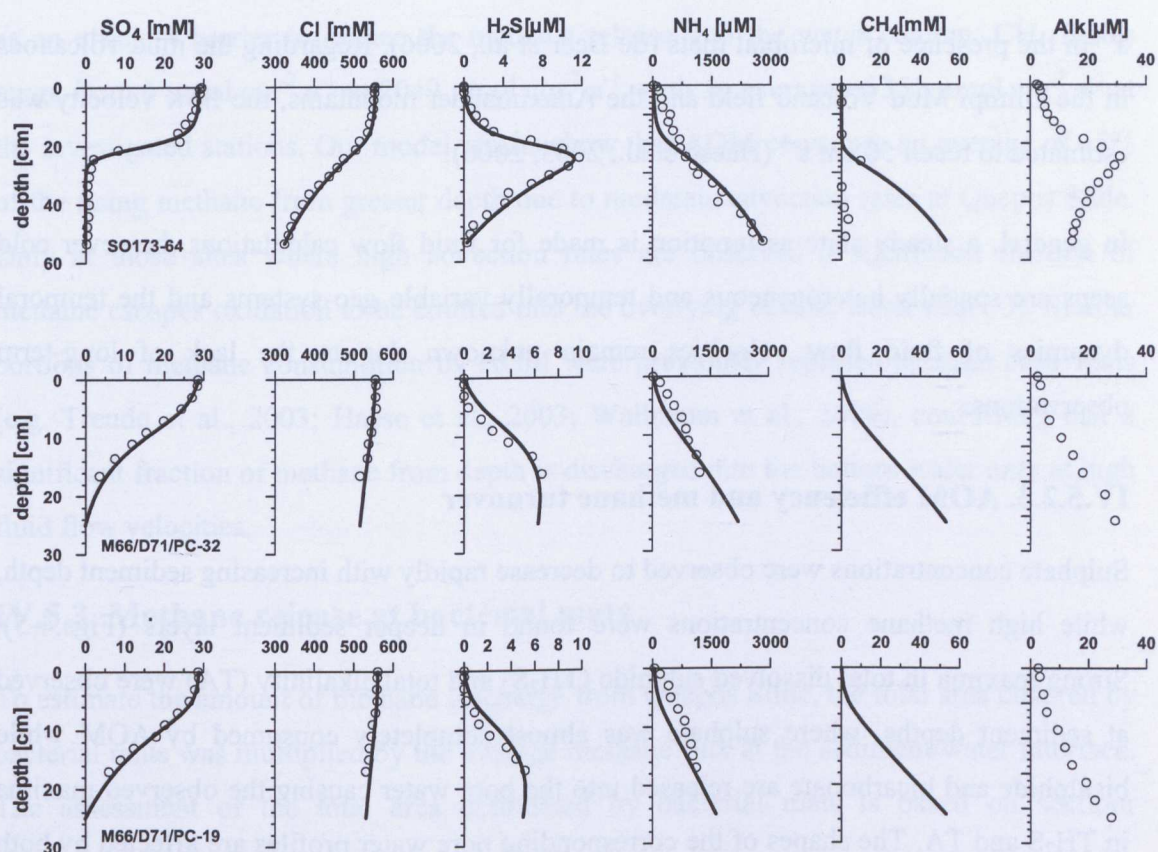


Figure 5. Measured (dots) and simulated (solid lines) concentration profiles of sulfate, chloride, total hydrogen sulfide (TH₂S), ammonium, methane and alkalinity in selected stations at Quepos Slide.

IV.5.2.2. Upward fluid flow velocities

The advection rates of the pore fluid range in total from 1 to 40 cm a⁻¹, with an average of 10 cm a⁻¹ (Tab. 3). These velocities are within the range of previously reported values for Quepos Slide in the field of bacterial mats (4 - 40 cm a⁻¹; Karaca et al., 2010), however they indicate low to moderate advective upflow compared to other cold vent sites. Flow velocities of 0.1 - 300 cm a⁻¹ were obtained at other cold vents with microbial mat formations at the continental margin off Costa Rica (Hensen et al., 2004; Linke et al., 2005; Karaca et al., 2010). Estimates of fluid flow velocities in sediments covered by bacterial mats on Hydrate Ridge average 20 cm a⁻¹ (Sommer et al., 2006) with a range of 10 to 250 cm a⁻¹ (Torres et al., 2002). The rate of fluid flow at the Håkon Mosby Mud Volcano was observed to be as high as 600 cm a⁻¹, but was found to decrease to 30 - 60 cm

a^{-1} in the presence of microbial mats (de Beer et al., 2006). Regarding the mud volcanoes in the Olimpi Mud Volcano field and the Anaximander mountains, the flow velocity was estimated to reach 50 cm a^{-1} (Haese et al., 2003, 2006).

In general, a steady state assumption is made for fluid flow calculations, however cold seeps are spatially heterogeneous and temporally variable geo-systems and the temporal dynamics of fluid flow velocities remain unknown due to the lack of long-term observations.

IV.5.2.3. AOM efficiency and methane turnover

Sulphate concentrations were observed to decrease rapidly with increasing sediment depth, while high methane concentrations were found in deeper sediment layers (Figs.4-5). Strong maxima in total dissolved sulphide (TH_2S) and total alkalinity (TA) were observed at sediment depths, where sulphate was almost completely consumed by AOM while bisulphide and bicarbonate are released into the pore water causing the observed maxima in TH_2S and TA. The shapes of the corresponding pore water profiles are affected by both transport processes and AOM. Thus, steep gradients in dissolved sulphate are not only caused by high AOM rates but also by the ascent of sulphate-free fluids.

Depth-integrated AOM rates vary between 56 and $1538 \mu\text{mol CH}_4 \text{ cm}^{-2} \text{ a}^{-1}$ (Tab. 3) and fall into the range of values reported at Hydrate Ridge (Boetius et al., 2000; Luff and Wallmann, 2003; Treude et al., 2003), where the highest AOM rates to date have been found ($3616 \mu\text{mol CH}_4 \text{ cm}^{-2} \text{ a}^{-1}$). Likewise, depth integrated AOM rates in Quepos Slide match those at other mud volcanoes like the Håkon Mosby Mud Volcano (Niemann et al., 2006), Dvurechenskii Mud Volcano (Lichtsclag et al., 2010; Wallmann et al., 2006) and the Kazan Mud Volcano (Haese et al., 2003). Hence, the investigated Quepos Slide can be regarded as one of the most active areas of the seafloor.

Pore water profiles showed that sulphate penetration depth controlled by the velocity of upward fluid flow and the methane concentration in the rising fluids is restricted to the upper centimetres of the sediment at those sites where high fluid flow velocities prevailed (SO173-63 and SO173-121-FLUFO-K4; Fig.4). High flow rates at those sites reduce the efficiency of AOM so that higher amounts of dissolved methane are emanating into the water column (Tab. 3). AOM is most efficient at low and intermediate flow rates and acts

as an efficient barrier to reduce the methane release into the water column. CH_4 fluxes range from $6 \mu\text{mol cm}^{-2} \text{a}^{-1}$ to $2049 \mu\text{mol cm}^{-2} \text{a}^{-1}$, with an average of $351 \mu\text{mol cm}^{-2} \text{a}^{-1}$ at the investigated stations. Our model results show that AOM consumes an average of 45% of the rising methane from greater depth due to moderate advection rates at Quepos Slide. Only at those sites where high advection rates are observed a significant fraction of methane escapes oxidation to be emitted into the overlying bottom water (Tab. 3). Similar portions of methane consumption by AOM were previously reported at other cold vents (e.g. Treude et al., 2003; Haese et al., 2003; Wallmann et al., 2006), confirming that a significant fraction of methane from depth is discharged into the bottom water only at high fluid flow velocities.

IV.5.3. Methane release at bacterial mats

To estimate the amount of methane discharge from Quepos Slide, the total area covered by bacterial mats was multiplied by the average methane flux at the sediment/water interface. The assessment of the total area dominated by bacterial mats is based on seafloor observations.

Based on the density of bacterial mat coverage on the seafloor, three different areas were determined (Fig. 6); (i) areas with the most abundant bacterial mats (51-100%, red zone), (ii) areas with relatively low abundances (11-50%, yellow zone), (iii) and areas with occasional bacterial mat occurrence (1-10%, green zone). The total area covered by bacterial mats was calculated by assuming that the highest ratio (100% of red zone; 50% of yellow zone; 10% of green zone) of sea floor area covered by bacterial mats (Tab. 4). Herewith, bacterial mats cover an area of 0.042 km^2 in the green zone, representing 10% of the total seepage area (0.42 km^2 ; Tab. 4; Fig. 6). The estimated area is covered by mats in this zone is used to extrapolate the total emission of dissolved methane to $0.15 \cdot 10^6 \text{ mol a}^{-1}$ by multiplying the average methane flux of $351 \mu\text{mol cm}^{-2} \text{a}^{-1}$ at the sediment/water interface. Similarly, methane emission in yellow zone, where 50% of the total area is covered by mats (0.04 km^2) results in $0.14 \cdot 10^6 \text{ mol a}^{-1}$. This value increases to $0.27 \cdot 10^6 \text{ mol a}^{-1}$ in the field of most abundant bacterial mats (red zone; 0.07 km^2). Accordingly, the overall amount of dissolved methane released from the entire survey area of Quepos Slide into the water column is estimated to be an order of $0.56 \cdot 10^6 \text{ mol a}^{-1}$.

Table 4. Dissolved methane fluxes at Quepos Slide via dewatering.

Total area (km ²)	Bacterial mat coverage	Area covered by bacterial mats	CH ₄ fluxes (in 10 ⁶ mol a ⁻¹)
0.423	1-10%	0.042	0.15
0.081	11-50%	0.04	0.14
0.076	51-100%	0.07	0.27
Σ=0.58		Σ=0.0152	Σ=0.56

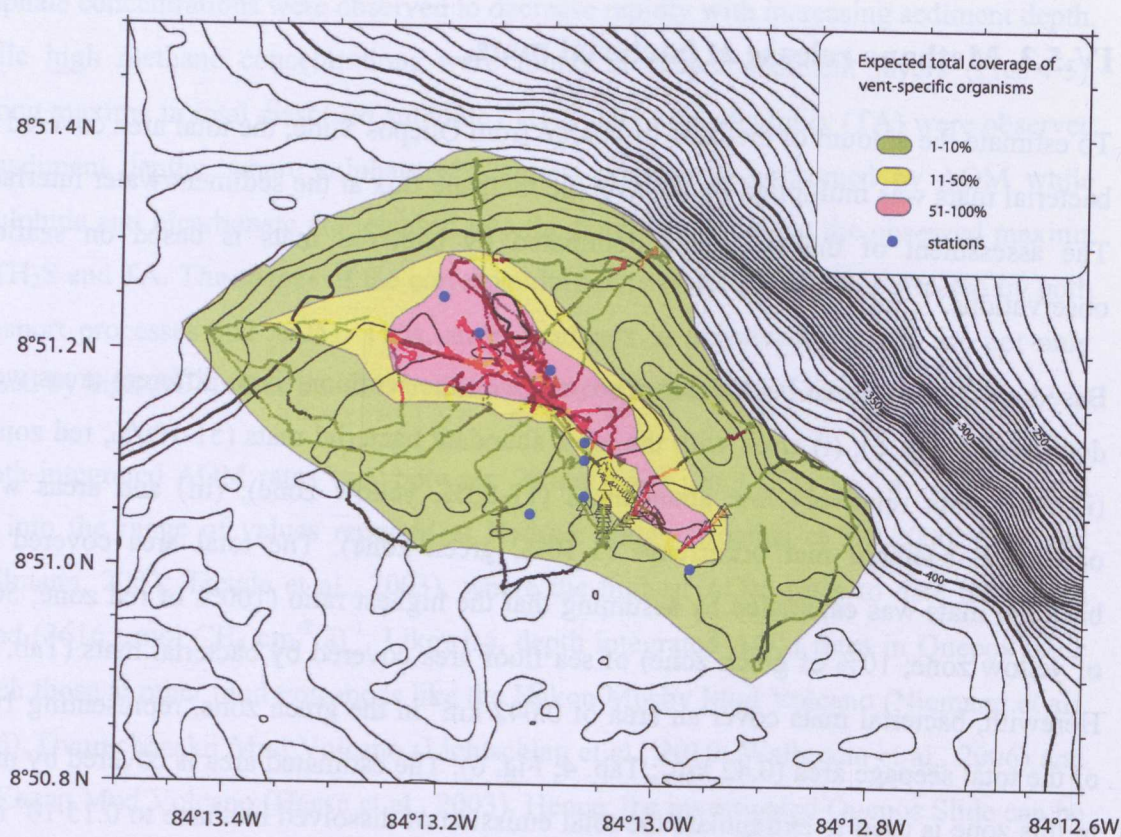


Figure 6. The map of bacterial mats at Quepos Slide together with coring stations. Light green represents a bacterial mat coverage ranging between 1-10 %, whereas yellow indicates a mean coverage of about 11-50% and red shows abundant coverage ranging between 51-100% of the total area.

This regional flux rate at Quepos Slide is comparable to flux estimates for methane transported via vent fluids ($0.19 - 0.57 \cdot 10^6 \text{ mol a}^{-1}$; personal unpublished data) and water column measurements ($0.07 - 0.6 \cdot 10^6 \text{ mol a}^{-1}$; Mau et al., 2006) for the bacterial mat sites of the major mound structures at the Costa Rica continental margin. Extrapolating over the 77 mound structures along the $\sim 460 \text{ km}$ long section of the Central America margin (Klaucke et al., 2008; Ranero et al., 2008; Sahling et al., 2008), Furi et al. (2010) calculated a total methane output of $3.1 \cdot 10^7 \text{ mol a}^{-1}$. Our methane flux value is similar to the average flux of $0.4 \cdot 10^6 \text{ mol a}^{-1}$ per mound according to Furi et al. (2010). Taking $0.5 \cdot 10^6 \text{ mol a}^{-1}$ as the average methane discharge, we derive a total methane output of $63 \cdot 10^6 \text{ mol a}^{-1}$ for the latest estimate of 112 various active methane seeps (e.g. mounds, faults, slides and seamount subduction tectonic features; Sahling et al., 2008) observed along the Central America margin.

Methane discharge has been quantified at a few cold seeps (mainly mud volcanoes). Compared to other very active systems like Håkon Mosby Mud Volcano ($5.4 \cdot 10^6 \text{ mol a}^{-1}$; Ginsburg et al., 1999), mud volcanoes offshore Barbados ($0.6 - 185 \cdot 10^6 \text{ mol a}^{-1}$; Henry et al., 1996), and Dvurechenskii Mud Volcano ($13 \cdot 10^6$ and $1.9 \cdot 10^6 \text{ mol a}^{-1}$; Lichtschlag et al., 2010 and Wallmann et al., 2006, respectively) the methane flux of $0.56 \cdot 10^6 \text{ mol a}^{-1}$ estimated in this study is a low methane discharge. However, calculations for those active systems integrate the total methane flux from the entire structures and do not represent the discharge from the areas covered by bacterial mats. At the areas covered by seep habitats (clast and siboglinid) a methane flux of $0.006 \cdot 10^6 \text{ mol a}^{-1}$ has been measured for the Captain Arutyunov Mud Volcano (Sommer et al., 2009). Solomon et al. (2008) investigated the total methane flux across the seafloor at Bush Hill to be $5.2 \cdot 10^6 \text{ mol a}^{-1}$ for the areas occupied by the chemosynthetic communities (i.e. tubeworms, mussels and bacterial mats). A benthic methane flux of up to $3.5 \cdot 10^6 \text{ mol a}^{-1}$ was found to be discharged in dissolved form in pore water as well as in the form of gas bubbles at the vent sites of the southern Hydrate Ridge (Heeschen et al., 2005). Our methane flux value cannot be directly compared to estimates from those sites. However it is a considerable seafloor methane flux from bacterial mats sites where the areal extent has been precisely estimated and it is ~ 6 times the flux from individual seeps off the UK continental shelf (Judd et al., 1997), up to 7 times of the global average seafloor methane flux from similar sized seeps and mud volcanoes (Etiope and Klusman, 2002; Etiope and Milkov, 2004). This illustrates that

submarine slides are important seepage sites of natural methane. However, the extent of methane seepage from submarine slides remains unknown on global scale.

IV.6. Conclusions

Sea floor methane emission from Quepos Slide bacterial mats sites at the submarine segment of the Costa Rica fore-arc margin was estimated taking into account the spatial variability of the seepage by relating the distribution patterns of bacterial mat coverage and a numerical model for methane dissolution into the water column. Model results illustrate that studied seeps transport a rather limited amount of methane into the water column due to medium to low advection rates ranging between 1 - 40 cm a⁻¹ (average 10 cm a⁻¹). Such advection rates allow high methane consumption by AOM and reduce the methane discharge into the water column by approximately 50%. As a major sink for methane in cold seep sediments, AOM consumes on average 45% of the methane flux from depth and leads to a moderate methane flux of average 351 μmol cm⁻² a⁻¹ from single spots into the bottom water. Depth integrated AOM rates (ranging between 56 and 1538 μmol CH₄ cm⁻² a⁻¹) are similar in magnitude to those at well studied active cold seeps (e.g. Hydrate Ridge) indicating that Quepos Slide should be regarded as one of the most active areas at the seafloor.

Based on detailed mapping, the overall amount of dissolved methane released from bacterial mats into the water column is estimated to be 0.56·10⁶ mol a⁻¹. This is a significant seafloor methane flux out of a single bacterial mat site, suggesting that submarine slides might be important seepage sites of natural methane if the methane flux from these structures is similar to the Quepos Slide flux. However, the global extent of methane seepage from submarine slides remains unknown to date, warranting a more extensive monitoring program.

References

- Aloisi, G., Wallmann, K., Haese, R. R., and Saliege, J. F., 2004. Chemical, biological and hydrological controls on the C-14 content of cold seep carbonate crusts: numerical modeling and implications for convection at cold seeps. *Chemical Geology* 213, 359-383.
- Berner, R. A., 1980. *Early diagenesis. A theoretical approach*. Princeton University Press, 241pp., New York.
- Boetius, A., Ravensschlag, K., Schubert, C. J., Rickert, D., Widdel, F., Giesecke, A., Amann, R., Jørgensen, B. B., Witte, U., and Pfannkuche, O., 2000. A marine microbial consortium apparently mediating anaerobic oxidation of methane. *Nature* 407, 623-626.
- Boetius, A. and Suess, E., 2004. Hydrate Ridge: a natural laboratory for the study of microbial life fueled by methane from near-surface gas hydrates. *Chem. Geol.* 205, 291 - 310.
- Bohrmann, G., Heeschen, K., Jung, C., Weinrebe, W., Baranov, B., Cailleau, B., Heath, R., Hühnerbach, V., Hort, M., Masson, D., and Trummer, I., 2002. Widespread fluid expulsion along the seafloor of the Costa Rica convergent margin. *Terra Nova* 14, 69-79.
- Boudreau, B. P., 1997. *Diagenetic models and their implementation: modelling transport and reactions in aquatic sediments*. Springer, Berlin, Heidelberg, Berlin, Heidelberg, New York.
- Brückmann, W., Rhein, M., Rehder, G., Bialas, J., and Kopf, A., 2009. SUBFLUX METEOR-Berichte 09-2, Universität Hamburg.
- de Beer, D., Sauter, E., Niemann, H., Kaul, N., Foucher, J. P., Witte, U., Schluter, M., and Boetius, A., 2006. In situ fluxes and zonation of microbial activity in surface sediments of the Hakon Mosby Mud Volcano. *Limnology and Oceanography* 51, 1315-1331.
- Dimitrov, L. I., 2002. Mud volcanoes - the most important pathway for degassing deeply buried sediments. *Earth-Sci. Rev.* 59, 49-76.
- Etiopie, G., 2004. New directions: GEM - Geologic emissions of methane, the missing source in the atmospheric methane budget. *Atmospheric Environment* 38, 3099-3100.
- Etiopie, G. and Klusman, R. W., 2002. Geologic emissions of methane to the atmosphere. *Chemosphere* 49, 777-789.
- Etiopie, G. and Milkov, A. V., 2004. A new estimate of global methane flux from onshore and shallow submarine mud volcanoes to the atmosphere. *Environmental Geology* 46, 997-1002.

- Feseker, T., Foucher, J. P., and Harmegnies, F., 2008. Fluid flow or mud eruptions? Sediment temperature distributions on Hakon Mosby mud volcano, SW Barents Sea slope. *Mar. Geol.* 247, 194-207.
- Füri, E., Hilton, D. R., Tryon, M. D., Brown, K. M., McMurtry, G. M., Bruckmann, W., and Wheat, C. G., 2010. Carbon release from submarine seeps at the Costa Rica fore arc: Implications for the volatile cycle at the Central America convergent margin. *Geochemistry Geophysics Geosystems* 11.
- Ginsburg, G. D., Milkov, A. V., Soloviev, V. A., Egorov, A. V., Cherkashev, G. A., Vogt, P. R., Crane, K., Lorenson, T. D., and Khutorskoy, M. D., 1999. Gas hydrate accumulation at the Haakon Mosby Mud Volcano. *Geo-Marine Lett.* 19, 57-67.
- Gubsch, S., 2010. Detektion und Quantifizierung von subaquatischen Porenwasserfreisetzungen geringer Intensitäten. PhD Thesis, University of Hamburg-Harburg, 174pp., Shaker Verlag, Hamburg.
- Haese, R., Hensen, C., and De Lange, G. J., 2006. Pore water geochemistry of eastern Mediterranean mud volcanoes: implications for fluid transport and fluid origin. *Mar. Geol.* 225, 191-208.
- Haese, R. R., Meile, C., Van Cappellen, P., and De Lange, G. J., 2003. Carbon geochemistry of cold seeps: methane fluxes and transformation in sediments from Kazan mud volcano, eastern Mediterranean Sea. *Earth Planet. Sci. Lett.* 212, 361-375.
- Heeschen, K. U., Collier, R. W., de Angelis, M. A., Suess, E., Rehder, G., Linke, P., and Klinkhammer, G. P., 2005. Methane sources, distributions, and fluxes from cold vent sites at Hydrate Ridge, Cascadia Margin. *Global Biogeochemical Cycles* 19.
- Henry, P., Foucher, J. P., Lepichon, X., Sibuet, M., Kobayashi, K., Tarits, P., Chamotrooke, N., Furuta, T., and Schultheiss, P., 1992. Interpretation of Temperature-Measurements from the Kaiko-Nankai Cruise - Modeling of Fluid-Flow in Clam Colonies. *Earth and Planetary Science Letters* 109, 355-371.
- Henry, P., Le Pichon, X., Lallemand, S., Lance, S., Martin, J. B., Foucher, J.-P., Fiala-Médioni, A., Rostek, F., Guilhaumou, N., Pranal, V., and Castrec, M., 1996. Fluid flow in and around a mud volcano field seaward of the Barbados accretionary wedge: results from Manon cruise. *J. Geophys. Res.* 101, 20,297-20,323.
- Hensen, C. and Wallmann, K., 2004. Methane fluxes and gas hydrate reservoirs in slope sediments along Costa Rica continental margin EGU, Nice, France.
- Hovland, M., Judd, A. G., and Burke, J. R. A., 1993. The global flux of methane from shallow submarine sediments. *Chemosphere* 26, 559-578.
- Hovland, M., Svensen, H., Forsberg, C. F., Johansen, H., Fichler, C., Fossa, J. H., Jonsson, R., and Rueslatten, H., 2005. Complex pockmarks with carbonate-ridges off mid-Norway: Products of sediment degassing. *Mar. Geol.* 218, 191-206.

- Imhoff, J. F., Sahling, H., Suling, J., and Kath, T., 2003. 16S rDNA-based phylogeny of sulphur - oxidising bacterial endosymbionts in marine bivalves from cold-seep habitats. *Marine Ecology-Progress Series* 249, 39-51.
- Judd, A., Davies, G., Wilson, J., Holmes, R., Baron, G., and Bryden, I., 1997. Contributions to atmospheric methane by natural seepages on the UK continental shelf. *Mar. Geol.* 137, 165-189.
- Judd, A. G., 2004. Natural seabed gas seeps as sources of atmospheric methane. *Environmental Geology* 46, 988-996.
- Karaca, D., Hensen, C., and Wallmann, K., 2010. Controls on authigenic carbonate precipitation at cold seeps along the convergent margin off Costa Rica. *Geochemistry Geophysics Geosystems*. 11, Q08S27, doi:10.1029/2010GC003062.
- Kessler, J. D., Reeburgh, W. S., Southon, J., Seifert, R., Michaelis, W., and Tyler, S. C., 2006. Basin-wide estimates of the input of methane from seeps and clathrates to the Black Sea. *Earth and Planetary Science Letters* 243, 366-375.
- Klaucke, I., Masson, D. G., Petersen, C. J., Weinrebe, W., and Ranero, C. R., 2008. Multifrequency geoaoustic imaging of fluid escape structures offshore Costa Rica: Implications for the quantification of seep processes. *Geochemistry Geophysics Geosystems* 9, Q04010, doi:10.1029/2007GC001708.
- Kvenvolden, K. A. and Rogers, B. W., 2005. Gaia's breath - global methane exhalations. *Marine and Petroleum Geology* 22, 579-590.
- Lichtschlag, A., Felden, J., Wenzhofer, F., Schubotz, F., Ertefai, T. F., Boetius, A., and de Beer, D., 2010. Methane and sulfide fluxes in permanent anoxia: In situ studies at the Dvurechenskii mud volcano (Sorokin Trough, Black Sea). *Geochimica et Cosmochimica Acta* 74, 5002-5018.
- Linke, P., Wallmann, K., Suess, E., Hensen, C., and Rehder, G., 2005. In-situ benthic fluxes from an intermittently active mud volcano at the Costa Rica convergent margin. *Earth and Planetary Science Letters* 235, 79-95.
- Luff, R. and Wallmann, K., 2003. Fluid flow, methane fluxes, carbonate precipitation and biogeochemical turnover in gas hydrate-bearing sediments at Hydrate Ridge, Cascadia Margin: Numerical modeling and mass balances. *Geochim. Cosmochim. Acta* 67, 3403-3421.
- Luff, R., Wallmann, K., Grandel, S., and Schlüter, M., 2000. Numerical modelling of benthic processes in the deep Arabian Sea. *Deep-Sea Res. II* 47, 3039-3072.
- Luyendyk, B., Kennett, J., and Clark, J. F., 2005. Hypothesis for increased atmospheric methane input from hydrocarbon seeps on exposed continental shelves during glacial low sea level. *Marine and Petroleum Geology* 22, 591-596.

- Mau, S., Sahling, H., Rehder, G., Suess, E., Linke, P., and Soeding, E., 2006. Estimates of methane output from mud extrusions at the erosive convergent margin off Costa Rica. *Mar. Geol.* 225, 129-144.
- Niemann, H., Losekann, T., de Beer, D., Elvert, M., Nadalig, T., Knittel, K., Amann, R., Sauter, E. J., Schluter, M., Klages, M., Foucher, J. P., and Boetius, A., 2006. Novel microbial communities of the Haakon Mosby mud volcano and their role as a methane sink. *Nature* 443, 854-858.
- Ranero, C. R., Grevenmeyer, I., Sahling, H., Barckhausen, U., Hensen, C., Wallmann, K., Weinrebe, W., Vannucchi, P., von Huene, R., and McIntosh, K., 2008. Hydrogeological system of erosional convergent margins and its influence on tectonics and interplate seismogenesis. *G-cubed* 9, Q03S04, doi:10.1029/2007GC001679.
- Ranero, C. R. and Von Huene, R., 2000. Subduction erosion along the Middle America convergent margin. *Nature* 404, 748-752.
- Reeburgh, W. S., 2007. Oceanic methane biogeochemistry. *Chemical Reviews* 107, 486-513.
- Sahling, H., Masson, D. G., Ranero, C. R., Hühnerbach, V., Weinrebe, W., Klauke, I., Bürk, D., Brückmann, W., and Suess, E., 2008. Fluid seepage at the continental margin offshore Costa Rica and southern Nicaragua. *G-cubed* 9.
- Schleicher, 2006, Bestimmung von ventspezifischen Faunenvergesellschaftungen am mittellamerikanischen Kontinentalrand mit Hilfe quantitativer Videoauswertung, Diploma Thesis, 68pp, University of Kiel, Kiel.
- Solomon, E. A., Kastner, M., Jannasch, H., Robertson, G., and Weinstein, Y., 2008. Dynamic fluid flow and chemical fluxes associated with a seafloor gas hydrate deposit on the northern Gulf of Mexico slope. *Earth and Planetary Science Letters* 270, 95-105.
- Sommer, S., Pfannkuche, O., Linke, P., Luff, R., Greinert, J., Drews, M., Gubsch, S., Pieper, M., Poser, M., and Viergutz, T., 2006. Efficiency of the benthic filter: Biological control of the emission of dissolved methane from sediments containing shallow gas hydrates at Hydrate Ridge. *Global Biogeochemical Cycles* 20.
- Tishchenko, P., Hensen, C., Wallmann, K., and Wong, C. S., 2005. Calculation of the stability and solubility of methane hydrate in seawater. *Chemical Geology* 219, 37-52.
- Torres, M. E., McManus, J., Hammond, D. E., de Angelis, M. A., Heeschen, K. U., Colbert, S. L., Tryon, M. D., Brown, K. M., and Suess, E., 2002. Fluid and chemical fluxes in and out of sediments hosting methane hydrate deposits on Hydrate Ridge, OR, I: Hydrological provinces. *Earth and Planetary Science Letters* 201, 525-540.
- Treude, T., Boetius, A., Knittel, K., Wallmann, K., and Jørgensen, B. B., 2003. Anaerobic oxidation of methane above gas hydrates. *Mar. Ecol. Prog. Ser.* 264, 1-14.

- Tryon, M. D., Wheat, C. G., and Hilton, D. R., 2010. Fluid sources and pathways of the Costa Rica erosional convergent margin. *Geochemistry Geophysics Geosystems* 11.
- Vannucchi, P., Ranero, C. R., Galeotti, S., Straub, S. M., Scholl, D. W., and McDougall-Ried, K., 2003. Fast rates of subducting erosion along the Costa Rica Pacific margin: Implications for nonsteady rates of crustal recycling at subduction zones. *Journal of Geophysical Research* 108, doi:10.1029/2002JB002207.
- von Huene, R., Ranero, C. R., Watts, P., 2004, Tsunamigenic slope failure along the Middle America Trench in two tectonic settings, *Marine Geology*, 203, 303-317.
- von Huene, R., Ranero, C. R., Weinrebe, W., and Hinz, K., 2000, Quaternary convergent margin tectonics of Costa Rica, segmentation of the Cocos Plate, and Central American volcanism, *Tectonics*, 19, 314-334.
- Wallmann, K., Drews, M., Aloisi, G., and Bohrmann, G., 2006. Fluid expulsion from the Dvurechenskii mud volcano (Black Sea): Part II. Methane fluxes and new estimates of global methane discharge into the ocean via submarine mud volcanism. *Earth Planet. Sci. Lett.* 248, 544-559.
- Wallmann, K., Linke, P., Suess, E., Bohrmann, G., Sahling, H., Schlüter, M., Dählmann, A., Lammers, S., Greinert, J., and Mirbach, N. V., 1997. Quantifying fluid flow, solute mixing, and biogeochemical turnover at cold vents of the eastern Aleutian subduction zone. *Geochim. Cosmochim. Acta* 61, 5209-5219.

Personal Information

Address : Mittelstr. 15
Zip code and city : D-24103 Kiel
Phone number (cell) : +49(0)179 9407863
E-mail : dkaraca@ifm-geomar.de
Date of Birth : May 30th 1978
Nationality : Turkish
Gender : Female

Educational Background

2006 - 2011 Ph.D Research in Marine Biogeochemistry
SFB 574 /University of Kiel-IFM-GEOMAR / Germany

2002 - 2004 M.Sc. Coastal Geosciences and Engineering
Coastal Research Laboratory / University of Kiel / Germany

1996 - 2000 B.Sc. Geological Engineering (High Honour Degree)
Faculty of Engineering / University of Ankara / Turkey

1992 - 1995 Science High School
Evrensel Science High School / Ankara / Turkey

